Instituto Tecnológico y de Estudios Superiores de Monterrey

Campus Monterrey

School of Engineering and Sciences

Rhythmic expression of microRNAs in entrained human breast cell lines

A dissertation presented by

Rafael Julián Chacolla Huaringa

Submitted to the

School of Engineering and Sciences

in partial fulfillment of the requirements for the degree of

Doctor

in

Biotechnology

Monterrey Nuevo León, June 30th, 2021

Dedication

To my parents, Julián Chacolla Paquita y Celia Huaringa Contreras, as well as my brother who was the inspiration to push my limits all times. Finally, to my wife, Ana Olimpia Balán and my daughter Rosalía who gave me the last breath.

Acknowledgements

I am infinitely grateful for the aid of genteel people such as workers and professors for their academic services from TEC de Monterrey and CONACyT for their financial support that have made things possible. There are a lot of people to thank for their support, but I have to mention three persons who changed the horizons of my scientific career through academic field:

Dr. Sean Scott and Dr. Victor Treviño for their support as advisors of this thesis, their help was invaluable for my research. My colleagues from Therapy Cell and Bioinformatics focus groups provide great moment along the period of thesis. Dr. Rocío Ortiz was a valuable support and appreciate her feedback on the heading of thesis.

Dr. Magdaleno Pérez and Dr Consuelo Cantú are valuable persons who changed my life on industry sector. I always have in mind their advices and support while I worked with them, as well as my friends forever.

My parents, Celia Huaringa and Julián Chacolla for their love, support and sacrifice through all these years. I have a special thanks to my brother William, because he is always an ideal image to follow. My friends from Peru are a great motivation every day and I thank them for their advices to never to give up on this challenge.

Rhythmic expression of microRNAs in entrained human breast cell lines

by

Rafael Julián Chacolla Huaringa

Abstract

Circadian rhythms is an essential system for temporal (~24 hours) regulation of molecular processes in diverse organisms. Dysregulation of circadian gene expression has been associated to pathogenesis of various disorders, including hypertension, depression, and diverse cancers. Recently, microRNAs (miRNAs) have been identified as key modulators of gene expression post-transcriptionally, and perhaps involved in circadian clock architecture or their output functions. The aim of the present study is to explore the temporal expression of miRNAs among entrained human breast cell lines. Thus, we evaluated the temporal (28 hours) expression of 2006 miRNAs in breast non-tumorigenic cell line, MCF-10A, and tumorigenic cell lines, MCF-7 and MDA-MB-231 using microarrays technology after serum shock entrainment. We determined miRNAs that exhibit rhythmic fluctuations in each breast cell line, and some of them across two or three cell lines. Afterwards, we confirmed rhythmic profiles exhibited by miR-141-5p, miR-1225-5p, miR-17-5p, miR-222-5p, miR-769-3p, and miR-548ay-3p in the above cell lines, as well as in ZR-7530 and HCC-1954 using RT-qPCR technology. Our results show that serum shock entrainment in breast cells lines induces rhythmic fluctuations of distinct sets of miRNAs, which have the potential to be related to endogenous circadian clock, but extensive investigation is required to elucidate that connection.

Keywords: microRNAs – rhythmic expression – entrainment – breast cancer

List of Figures

Figure 1. Physiological functions regulated by circadian system. This system core consists of hypothalamic pacemaker, which is located SCN and communicates through various neural and endocrine signals to drive diverse physiological levels. An individual progress through the regular 24-h cycle of sleep (grey shading) and wakefulness, thus, his metabolism is adjusted accordingly demands and opportunities of the solar day. Melatonin, core temperature and serum cortisol are well-known biological variables with circadian regulation. Image taken from [50]. 18
Figure 2. Architecture of mammalian circadian clock system. The circadian clock mainly consist of three components: the inputs, ~24-h clock and the outputs. The SCN is the central pacemaker at the top of the hierarchy, which is synchronized by the external 24-h cycle and in coordinates physiological outputs. Thus, whole clock machinery is important for robust operation of the entire body, regulating rhythms such as locomotion, body temperature and others. Image taken from [63]. 19
Figure 3. Clock molecular network. The E-box mediated the negative feedback of per and cry proteins towards transcriptional complex CLOCK/BMAL1. Additionally, recent investigations also suggest negative feedback loop with the nuclear receptors *Rev-erb-α* and *Rev-erb-β* through RORE enhancers, due they might generate self-sustained oscillations. 21
Figure 4. The circadian expression in central and peripheral clocks. The SCN promote electrical and humoral signals to synchronize phases of local circadian clocks oscillations, which is dependent of peripheral organ. 21
Figure 5. Overview of miRNA biogenesis pathway. The miRNAs are initially transcribed as primary as pri-miRNAs by Pol II in the nucleus. Thus, these are cleaved by microprocessor to produce pre-miRNAs, which are then exported from nucleus to cytoplasm. Image taken from [82]. 24
Figure 6 The miRNA involvement in hallmarks of cancer. Abnormal miRNA expression affects signaling pathways at diverse physiological levels to enhance tumorigenesis. This image depict representative miRNAs that have been studied to act as oncogenes or tumor suppressor. Image taken from [99] 26
Figure 7 Components of the breast. Image taken from [108]..... 28
Figure 8. Establishment of cell culture to entrainment of cell lines. The entrainment initiates when cultured cells have a confluence greater of 90%. Thus, the batch is split on 2 batches for mRNA and miRNA expression. Particularly, miRNA expression required thirteen 6-well plates (triplicates, each one consist of 2 wells) for covering 48h period. The mRNA expression required five 6-well plates (duplicates) for covering 48h period. Except miRNA expression in MCF-7 was done by triplicate. 34
Figure 9. Comparison of total RNA from cellular fractions before and after purification. The purified RNA was used for microarray assays 57
Figure 10. Electropherogram plot. This image depicts the parameters evaluated for evaluating RNA integrity. Markers 18S and 28S, and ladder are reference parameters. 57
Figure 11. Temporal expression profiles of *BMAL1* and *PER2* genes in entrained human breast non-tumorigenic cell line, MCF-10A. The expression of *BMAL1* and *PER2* was measured by RT-qPCR assays. Samples were collected every 4-h for 48-h. Data points

(mean of duplicates) were normalized using *GAPDH* gene, and corrected to the first time point (t = 0). 60
Figure 12 Temporal expression profiles of *BMAL1* and *PER2* genes in entrained MCF-7 cells. In addition, expression profiles in MCF10A cells are added for comparison purposes. The expression of *BMAL1* and *PER2* genes was measured by RT-qPCR assays. Samples were collected every 4-h for 48-h. Data points (mean of triplicates ± SEM) were normalized using GAPDH gene relative to the first time point (t = 0). Dotted gray lines at 12-h and 40h were added to show the period where profiles have robustness. 62
Figure 13 Temporal expression profiles of *BMAL1* and *PER2* genes in entrained MDA-MB-231 cells. In addition, expression profiles in MCF10A cells are added for comparison purposes. The expression of *BMAL1* and *PER2* gene was measured by RT-qPCR assays. Samples were collected every 4-h for 48-h. Data points (mean of triplicates ± SEM) were normalized using GAPDH gene relative to the first time point (t = 0). Dotted gray lines at 12-h and 40h were added to show the period where profiles have robustness. 63
Figure 14 Temporal expression profiles of *BMAL1* and *PER2* genes in entrained ZR-7530 cells. In addition, expression profiles in MCF10A cells are added for comparison purposes. The expression of *BMAL1* and *PER2* genes was measured by RT-qPCR assays. Samples were collected every 4-h for 48-h. Data points (mean of triplicates ± SEM) were normalized using GAPDH gene relative to the first time point (t = 0). Dotted gray lines at 12-h and 40h were added to show the period where profiles have robustness. 64
Figure 15 Temporal expression profiles of *BMAL1* and *PER2* genes in entrained HCC-1954 cells. In addition, expression profiles in MCF-10A cells are added for comparison purposes. The expression of *BMAL1* and *PER2* genes was measured by RT-qPCR assays. Samples were collected every 4-h for 48-h. Data points (mean of triplicates ± SEM) were normalized using GAPDH gene relative to the first time point (t = 0). Dotted gray lines at 12-h and 40h were added to show the period where profiles have robustness. 65
Figure 16. Temporal expression profile of *SERPINB1* gene in entrained MCF-7 cells. The profile expression of *SERPINB1* gene was done by RT-qPCR assays in serum-shocked MCF-7 cells during 48 hours (4-hour intervals). Data points (mean of triplicates ± SEM) were normalized using GAPDH gene relative to the first time point (t = 0). Dotted gray lines at 12-h and 40h were added to show the period where profiles have robustness. 66
Figure 17 Comparison of background and foreground obtained from microarrays assays in MCF-10A. The foreground plot obtained from cyRNA samples has solid signal intensities (green) and background evidenced normal pattern. However, The foreground plot obtained from nuRNA samples has few dots and lower signal intensities (red) and background evidenced more dots and higher signal intensities. 68
Figure 18. Distribution of cosine correlation, period and phase obtained from analyzing 28h temporal expression of 2006 miRNAs in MCF-10A, MCF-7 and MDA-MB-231 cells. 69
Figure 19 Evaluation of the cosine correlation, period and phase distributions in experimental and randomized data. Experimental data consisted of miRNA temporal expression in MCF- 10A, MCF-7 and MDA-MB-231 cells. Randomized data consisted of five types of data (by triplicate) decomposed from 5 types of randomization methods: TL, CW, RW, CRW and CRWB. Panel (A) shows the distributions of cosine correlation, panel (B) period, and panel (C) phase among experimental and randomized data. Panel

(D) shows cosine correlation compared to the period for experimental and randomized (CRWB) data. An arrow mark regions in which miRNAs with large cosine correlation is highly associated to non-periodic values in randomized experiments whereas experimental data do not show such associations. Panel (E) shows plots of the period values in experimental and randomized (CRWB) data (two replicates). Red dots represent miRNAs fulfilling the selection criteria in correlation and period values. 71
Figure 20 Correlations plots from miRNA profiling in breast cell lines. They illustrate the disposition of the clusters (based miRNA expression) identified for each breast cell line. 73
Figure 21. Heatmaps of temporal expression (28h) of miRNA profiling in breast cell lines. The heat maps depict the expression level of miRNAs over 28 h (between 12–40h) in MCF-10A, MCF-7 and MDA-MB-231 cells. Additionally, heat maps show 6 different clusters of miRNAs that depict marked phases. Brown colors represent higher expression values, while yellow colors represent lower expression values. Expression values are z-scaled relative to each cell line. 73
Figure 22. Venn diagram of 143, 183, and 147 miRNAs that exhibited rhythmic expression over 28 h in MCF-10A, MCF-7, and MDA-MB-231 cells. The diagram also shows miRNAs that exhibited rhythmicity across cell lines and were selected for RT-qPCR validation (red). 74
Figure 23. Expression profiles of miR-141-5p, miR-1225-5p, and miR-17-5p across breast cell lines. The rhythmic expression was evaluated by RT-qPCR assays in serum-shocked MCF-10A, MCF-7, MDA-MB-231, ZR-7530, and HCC-1954 cells over 48 h (4h intervals). (A) miR-141-5p exhibits rhythmic profiles in MCF-10A, MCF-7 and HCC-1954 cells; (B) miR-1225-5p exhibits rhythmic profiles in ZR-7530 and HCC-1954 cells; (C) miR-17-5p exhibits rhythmic profiles in MDA-MB-231 and HCC-1954 cells. Data points (means of three biological replicates ± standard error of the mean [SEM]) were normalized using miR-106a-5p relative to the first time point (t = 0). The p-value and period values of rhythmic profiles were obtained from the MetaCycle analysis and are illustrated at the top of each plot. Expression profiles with p-values less than 0.05 were considered rhythmic. For comparison purposes, the gray lines in the graphs concerning MCF-10A, MCF-7, and MDA-MB-231 illustrate the expression profiles obtained from the microarray data, which were scaled to the expression profile obtained from RT-qPCR assays. Dashed gray lines at 12 h and 40 h were added to show the period in which profiles were measured by microarray. 77
Figure 24 Expression profiles of miR-769-3p, miR-1225-5p, and miR-222-5p across MCF-10A, MCF-7 and MDA-MB-231 cells. The rhythmic expression was evaluated by RT-qPCR assays in serum-shocked MCF-10A, MCF-7, and MDA-MB-231 cells over 48 h (4 h intervals). (A) Rhythmic profiles of miR-769-3p exhibited in MCF-7 and MDA-MB-231 cells. (B) Rhythmic profiles of miR-222-5p exhibited in MCF-10A and MCF-7 cells. Data points (means of three biological replicates ± SEM) were normalized using miR-106a-5p relative to the first time point (t = 0). The p-values and period values of rhythmic profiles were obtained from MetaCycle analysis and are illustrated at the top of each plot. The p-values lesser than 0.05 were considered as rhythmic expression statistically significant. For comparison purposes, the more lightly colored lines illustrate the expression profiles obtained from microarray assays, which were scaled to the expression profiles obtained

from RT-qPCR assays. Dashed gray lines at 12 and 40 h were added to show the periods in which the profiles were measured by microarrays. 79
Figure 25 Expression profiles of miR-548ay-3p in MCF-10A, MCF-7, MDA-MB-231, ZR-7530 and HCC-1954 cells. The rhythmic expression was evaluated by RT-qPCR assays in serum-shocked 5 human breast cell lines over 48 h (4 h intervals). Data points (means of three biological replicates ± SEM) were normalized using miR-106a-5p relative to the first time point (t = 0). The p-values and period values of rhythmic profiles were obtained from MetaCycle analysis and are illustrated at the top of each plot. The p-values lesser than 0.05 were considered as rhythmic expression statistically significant. For comparison purposes, the more lightly colored lines illustrate the expression profiles obtained from microarray assays, which were scaled to the expression profiles obtained from RT-qPCR assays. Dashed gray lines at 12 and 40 h were added to show the periods in which the profiles were measured by microarrays. 80
Figure 26. Overview of the interaction between circadian clock and miRNAs, specifically with rhythmicity. Continuous lines between concepts represent known facts. Dashed lines represent unknown information. Circadian control inspired in [230]. 83

List of Tables

Table 1. Characteristics of the human breast cell lines used in this study 31
Table 2. List of primers for *BMAL1*, *PER2*, *SERPINB1* and *GAPDH* genes 41
Table 3. List of primers for miRNA validation. 42
Table 4. Cycling parameters for miRNA reverse transcription 44
Table 5. Pools for pre-amplification of cDNA 45
Table 6. RNA concentration and quality parameter of MCF-10A 58
Table 7. Primers features 59
Table 8. Circadian features of clock genes displayed in MCF-7 cells 62
Table 9 Circadian features of clock genes displayed in MDA-MB-231 cells 63
Table 10 Circadian features of clock genes displayed in ZR-7530 cells 64
Table 11 Circadian features of *BMAL1* and *PER2* genes displayed in HCC-1954 cells 65
Table 12 Circadian features of *SERPINB1* gene displayed in MCF-7 cells 66

Contents

Abstract v

List of Figures vi

List of Tables x

Introduction 14

1.1 Motivation 15
1.2 Problem Statement and Context 16
1.3 Research Question 16
1.4 Solution overview 16

Theoretical Framework 17

2.1 Biological clocks as central feature of life 17
2.1.1 Circadian rhythm in living organisms - human 17
2.1.2 Circadian rhythm as a hierarchical network 18
2.1.3 Molecular circadian clock 19
2.1.4 Circadian clock-mediated whole transcriptome 20
2.1.5 Circadian clock and posttranscriptional mechanisms 21
2.2 Significance of miRNAs 22
2.2.1 Basic structure and biogenesis of miRNAs 23
2.2.2 Nomenclature of miRNAs 25
2.2.3 MiRNA in normal biological processes 25
2.2.4 MiRNA in cancer 25
2.3 Breast Cancer 27
2.3.1 Breast biology 27
2.3.2 Breast cancer and circadian clock 28
2.3.3 Breast cancer and microRNAs 29

Materials and Methods 30

3.1 Human cell cultures 30
3.1.1 Human epithelial breast tumorigenic and non-tumorigenic cell lines 30
3.1.2 Cell culture procedures 31
3.1.3 Serum shock synchronization (Entrainment) 32
3.2 Cellular assays 34
3.2.1 Cytoplasmic/nuclear fractionation for use in miRNA expression 34
3.3 Molecular assays 35
3.3.1 Total RNA purification for mRNA expression 35
3.3.2 Total RNA isolation for miRNA expression 36
3.3.3 RNA precipitation for every RNA sample 37

3.3.4 Total RNA quantification 38
3.3.4.1 Quantification for mRNA expression 38
3.3.4.2 Quantification for miRNA expression 38
3.3.5 Assessment of RNA integrity 39
3.3.6 Primer design for expression assays 40
3.3.6.1 Primer design for mRNA expression 40
3.3.6.2 Primer design for miRNA expression 41
3.3.7 Synthesis of complementary DNA (cDNA) 43
3.3.7.1 cDNA for mRNA expression 43
3.3.7.2 cDNA for miRNA expression 43
3.3.8 Pre-amplification of cDNA for miRNA expression 44
3.3.9 Quantitative real-time polymerase chain reaction (qPCR) 45
3.3.9.1 Assessment of qPCR assay 45
3.3.9.2 Quantitative RT-qPCR for mRNA Expression 46
3.3.9.3 Quantitative RT-qPCR for miRNA Expression 47
3.3.10 Data analysis 47
3.3.10.1 Data analysis of mRNA Expression 48
3.3.10.2 Data analysis of miRNA Expression 48
3.3.11 DNA microarray assays 49
3.3.11.1 DNA microarrays overview 49
3.3.11.2 Microarray assays for miRNA expression – Sample preparation and labeling 50
3.3.11.3 Microarray assays for miRNA expression – Hybridization 51
3.3.11.4 Microarray assays for miRNA expression - Microarray wash 52
3.3.11.5 Microarray assays for miRNA expression - Scanning and Feature Extraction 52
3.3.12 Rhythmic expression analysis 53
3.3.12.1 Rhythmic expression analysis for microarray data 53
3.3.12.1 Rhythmic expression analysis for qPCR data 53
3.3.13 Identification of Targeted mRNAs and Pathway Analysis 54

Results and discussion 55

4.1 Entrainment of the circadian clock in human breast cell cultures 55
4.1.1 The Human breast clock 55
4.1.2 Optimization of gene expression protocol 56
4.1.2.1 Total RNA purification for microarray assays 56
4.1.2.2 RNA Integrity of samples for microarray assays 56
4.1.2.3 Total RNA concentration for RT-qPCR assays 58
4.1.2.4 Efficiency of primers. 58
4.1.3 Rhythmic expression of clock genes displayed in MCF-10A cell lines 59
4.1.4 Rhythmic expression of clock genes displayed on tumorigenic breast cell lines 61
4.1.4.1 Temporal expression of BMAL1 and PER2 genes in MCF-7 cells 62
4.1.4.2 Temporal expression of BMAL1 and PER2 genes in MDA-MB-231 cells 63
4.1.4.3 Temporal expression of BMAL1 and PER2 genes in ZR-7530 cells 64
4.1.4.4 Temporal expression of BMAL1 and PER2 genes in HCC-1954 cells 65
4.1.4.5 Temporal expression of SERPINB1 gene in MCF-7 cells 66
4.2 Rhythmic expression of miRNAs displayed in human breast cell lines 67
4.2.1 Microarray assays for miRNA expression 67
4.2.1 Statistical analysis of miRNA rhythmic profiles 67
4.2.2 Determination of miRNAs with rhythmic expression 72
4.2.3 Validation of rhythmic expression profiles using RT-qPCR 74
4.3 Identification of the Target mRNAs in a Group of miRNAs 81

Conclusions 82

Appendix A 85

Abbreviations and acronyms 85

Appendix B 86

mRNA expression performed in human breast cell lines 86

Appendix C 91

Circadian Features of miRNAs obtained from cosine-fitting function 91

Appendix D 104

Circadian Features of validated miRNAs obtained from MetaCycle 104

Appendix E 106

Pathways related to targeted genes of validated miRNAs 106

Published Papers 144

Curriculum Vitae 163

Chapter 1

Introduction

The circadian clock conducts the biological timekeeping of most species in cells by regulating physiological processes with a periodicity of 24-hours approximately [1]. In particular, extensive evidence shows that mammalian cells present synchrony between their external and internal environment, which is important for their well-being and survival [2], thus, lack of synchronicity might trigger physiological disorders, such as depression, diabetes, hypertension and cancer [3], [4].

Meanwhile, regarding molecular basis, the circadian system has been studied in diverse molecular levels, such as transcription, translation, protein-protein interaction and phosphorylation, which might participate in the biological orchestra of 24-hour environmental period [5], [6]. To date, the scientific community has revealed that circadian system has key actors, such as “clock” genes and their protein products which are settle to organize an auto-regulatory feedback system [7], [8], but the knowledge about how these processes interact with each other is yet unknown.

Recently, new insights about post-transcriptional regulatory events have been recognized as key factors of the circadian system [9]. The microRNAs (miRNAs) are a group that regulate the gene expression and subsequent protein translation [10], [11]. The link between circadian behavior and miRNAs, genes, and proteins is well studied. In 2006, a study in mice liver, it revealed that up to 20% of the soluble proteins show a circadian expression, whereas only about 10% of the genes show cyclic behavior, then both evidences suggest certain regulation by miRNAs [12]. In addition to the previous statement, it has also been reported that particular miRNAs have rhythmic patterns of expression through time periods in mice [13], [14], and rats cells [15], [16]. However, there are also evidences that circadian pattern expression of miRNAs might relate to breast cancer. During last decade, there has been an increasing amount of studies linking alterations of miRNA expression to breast cancer cells [17], [18]. However, in 2015, the concept turned around, a study revealed that circadian disruption induces changes of

miRNA levels in mammary tissues of rats with potentially malignant consequences [19]. All this evidence still needs to be validated, and more specifically, the determination of possible circadian pattern expression given by miRNAs in breast cancer cells.

Taken together, these findings suggest a biological relationship between the circadian system and miRNA expression. We aimed to explore miRNAs temporal expression in human breast cell lines. For this purpose, we initiated the study by establishment of cell culture, entrainment of breast cell lines and obtaining cell-samples at 4-hour intervals through 48 hours. Thus, miRNA temporal expression was evaluated in three human breast cell lines, MCF-10A, MCF-7, and MDA-MB-231 cells over a period of 28 hours. These results were used to determine rhythmic miRNAs patterns. Based on this analysis, six miRNAs were selected to confirm the rhythmic profile by RT-qPCR assays through 48 hours, this confirmation was tested in normal breast cell lines MCF-10A, and four breast cancer cell lines, MCF-7, MDA-MB-231, ZR-7530 and HCC-1954.

1.1 Motivation

Since 1960s, it has been reported that circadian rhythm disruptions might lead to an increased likelihood of mammary tumor development. This statement was due to the expression that some circadian genes are the key components in tumor progression [20]. In previous decades, studies have suggested those alterations in circadian rhythms are linked to huge molecular events [21], such as involved in genomics [22], transcriptomics [23], proteomics [24], metabolomics [25], microbiome [26], etc. However, the concept of rhythmic expression, as a possible behavior observed in those molecular events is still not well studied. Specifically, miRNAs, a group of molecules studied in the transcriptomics field, have insufficient evidence about possible rhythmic expression behavior among normal and cancer breast cell lines. This investigation might add some evidence about the connection of miRNA rhythmic expression in breast cancer.

1.2 Problem Statement and Context

The scientific advances regarding circadian rhythm in breast cancer is currently increasing day-to-day. However, there are still gaps due there are a lot of molecular intermediates or events, which make it harder to build a possible biological explanation for this matter. Thus, disruption of the circadian rhythm has been indicated as a risk factor for breast cancer in epidemiological studies [27], [28]. Additionally, some molecular evidences intent to explain the relationship between circadian clock and breast cancer [29], [30]. However, seen from another angle, there are molecular intermediates, such as miRNAs, on which their expression is also related to breast cancer [31], [32]. Although, all those evidences are increasing day-to-day, there is insufficient evidence about the connection of all these pieces in order to understand the true connection between circadian clock and miRNAs expression behavior in breast tumorigenic cells.

1.3 Research Question

Might miRNAs exhibit rhythmic expression in human non-tumorigenic and tumorigenic breast cell lines?

1.4 Solution overview

In this research, I designed a methodology to determine if miRNAs might show certain rhythmic patterns among breast cell lines. This research methodology has three phases:

A. Entrainment of human breast cell lines.
B. Determination of miRNAs with rhythmic pattern expression (period of 28 hours) by microarrays in three human breast cell lines, MCF-10A, MCF-7, and MDA-MB-231.
C. Validation the rhythmic expression of six microRNAs (period of 48 hours) by RT-qPCR in human breast cell lines, MCF-10A, MCF-7, MDA-MB-231, ZR-7530 and HCC-1954.

Chapter 2

Theoretical Framework

2.1 Biological clocks as central feature of life

Timing regarding physiology, behavior and cognitive processes in organisms from bacteria to mammalian is mainly orchestrated by a complex biochemical feedback system, which endogenously generate or promote certain rhythmic phenomena, called oscillations, termed circadian rhythms [33]–[35]. Biological timing systems function to anticipate and adapt an organism to events occurring within its environment [36], [37], such as increased efficiency of metabolic processes [38], circadian regulation of the cellular response to DNA damage [39] and possibly has a role in the cellular coordination of growth of malignant cells, cancer [40]–[43].

2.1.1 Circadian rhythm in living organisms - human

Almost all living organisms have evolved to co-ordinate their activities according the daily environmental cycles (light/darkness) caused by the rotation of earth around the sun. Biological processes that cycle in approximately 24-hour intervals (light/darkness) are called daily circadian rhythms [44]. In fact, the term ‘circadian’ is came from Latin words “circa” meaning around and “diem” or “dies” meaning day together translating to “approximately one day”.

The circadian rhythms are generated and sustained by the cell autonomous circadian clock system, which is a molecular machinery that drives and regulates a wide variety of physiological event, such as cyanobacteria cell division [45], fungal sporulation [46], plant growth and flowering time [47], and sleep/wake cycles in animals [48], [49]. Specifically, in humans, the circadian system is responsible for most physiological and behavioral functions across days and nights [50], see Figure 1, such as sleep-wake cycle [51], feeding behavior [52], core body temperature [53], hormone levels [54], blood pressure [55], metabolism [56], immune system [57], gut microbiome [58], etc.

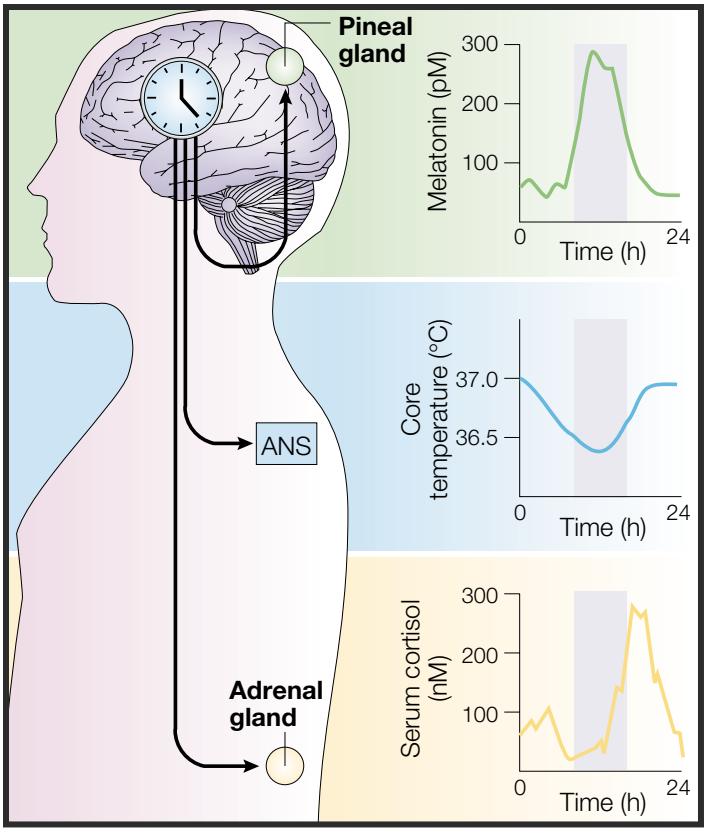

Figure 1. Physiological functions regulated by circadian system. This system core consists of hypothalamic pacemaker, which is located SCN and communicates through various neural and endocrine signals to drive diverse physiological levels. An individual progress through the regular 24-h cycle of sleep (grey shading) and wakefulness, thus, his metabolism is adjusted accordingly demands and opportunities of the solar day. Melatonin, core temperature and serum cortisol are well-known biological variables with circadian regulation. Image taken from [50].

2.1.2 Circadian rhythm as a hierarchical network

Circadian rhythms are regulated by an internal molecular timing system, circadian clock, which is an endogenous, self-sustaining network composed of three main components: input pathways, the central pacemaker and output pathways [59]–[61]. Nearly every mammalian cell type contains a circadian clock, giving rise to a multi-oscillator system *in vivo* [62], [63], see Figure 2. These oscillators can be divided into two classes: the central pacemaker and peripheral oscillators [50].

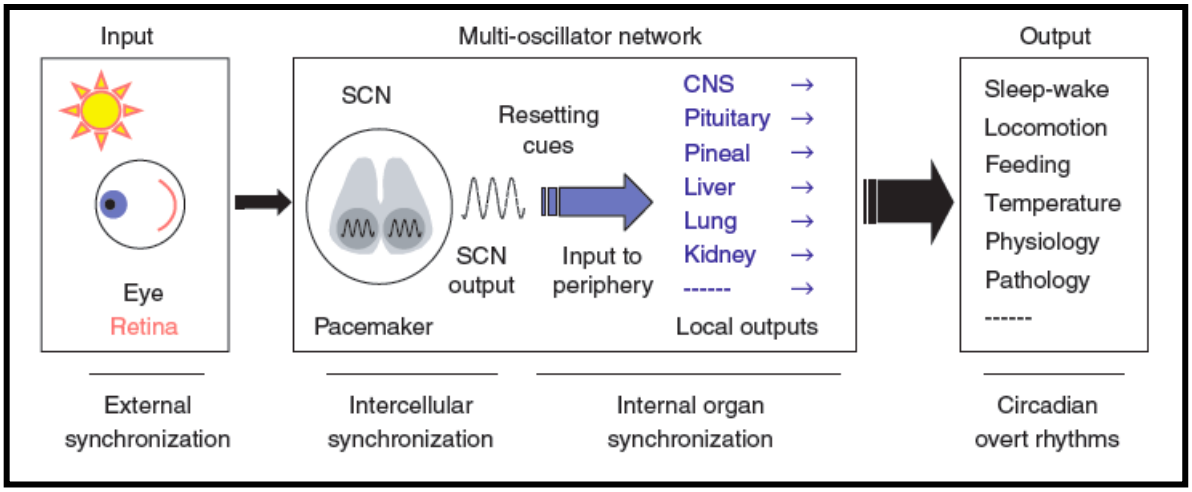

Figure 2. Architecture of mammalian circadian clock system. The circadian clock mainly consist of three components: the inputs, ~24-h clock and the outputs. The SCN is the central pacemaker at the top of the hierarchy, which is synchronized by the external 24-h cycle and in coordinates physiological outputs. Thus, whole clock machinery is important for robust operation of the entire body, regulating rhythms such as locomotion, body temperature and others. Image taken from [63].

In mammals, this pacemaker is located at suprachiasmatic nucleus (SCN) of the anterior hypothalamus, which is composed of approximately 20,000 neurons, each of which can produce coordinated circadian outputs that regulate the gene expression to promote circadian alteration in physiology and behavior [64].

On the other hand, the peripheral oscillators are a cell-autonomous clock systems found in peripheral organs or tissues, such as the heart, liver, lung and skeletal muscle. The peripheral clocks are synchronized differently than the SCN as they do not receive direct light input [50]. Instead, they respond to other stimuli, such as feeding, hormones, or metabolites, which have yet to be fully characterized as well as the mechanisms by which these clocks communicate with one another [50], [65].

2.1.3 Molecular circadian clock

The circadian rhythms of every mammalian cell from SCN or peripheral tissues are regulated by their own internal molecular timing system, circadian clock, which is an endogenous, self-sustaining network composed of three interlocking transcription-

translation feedback loops (TTFL) [66]. Each of these loops is defined by its components act: the E-box, RRE, and D-box loop.

The E-box loop is also called core loop and is needed for cycling on clock system. It contains transcription factors, such as bmal1 (official name: arntl) and clock, which dimerize and activate transcription of target genes through E-boxes (CACGTG), the Period genes (*PER1, PER2, PER3*) and Cryptochrome genes (*CRY1, CRY2*). Particularly, per and cry proteins dimerize and repress the transcription of *BMAL1* and *CLOCK* genes [59], [67], [68]. Subsequently, the RRE and D-box loop are actor, which are interlocked with core loop, and at date, they are considered to play important roles in phase resetting (conferring input to synchronize clock to the external environment), stabilizing the core loop, and in regulating some clock outputs (See Figure 3). The RRE consists of ROR transcriptional activators (RORa, RORb, RORc) and REV-ERB transcriptional repressors (REV-ERBα, REV-ERBβ) [59], [67].

Briefly, BMAL1/CLOCK complex activates the transcription of *ROR* and *REV-ERB* genes through E-boxes on their promoter sequences. Specifically, RORs and REV-ERBs competitively bind to RRE sequence ([A/T]A[A/T]NT[A/G]GGTCA), allowing them to feedback on the core loop through the RRE in the bmal1 and clock promoters. The D-box loop consists of the transcription activator DBP and the repressor E4BP4 (official name: NFIL3). BMAL1/CLOCK activates transcription of *DBP* gene; while *E4BP4* transcription is controlled by an RRE in its promoter. DBP and E4BP4 act as transcription activator and repressor, respectively, through binding to D-boxes (TTA[T/C]GTAA) in target genes, including the *PER* genes [59], [67].

2.1.4 Circadian clock-mediated whole transcriptome

These circadian components above orchestrate a robust 24-h timekeeper that drives oscillations in output gene expression [69]. In fact, approximately 10% of the genome exhibits circadian cycles in any tissue, but in a tissue-specific manner, such as liver, heart, kidney, lung, etc. [70]–[73]. The respective roles of the central pacemaker

and peripheral clocks observed in certain transcripts of transcriptome entails several physiology and behavior changes that remain unknown [74].

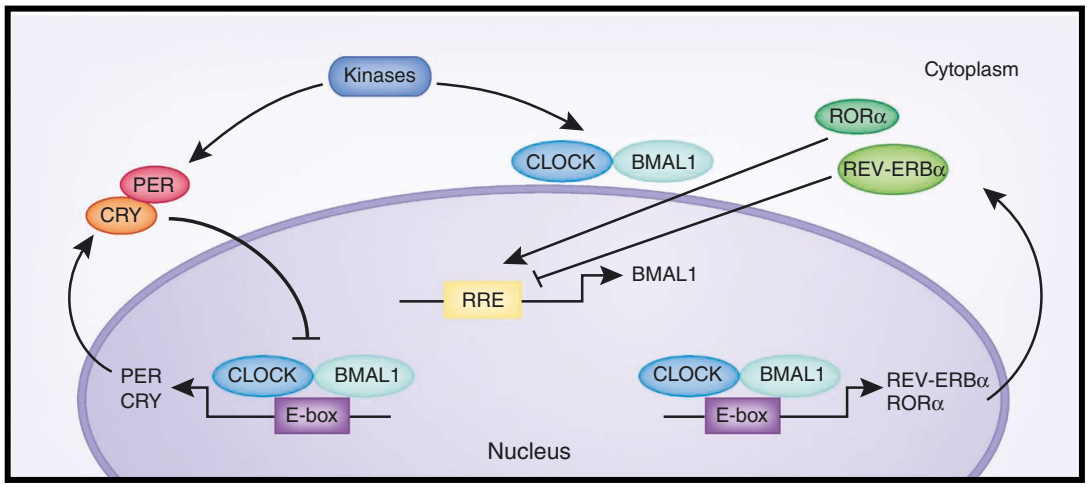

Figure 3. Clock molecular network. The E-box mediated the negative feedback of per and cry proteins towards transcriptional complex CLOCK/BMAL1. Additionally, recent investigations also suggest negative feedback loop with the nuclear receptors *Rev-erb-α* and *Rev-erb-β* through RORE enhancers, due they might generate self-sustained oscillations.

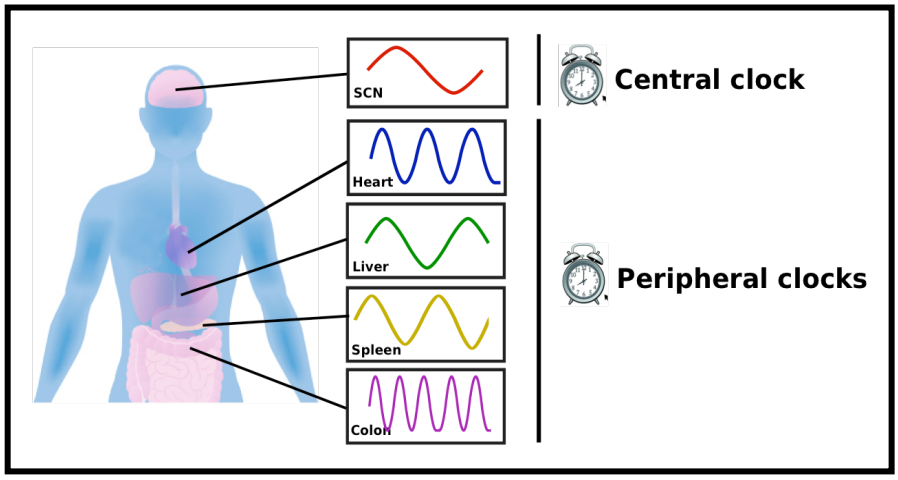

Figure 4. The circadian expression in central and peripheral clocks. The SCN promote electrical and humoral signals to synchronize phases of local circadian clocks oscillations, which is dependent of peripheral organ.

2.1.5 Circadian clock and posttranscriptional mechanisms

According to how circadian rhythm has been discussed till now, it is a fundamental

system in diverse organisms, and it is composed of transcripts and proteins that are interacting in a cell-autonomous transcriptional feedback loop. Interestingly, if these components are stimulated, repressed or affected, then they can dramatically alter the circadian clock system [75], [76]. To date, there has been reported several post-transcriptional mechanisms and components that could interact with circadian clock and adjust the timing of the clock (approximately 24 h) for further implications in health and disease [77].

One of the hallmarks regarding transcriptional feedback loop is the daily oscillation of clock-related RNA and proteins [78]. To sustain such oscillations, some posttranscriptional modifications are needed to avoid the generation of a steady state [5]. Hence, diverse events in gene expression, including RNA events, such as RNA processing, RNA export, RNA decay, and RNA translation are required for controlling circadian clock system. Thus, when transcription is initiated, one of the first events that occur in the nucleus is the addition of a “cap” structure by the heterodimeric cap-binding complex.

Subsequently, the intronic sequences are removed, a process called splicing, and the polyadenylation complex cleaves and adds a poly(A) tail to the 3’ end of the transcript (Fig. 1). All these processes are interlinked by affecting downstream events, such as RNA export and translation.

It is well-known that daily oscillations of RNA and/or proteins are a central feature of circadian clock system. Cycling mRNAs are generally considered to be under transcriptional regulation. Nevertheless, rhythmic synthesis would require an oscillating mRNA with a certain short half-life, and/or the oscillating mRNA could be regulated post-transcriptionally. Thus, stable RNA expression throughout the circadian cycle could damp or abolish the amplitude of the oscillation expression.

2.2 Significance of miRNAs

The miRNAs are a large family of small non-coding RNAs (~22 nucleotides approximately) that are responsible of gene expression by for post-transcriptional

regulation [79]. The regulation of the expression of target genes occurs through imperfect base pairing of the 3' untranslated region (3' UTR) of messenger RNAs (mRNAs) thereby dampening mRNA expression [11].

The miRNAs can be found encoded in intergenic regions, exons or introns. In humans, around half of all known miRNAs are expressed from non-protein-coding transcripts [80]. Considering that more than 1,000 individual miRNAs have been identified in humans [81], then an individual miRNA might target one to thousands of different mRNAs, and this mRNA can be coordinately inhibited by different miRNAs, the miRNA biogenesis pathway therefore has a key role in gene regulatory networks [10].

2.2.1 Basic structure and biogenesis of miRNAs

The miRNA biogenesis is an evolutionary conserved mechanism among species. Approximately 30% of miRNAs are processed since introns of coding genes, and other group of miRNAs are expressed from dedicated miRNA gene loci [82]. In the nucleus, the first stage in miRNA biogenesis (illustrated in Figure. 5) is the transcription by RNA polymerase II (Pol II), resulting in the primary form (pri-miRNA), which includes a 5' cap and a 3' poly-A tail [10]. An individual pri-miRNA can produce a single miRNA or clusters of two or more miRNAs that will be processed from a common primary transcript [82]. Each pri-miRNA has a secondary structure, a hairpin, which contains the sequence of a mature miRNA [83]. These hairpins are recognized by the enzyme-complex referred as microprocessor where the RNase III type endonuclease, called Drosha is a key component [84]. Drosha introduces a cut in the stem of the hairpin within the pri-miRNA that releases a shorter hairpin (with the stem ≈ 33 nt), called the precursor-miRNA (pre-miRNA) [84]. Afterwards, the pre-miRNA is exported out of the nucleus into the cytoplasm, assisted by Exportin 5 complex, which uses Ran-GTP and only binds strongly to correctly processed pre-miRNAs [85].

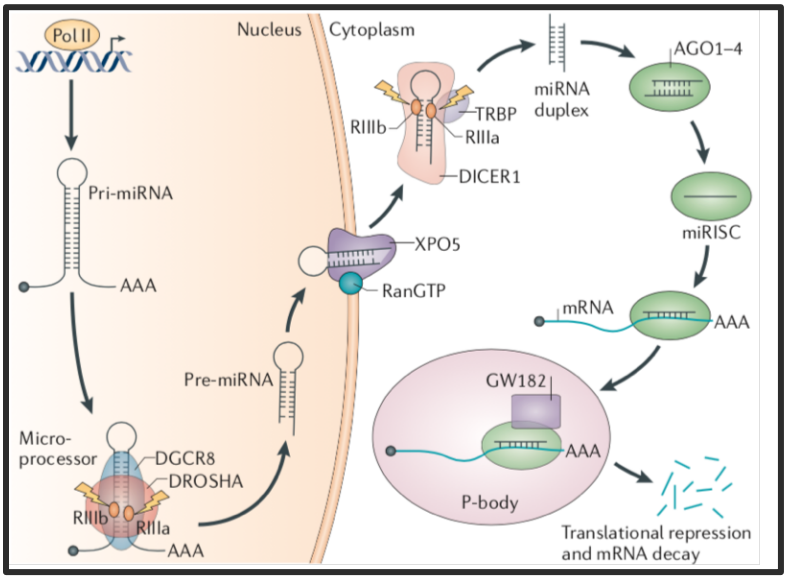

Figure 5. Overview of miRNA biogenesis pathway. The miRNAs are initially transcribed as primary as pri-miRNAs by Pol II in the nucleus. Thus, these are cleaved by microprocessor to produce pre-miRNAs, which are then exported from nucleus to cytoplasm. Image taken from [82].

In the cytosol, a final processing step, it is required to produce mature miRNAs. It is carried out by another RNAse III nuclease, DICER1, which cuts out the loop in the pre-miRNA to its ~22 bp, double stranded form, known as the miRNA duplex [86]. This cut process is assisted by TRBP (transactivation-responsive RNA-binding protein) [84]. Additionally, TRBP links DICER1 with argonaute proteins (ago1, ago2, ago3 or ago4) to participate in miRNA-induced silencing complex (miRISC) [87]. Thus, one strand of the mature miRNA linked to argonaute protein and retained in the miRISC complex, which guide together with GW182 family to complementary target mRNAs for post-transcriptional gene repressing [88]. This last molecular event occurs in the processing bodies (P-bodies), which are cytoplasmic ribonucleoprotein (RNP) granules primarily composed of repressed mRNAs and proteins related to mRNA decay [89].

In the last decade, post-transcriptional regulation of miRNA expression is a matter that has begun to receive more attention, because there is certain evidence that every step of the miRNA biogenesis is subject to regulation and might considerably change the path of miRNA expression [83].

2.2.2 Nomenclature of miRNAs

The first miRNA identified have been shown a possibly regulatory role in *Caenorhabditis elegans* in 2001 [90]. Afterward, other miRNAs were discovered in plants [91]. Discovery of these small RNAs revolutionized our understanding regarding regulation of gene expression, thus, miRNAs became a major focus of many worldwide research groups.

Numerous investigations carried out a rapid accumulation of a vast number of new miRNAs, thus a central registry and repository database, 'microRNA Registry' (miRBase) was first established in 2002 [92], [93].

2.2.3 MiRNA in normal biological processes

The miRNAs are potent regulators of gene expression and have been known to participate in key roles of normal development. Many studies have shown miRNAs featuring in normal muscle development, embryonic development and lymphocyte differentiation [54]. However, in relation to normal breast physiology, little research has been carried out. One study showed that 7 groups of miRNAs are associated with distinct phases of the breast development when examined in juvenile and adult mouse mammary glands [55]. Research such as this is critical, as an understanding of normal miRNA function will allow scientists to understand how aberrant miRNA function influences carcinogenesis.

2.2.4 MiRNA in cancer

Cancer development involves multiple-step alterations in oncogenes and tumour suppressor genes through a period of time. Abundant data have already been published in regards to how important the role of miRNAs is among many pathways involved in the pathogenesis of cancer. In 2002, a report provided the first evidence about the connection between microRNAs and cancer, this research showed miR-15 and miR-16 located at a

genomic region frequently silenced in chronic lymphocytic leukemia [94]. Since this evidence, numerous researchers started to investigate diverse angles regarding this biological connection [95], one of them, the levels of expression of several microRNAs in a wide range of human cancers [96], [97]. Furthermore, there are scientific evidences where miRNAs showed tissue-specific expression signatures and promoted or suppressed tumour development and progression, thereby influencing all the hallmarks of cancer postulated by Hanahan and Weinberg [98].

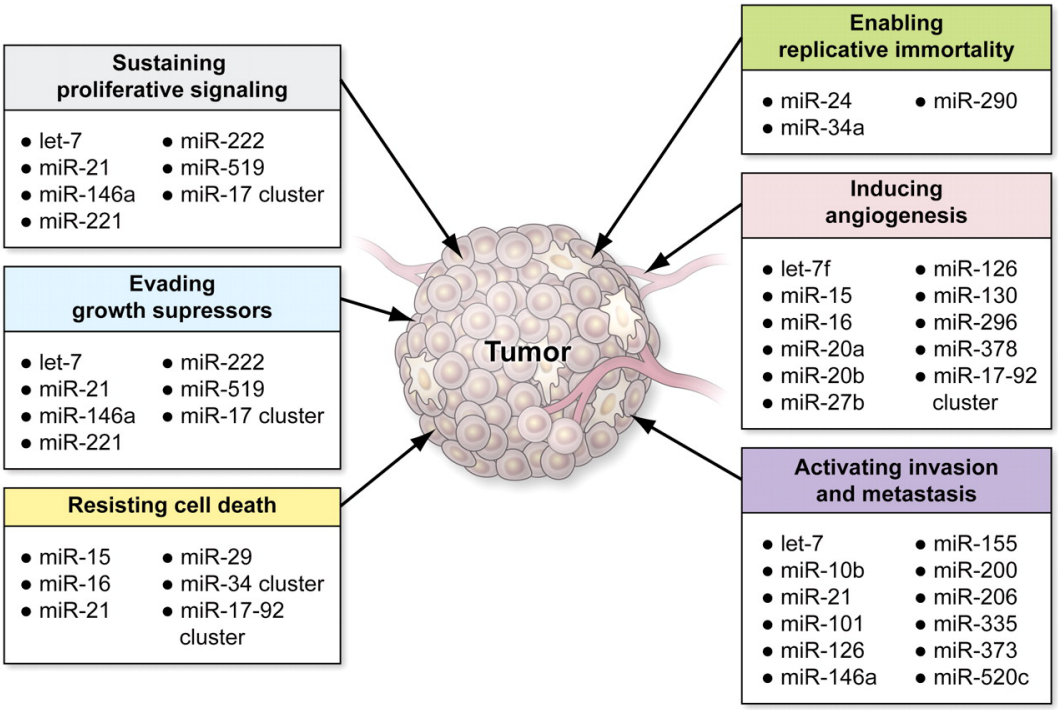

Figure 6 The miRNA involvement in hallmarks of cancer. Abnormal miRNA expression affects signaling pathways at diverse physiological levels to enhance tumorigenesis. This image depict representative miRNAs that have been studied to act as oncogenes or tumor suppressor. Image taken from [99]

The miRNAs can function as oncogenes or tumour suppressors in the majority of cancers. Tumour suppressor miRNAs are usually down-regulated in cancer and the majority of the miRNAs are considered tumour suppressors [100]. Oncogenic miRNAs, also known as oncomiRs, tend to up-regulate oncogenes or suppress tumour suppressor genes [101]. However, few miRNAs have been already described as truly tumour suppressors, with functional data published. Curiously, some miRNAs can act as both suppressors and oncogenes, depending on the microenvironment [102].

2.3 Breast Cancer

Breast cancer is one the most frequent cancer types among women around the world [103]. Despite the huge scientific progression in breast cancer investigation, much is still needed to better understand this heterogeneous disease. In the past years, the incidence of breast cancer has been increasing due to improved life expectancy and lifestyle choices such as birth control pills, smoking, alcohol consumption, and urbanization [104]. Thus, there are intrinsic factors conditioning the occurrence of breast cancer is the familial susceptibility. Several studies have identified genes whose function is associated with an increased risk of occurrence of malignant breast cancer. The most important genes, *BRCA1* and *BRCA2* (breast cancer susceptibility 1 and 2) are known as tumor suppressor genes in a cell [105]. However, last years, there are evidences that miRNAs have some biological participation on breast cancer initiation, progression and survival [106].

2.3.1 Breast biology

Breast tissue is mainly composed of lobes (lobules), ducts (hollow tubes) and stroma. Each lobule contains a network of milk producing glands, each terminating into the papilla (nipple) via small ducts lined with myoepithelial cells [107]. The milk ducts and lobules lie within adipocytes and connective tissue as shown in Figure 7 [108]. Around 80% of breast cancers occur in the ductal region, while the remaining 20% seem to originate in the lobules.

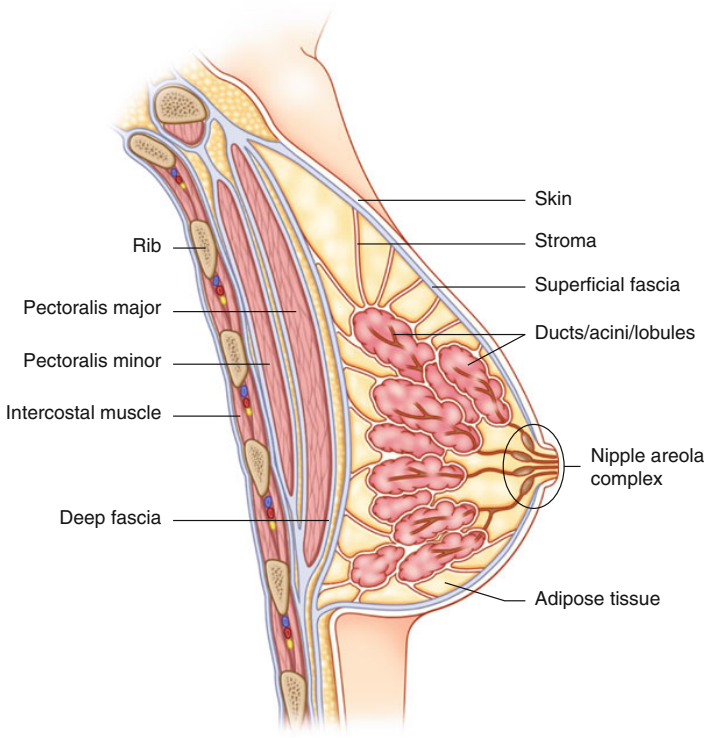

Figure 7 Components of the breast. Image taken from [108]

Despite the huge scientific progression in breast cancer investigation, much is still needed to better understand this heterogeneous disease, but it is generally thought this malignancy is involved in a complex interaction of endogenous and factors by affecting multiple genetic changes in cells.

2.3.2 Breast cancer and circadian clock

Breast tissue consists of a network of branched epithelial ducts surrounded by a basement membrane, which is almost covered with fibroblast-rich and adipose-rich stromal extracellular matrix [109]. Clock expression have been discovered within breast epithelium mice [110]. Particularly, mutations of specific circadian genes disrupt behavioral and molecular rhythms in mice [111], [112]. Additionally, such mutations also reveal that cellular clocks participates in the carcinogenesis development. Altered functioning of clock-controlled circadian genes has been found to be involved in the process of carcinogenesis [113]–[115].

In the past decades, there have been a some reports whose showed differences in expression of circadian genes in breast tumor cells as compared to normal cells [116], [117].

2.3.3 Breast cancer and microRNAs

Research that is more recent has demonstrated the importance of miRNAs in breast cancer biology. Past decades, miRNAs have been extensively associated with breast cancer. The use of genome-wide approaches has enabled the production of miRNAs fingerprints in tumors and in its normal counterpart. As a result, miRNA expression patterns allow to discriminate with high accuracy, and the tissue of origin of poorly differentiated tumors to be identified [118]. Indeed, several miRNAs have been associated with different subtypes of breast cancer, such as luminal, HER2, basal-like and normal-like [119]. Particularly, ER+ and HER2 have been shown to be targeted and regulated by miRNAs, and in turn, the ER+ growth pathway has been shown to regulate some miRNAs [120]. Thus, pathological status of breast cancer is key factor in the regulation and behavior of miRNAs.

Chapter 3

Materials and Methods

3.1 Human cell cultures

3.1.1 Human epithelial breast tumorigenic and non-tumorigenic cell lines

The biological complexity of breast cancer has been studied by multiple gene expression studies whose proposed a stratification of breast tumors in four subtypes, such as luminal A, luminal B, HER2 over-expressing and basal-like [121]–[124]. These molecular subtypes were largely studied in contrast with traditional classification of breast tumors [125], based on the status of estrogen receptor (ER), progesterone receptor (PR), and human epidermal growth factor receptor-like 2 (HER2/neu). Furthermore, this stratification was also studied in breast cell lines, which most researchers used to start novel hypotheses. This research has begun the determination of expression changes of miRNAs by entrained tumorigenic and non-tumorigenic breast cell lines.

Non-tumorigenic cell line, MCF-10A cells have not expression of ER, PR and HER2/neu markers like basal subtype, but has a fibrocystic origin and is considered a non-tumorigenic cell line [126]. There are tumorigenic cell lines, such as MCF-7 (ER^+ and/or, PR^+ and $HER2/neu^-$) and ZR-7530 (ER^+ and/or, PR^+ and HER2/neu), which are considered as luminal subtype due status of ER positive, as well as those cell lines have expression of markers of the luminal epithelial layer of normal breast ducts cells. In addition, HCC-1954 cells (ER^-, PR^-, $HER2/neu^+$) are well known for overexpression of HER2/neu and adjacent genes on chromosome 17q12 [127], [128]. Finally, MDA-MB-231 cells (ER^-, PR^- and $HER2/neu^-$) are characterized for negative expression of the three markers, which are consistent with basal-like tumors, TNBC and also associated with an unfavorable outcome [127], [128]. The features of the above-described cell lines used in this research work are summarized in Table 1.0.

Table 1. Characteristics of the human breast cell lines used in this study

Cell line	Phenotype	Tumorigenic	Age / Ethnicity	Source	Disease
MCF-10A	Normal	No	36/C	SM	Fibrocystic disease
MCF-7	Luminal A	Yes	69/C	PE	Metastasic adenocarcinoma
MDA-MB-231	Basal-like	Yes	51/C	PE	Metastasic adenocarcinoma
ZR-7530	Luminal B	Yes	47/B	MAF	Ductal carcinoma
HCC-1954	HER2/neu	Yes	61/EI	PT	Ductal carcinoma grade III

Abbreviations: C, Caucasian; B, Black; EI, East Indian; SM, Subcutaneous Mastectomy; PE, Pleural Effusion; MAF, Malignant Ascitic fluid; PT, Primary Tumor.

The human breast cell lines, MCF-10A (ATCC® CRL-10317™), MCF-7 (ATCC® HTB-22™) and HCC-1954 (ATCC® CRL-2338™) were purchased from the American Type Culture Collection (ATCC®, Rockville, MD, USA). Meanwhile, MDA-MB-231 and ZR-75-30 cell lines were obtained from Dr. Nadia Jacobo Herrera from Instituto Nacional de Ciencias Médicas y Nutrición "Salvador Zubirán" in Mexico City.

3.1.2 Cell culture procedures

Breast cell lines were maintained in culture flasks of 25-cm^2 or 75-cm^2 (Corning Inc., Corning, NY, USA), containing among 8-10mL and 20-25mL of culture medium, respectively. Cell lines were subcultured after every 48 to 72 hours by adding 0.25% [w/v] Trypsin/EDTA (Biowest, Mountain View, CA, USA), specifically, 1.0 mL for cultures in T25cm^2 and 4.0 mL for cultures in T75cm^2 flask. This enzymatic process, trypsinization made to dissociate adherent cells from the vessel in which cells are being cultured. Afterwards, the cells were collected from flasks and placed in tubes of 50mL for washing (3ml per T25-cm^2 and 10ml per 75-cm^2) with Gibco PBS buffer (Thermo Fisher Scientific, Grand Island, NY, USA) by centrifugation at 400x*g* for 5 minutes at room temperature. All subcultures were propagated in an incubator at 37°C under an atmosphere of 5.0% CO_2 and 95.0% air. The above procedures were performed to achieve near 100% confluence in cultured cells, which will be ready for serum synchronization (entrainment). Additionally,

mediums and solutions were warmed at 37°C in a water bath previously. All cultured cells were handled with aseptic techniques.

MCF-10A cells were grown in Mammary Epithelial Basal Medium® supplemented with SingleQuots® from the MEGM® BulletKit® (Lonza, Walkersville, MD, USA). The first medium changing occurred after 24h, while the complete medium was changed every three days.

ZR-75-30 and HCC-1954 cells were grown in Gibco® Roswell Park Memorial Institute (RPMI)-1640 medium (Thermo Fisher Scientific, Grand Island, NY, USA) supplemented with 10% and 15% heat-inactivated Gibco® Fetal Bovine Serum (FBS) (Thermo Fisher Scientific, Grand Island, NY, USA), respectively. Meanwhile, MCF-7 and MDA-MB-231 cells were grown in Gibco® Dulbecco's Modified Eagle Medium, which features a nutrient mixture of D-MEM and F-12 (Thermo Fisher Scientific, Grand Island, NY, USA), supplemented with 10% heat-inactivated FBS. Each culture medium was supplemented with Gibco® Penicillin-Streptomycin antibiotics (Thermo Fisher Scientific, Grand Island, NY, USA).

3.1.3 Serum shock synchronization (Entrainment)

In 1998, first evidence, Balsalobre *et al.*, described the serum shock protocol [129]. However, current protocol of serum shock was modified according to Rossetti and collaborators in 2012 [130]. This protocol was strictly performed across all breast cell lines without modifications. Below is listed each procedure (see Figure 8):

- Cultured-cells contained in 75-cm^2 flasks were seeded and maintained in 6-well plates with basal medium plus 10% of bovine serum.
- The basal medium is removed from 6-well plates, and then cells were washed twice with PBS buffer (Thermo Fisher Scientific, Grand Island, NY, USA) to remove residual growth factors. For MCF-10A, ZR-75-30, and HCC-1954, the basal medium was RPMI-1640, while for MCF-7 and MDA-MB- 231 was D-MEM/F-12.

- The above procedure was performed till achieving 500,000 cells approximately by each well (greater 95% of confluence), and then the entrainment procedure is properly ready to be performed.
- Add free-serum basal medium on cultured-cells.
- Leave cultured-cells starving overnight (12-16h).
- After starving, the basal medium was removed and discarded from cultured-cells, and then were serum shocked with growth basal medium supplemented with 50% horse serum (Biowest, Mountain View, CA, USA) and incubated for 2 hours at 37°C, 5% CO_2.
- After serum shocked, horse serum was removed and cultured-cells were washed with PBS and new free-serum basal medium was poured into each well. The 6-well plates were placed back into incubator at 37°C, 5% CO_2.
- The first time point was taken at the moment of serum shock (t = 0), while the rest of cells were harvested every 4 hours till a period of 48 hours, completing 13 time-points.
- Each time-sample was collected separately by duplicate for mRNA expression (except, triplicate from MCF-7), while by triplicate (two wells from 6-well plate were merged to build one replicate) for miRNA expression.
- The collected samples for mRNA expression were homogenized directly in the plate using TRI Reagent® solution (see Section 3.3.1 for further details).
- The collected samples for miRNA expression were first processed by cytoplasmic/nuclear fractionation protocol (see Section 3.2.1 for further details).

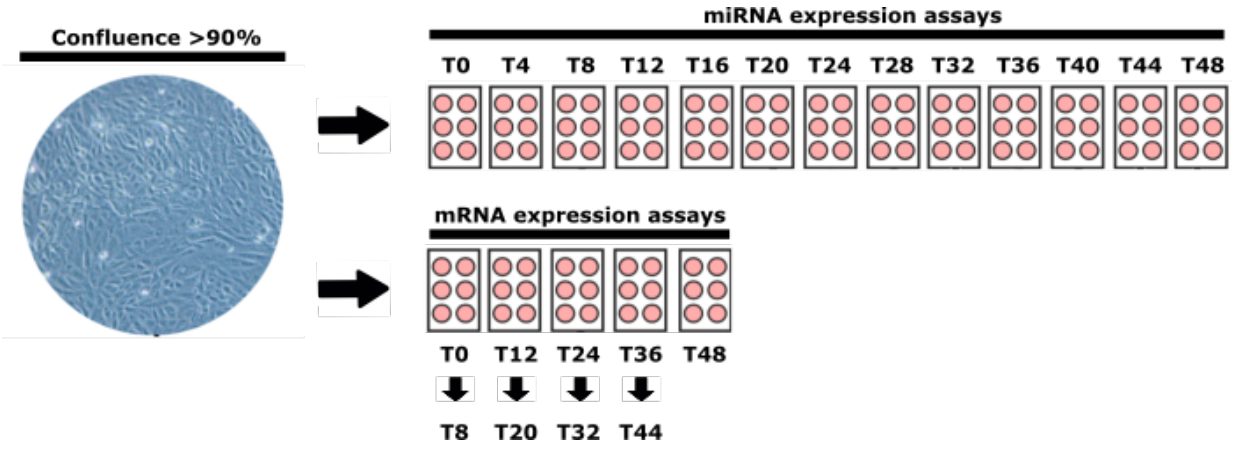

Figure 8. Establishment of cell culture to entrainment of cell lines. The entrainment initiates when cultured cells have a confluence greater of 90%. Thus, the batch is split on 2 batches for mRNA and miRNA expression. Particularly, miRNA expression required thirteen 6-well plates (triplicates, each one consist of 2 wells) for covering 48h period. The mRNA expression required five 6-well plates (duplicates) for covering 48h period. Except miRNA expression in MCF-7 was done by triplicate.

3.2 Cellular assays

3.2.1 Cytoplasmic/nuclear fractionation for use in miRNA expression

The isolation of cytoplasmic and nuclear fractions were done in order to evaluate the level expression of miRNAs separately, because there is evidence that miRNAs might have different expression patterns between cell compartments [131]–[134].

The Nuclear/Cytosol Extraction kit (BioVision, Mountain View, CA, USA) was used for cell fractionation, separation of nuclear fraction from the cytoplasmic fraction of mammalian cells according to manufacturer´s instructions. The protocol started with collection of cultured cells (described previously) where cells were pelleted and washed twice with 10 mL PBS, followed by centrifugation for 5 min at 600 x g at 4°C. Next procedure consists properly the isolation of cytoplasmic fraction, cells were resuspended in 200µL cytosol extraction buffer A (CEB-A) containing 1x protease inhibitor cocktail and 1mM dithiothreitol (DTT), vortexed for 15 seconds and incubated on ice for 10 min. Next, add 11 µL of cytosol extraction buffer B (CEB-B) to the cells followed of vortexing and incubation on ice for 1 min. Next, cells were vortexed quickly before being centrifuged at

16,000 x g for 5 minutes in a 4˚C microcentrifuge. Finally, the supernatant (cytoplasmic fraction) was removed and place onto sterile tube and stored at -80°C.

The next procedure consists of properly isolate the nuclear fraction. The pellet (nuclear fraction) was resuspended in 100 µL of ice-cold Nuclear Extraction Buffer Mix, vortexed on highest setting for 15 sec and returned the tubes to ice. Repeat this previous step for every 10 min for a total 40 min. Next, the tubes were centrifuged for 10 min at 16,000 x g, immediately transfer the supernatant (nuclear fraction) to sterile 1 mL tubes and place them on ice. The fractions were stored at -80°C till further processing.

3.3 Molecular assays

3.3.1 Total RNA purification for mRNA expression

Total RNA was isolated by using TRI Reagent® (Sigma-Aldrich, St. Louis, MO, USA) following the manufacturer's instructions. Trizol reagent is the most well-known phenol/chloroform-based method for isolating ordinary RNA and small RNAs [135].

The cultured-cells were homogenized directly in each 6-well plate, after removing culture medium, in 1mL of TRI Reagent®, a monophasic solution containing phenol and guanidine thiocyanate, which rapidly lyses cells and inactivates nucleases. Homogenates were placed in tubes of 1.5mL and incubated for 5 minutes at room temperature to allow nucleoprotein complexes to completely dissociate. Finally, tubes contained homogenates were stored at –70°C for further isolation.

Once all samples were collected through 48 hours, then tubes were incubated for 10 minutes at room temperature, then tubes were centrifuged at 13,000x*g* for 5 minutes at 4°C in order to remove insoluble material from homogenates. Afterwards, 100µL of 1-bromo-6-chloropropane (BCP; Sigma-Aldrich, St. Louis, MO, USA) was added to the tubes, then they were immediately mixed by vortexing at maximum speed for 15 seconds, incubated for 5 minutes at room temperature, and centrifuged at 13,000x*g* for 5 minutes at 4°C in order to separate the mixture into 3 phases for further RNA isolation.

The above steps allowed having 3 phases, an organic phase (phenol-BCP phase) placed on the bottom of tube, an interphase, and upper aqueous phase. The aqueous phase contains the RNA material, while DNA and proteins are immerse in interphase and organic phases. Thus, 400µL of the upper phase was taken off from tubes and placed in new 1.5mL tubes, then they were washed with 500µL of 75% molecular biology grade ethanol (Sigma-Aldrich, St. Louis, MO, USA) and centrifuged for 5 minute at 13,000x*g* at room temperature, by three times in order to efficiently remove away all contaminants.

After washes, the RNA was concentrated in the bottom of the tube in an aqueous pellet, then pellets were dried by leaving tubes with caps open on incubator at 43ºC. Next, pellets were resuspended in 50 uL prewarmed nuclease-free water. Finally, RNA samples were stored at –70°C till further process.

3.3.2 Total RNA isolation for miRNA expression

Total RNA, including small RNA enrichment was isolated by using MIRVANA miRNA Ambion® Kit (Thermo Fisher Scientific, NY, USA) based manufacturer's instructions [136]. The nuclear and cytoplasmic fractions are 2 types of samples, which were performed simultaneously with the same protocol for small RNA enrichment isolation.

The 100 uL of fractions were placed in 1.5 mL tubes and homogenized in 500 uL of Lysis/Binding Solution to prepare the mixture for enrichment process. Next, 60 uL of miRNA Homogenate Additive were added to homogenates and incubate them for 10 min on ice. Next, 600 uL of Acid-Phenol:Chloroform were added and immediately vortexed for 1 min, then centrifuged at 10,000xg for 5 min at room temperature to separate the aqueous and organic phases. Finally, recover the aqueous upper phase and transfer it to a 1,5 mL new tube for further small RNA enrichment isolation.

Add 1.25 volumes of 100% ethanol at room temperature to the aqueous phase previously collected. Next, place mixture up to 700 µL onto the filter cartridge. For samples larger than this, apply the mixture in successive applications to the same filter cartridge and centrifuge for 15 seconds at 10,000 x g to pass the mixture through the filter cartridge. Then, discard the flow-through, and repeat till all the mixture is through the filter cartridge. Next, wash the filter cartridge with 700 µL miRNA Wash Solution 1, then wash the Filter Cartridge twice with 500 µL Wash Solution 2/3, and elute small RNA enrichment with 100 µL 95°C nuclease-free water. Finally, RNA samples obtained from cytoplasm (cyRNA) and nuclear (nuRNA) fractions were stored at –70°C till further processing.

3.3.3 RNA precipitation for every RNA sample

The RNA precipitation is a procedure to concentrate and desalt RNA samples with higher concentration of salts or any other contaminants [137]. After precipitation, recovered RNA samples were suitable for using in downstream applications, including cDNA synthesis, real-time PCR, and microarrays. The procedure based on ethanol precipitation was identically applied to RNA samples from cultured-cells (3.3.1) and cellular fractions (3.3.2).

All RNA samples were thawed on ice. RNA samples were combined with 3M sodium acetate at pH 5.2 (Sigma-Aldrich, St. Louis, MO, USA) in a proportion 1:10 and 2.5 volumes of ice-cold 100% molecular biology grade ethanol (Sigma-Aldrich, St. Louis, MO, USA), then the mixture was mixed by moderate vortexing. Next, the mixture was incubated for 30 minutes at -70°C and centrifuged for 30 minutes at 13,500 × g at 4ºC. The supernatant was carefully aspirated to avoid losing the RNA pellet. Next,

The pellet was washed with 1mL of 70% ethanol ice-cold centrifuged for 5 minutes at 15,000 × g at 4ºC, and the supernatant was removed. This washing process was repeated 3 times. Next, after washes, the RNA was concentrated in the bottom of the tube in an pellet, then pellets were dried by leaving tubes with caps open on incubator at

65ºC. Next, pellets were resuspended in 50 uL prewarmed nuclease-free water. Finally, RNA samples were stored at –70°C till further process.

3.3.4 Total RNA quantification

3.3.4.1 Quantification for mRNA expression

Total purified RNA samples were quantified individually using the Take3 Micro-Volume plate (BioTek Instruments Inc., Winooski, VT, USA) and SynergyTM HT Multi-Mode Microplate Reader (BioTek Instruments Inc., Winooski, VT, USA) by measuring its absorbance at 260nm (A260). Take3 Micro-Volume plate allowed the quantification of up to sixteen samples with a nominal pathlength of 0.5mm for microvolume analysis. The procedure started dispensing 2 µL of each sample onto the Take3 Micro-Volume plate to measure the absorbance and calculate the ratios. The spectrophotometer was blanked with nuclease-free molecular water.

Measuring ratios of absorbance at 260 and 230 or 280nm allowed assessing the purity of RNA samples. The total RNA isolated has an A260/A280 ratio of 1.8–2.1 and an A260/A230 ratio of 1.7-2.2.

3.3.4.2 Quantification for miRNA expression

The cyRNA and nuRNA samples were quantified individually using the NanoDrop equipment (Thermo Scientific, NY, USA), because NanoDrop spectrophotometer is well-known to display low level of variation between measurements [138]. Prior to measurement, the NanoDrop was blanked with 2 µL of the same nuclease-free water that RNA was eluted in previously. The procedure started dispensing 1 µL of each sample onto the pedestal and absorbance measured. The NanoDrop software calculates total RNA concentration value based on the absorbance values obtained. Each sample was quantified by twice and averaged for further procedures.

Measuring ratios of absorbance at 260 and 230 or 280nm allowed assessing the purity of RNA samples. The isolated RNA samples should be fit on following ranges A260/A280 ratio of 1.8 – 2.1 and an A260/A230 ratio of 1.7 - 2.2.

3.3.5 Assessment of RNA integrity

Integrity of RNA is a very critical key in downstream RNA based quantitative analysis, because low-quality RNA can compromise the results of such experiments [139]. The integrity of cyRNA and nuRNA samples was assessed by Experion automated electrophoresis system (Bio-Rad Laboratories, Hercules, CA, USA). The Experion system included automated electrophoresis station, priming station, vortex station for RNA analysis, and Experion^{TM} RNA HighSens Analysis kit, which included chips and reagents for assessment of RNA. The procedures were performed according to the manufacturer's instructions.

Initially, limiting any contamination during RNA integrity analysis, electrodes of the Experion system were cleaned by 800 uL of Experion electrode cleaner (Bio-Rad Laboratories, Hercules, CA, USA), twice. Thus, electrodes were rinsed with 500 uL of DEPC treated water (Bio-Rad Laboratories, Hercules, CA, USA) for 5 minutes using electrode cleaning chip. At the end lid was kept open for 60 second to evaporate remaining water contained on electrodes. In parallel, RNA stain, RNA loading buffer and RNA gel from Experion^{TM} RNA HighSens Analysis kit were placed outside to achieve room temperature for 20 minutes. Also, RNA stain was wrapped in aluminum foil to avoid its light sensitive degradation. RNA gel was filtered from filter tube at 2000 RPM for 10 minutes. Next, 65 uL of filtered gel was mixed with 1 uL RNA stain in an RNase-free tube and kept solution protected from light. Meanwhile, RNA ladder was removed from -20˚C and thawed it on ice for 10 minutes. Next, 1 uL of RNA ladder and 3uL of cyRNA and nuRNA samples were taken into RNase-free tubes. RNA ladder and RNA samples were denatured at 70˚C for 2 minutes. Ladder and samples were immediately placed on ice for 5 minutes, spun down for 2-5 seconds and stored on ice until needed. Next, 9uL of the gel-stain solution was taken in well labeled as GS on RNA HighSens chip without

forming any air bubble. Chip was primed by setting appropriate pressure for sufficient time on priming station. Chip was inspected for any air bubbles in micro channels and for incomplete priming. Next, another 9 uL of gel-stain solution was taken into other well labeled by GS. Next, 9uL of filtered gel was taken to well labeled as G. Then, 5 uL of Loading buffer was taken to each sample well 1-12 including ladder well where 1 uL RNA ladder was taken to the well labeled as L as well RNA samples were taken to all wells numbered as 1-12. Chip was placed tightly and vortexed for 60 seconds on vortex station. Primed chip loaded with RNA samples and ladder was then kept on electrophoresis station for 5 minutes and electrophoresis run was started. After completion of the run, electrodes were cleaned with 800 uL DEPC water filled in a cleaning chip. Electropherograms were analyzed by Experion software version 3.2

The RNA integrity analysis was determined from a ratio metric calculation from integrals of the 18s rRNA and 28s rRNA peak areas on the generated electropherogram. Peak identification was determined by using internal reference ladder provided with the kit allowed for accurate peak alignment and identification. This calculation returned a number between 0 and 10, deemed the RNA quality indicator (RQI). The threshold for appropriate quality RNA was set at RQI > 7 [140].

3.3.6 Primer design for expression assays

3.3.6.1 Primer design for mRNA expression

Primers for gene expression were selected based on rhythmic expression clock genes already validated [141]. All the primers and probes used were designed using Primer3 (available at http://primer3.wi.mit.edu/) [142] with the following specifications:

- Optimal primer length – 20 bases
- Probe length – 18 to 25 bases.
- Product size – 100 to 150 bases for optimum PCR efficiency.
- Tm – 58°C to 60°C (Optimal Tm – 59°C).
- Probe Tm – 68°C to 70°C.

- % GC – 30% to 80%.
- 3’ end – last five nucleotides contain no more than two G + C residues.
- Probe 5’ end without G residue.
- Product should span an intron to prevent amplification of genomic DNA.

The primer pairs did not form any significant secondary structure, such as hairpins, homodimers and heterodimers. In addition, the primer sequences were tested virtually at the NCBI-BLAST tool (available at http://www.ncbi.nlm.nih.gov/tools/primer-blast/) to check that the primers correspond specifically to the selected targets and to verify the expected product size [143]. All primers were synthetized by Alpha DNA (Montreal, QC, Canada)

Table 2. List of primers for *BMAL1*, *PER2*, *SERPINB1* and *GAPDH* genes

Gene	Primer	Sequence (5′→3′)	NCBI RefSeq
BMAL1	Forward	CATTGTGCACAGAAGCATCA	NM_001178.4
	Reverse	ACAAGGAAGAATAAACGGCTTT	
PER2	Forward	TGCCAAAATCTTACTCTGCTG	NM_022817.2
	Reverse	GGCATCACGTAAACAAATTCA	
SERPINB1	Forward	AGGTTCATTCAAGATTCCAGAGT	NM_030666.3 70
	Reverse	AGTTTCAGAATATAAGACGCTCCA	
GAPDH	Forward	AGCCACATCGCTCAGACAC	NM_002046.4
	Reverse	TGGCAACAATATCCACTTTACCAGA	

3.3.6.2 Primer design for miRNA expression

In order to identify miRNAs, the stem-loop primers method is a novel strategy in miRNA research in diverse species [144], [145]. Particularly, stem-loop sequences are designed as a hairpin and possesses a 3′ overhang complementary to the miRNA. Also, miRNA-specific forward primers with a 5′ adapter are designed based on miRNA sequences, which were used from mature accession [93], while reverse primers were universal

primers, due these primers works along stem-loop and forward primers, thus, these features allow a high specificity and increased flexibility in the design of primers [146]. All primers were synthetized by Alpha DNA (Montreal, QC, Canada).

Table 3. List of primers for miRNA validation.

miRNA	Primer	Sequence (5′→3′)	Mature Accession Number
hsa-miR-141-5p	Stem-loop	GTC GTA TCC AGT GCA GGG TCC GAG GTA TTC GCA CTG GAT ACG AC TCCAAC	MIMAT0004598
	Forward	CAC GCA CAT CTT CCA GTA C	
hsa-miR-1225-5p	Stem-loop	GTC GTA TCC AGT GCA GGG TCC GAG GTA TTC GCA CTG GAT ACG AC CCCCCC	MIMAT0005572
	Forward	CAACAGTGGGTACGGCCCA	
hsa-miR-17-5p	Stem-loop	GTC GTA TCC AGT GCA GGG TCC GAG GTA TTC GCA CTG GAT ACG AC CTACCT	MIMAT0000070
	Forward	CAC GCA CAA AGT GCT TAC A	
hsa-miR-769-3p	Stem-loop	GTC GTA TCC AGT GCA GGG TCC GAG GTA TTC GCA CTG GAT ACG AC AACCAA	MIMAT0003887
	Forward	CAA CAC TGG GAT CTC CGG	
hsa-miR-222-5p	Stem-loop	GTC GTA TCC AGT GCA GGG TCC GAG GTA TTC GCA CTG GAT ACG AC AGGATC	MIMAT0004569
	Forward	CAG CAC TCA GTA GCC AGT	
hsa-miR-548ay-3p	Stem-loop	GTC GTA TCC AGT GCA GGG TCC GAG GTA TTC GCA CTG GAT ACG AC TGCAAG	MIMAT0025453
	Forward	CAG CAC AAA ACC GCG AT	
hsa-miR-106a-5p	Stem-loop	GTC GTA TCC AGT GCA GGG TCC GAG GTA TTC GCA CTG GAT ACG AC GCTACC	MIMAT0000103
	Forward	CAC GCA AAAAGTGCTTACAGT	
	Universal	TCG TA TCC AGT GCA GGG T	

3.3.7 Synthesis of complementary DNA (cDNA)

3.3.7.1 cDNA for mRNA expression

The total RNA samples were reverse transcribed to cDNA using AffinityScript Multi-Temperature cDNA synthesis kit (Agilent Technologies, CA, USA) based on manufacturer ‘s instructions.

Firstly, RNA samples and reagents provided in the kit were thawed on ice. Protocol started by preparing cDNA synthesis reaction, which contains 500 ng of total RNA, 3 uL of random primers (0.1 ug/ml) and enough RNase-free water to total volume 15.7 uL. Next, the mixture is incubated at 65°C for 5 minutes and placed at room temperature for 10 min to allow the primers to anneal to the RNA. Next, the mixture was combined with 2.0 uL of 10X AffinityScript RT Buffer, 0.8 uL of dNTP mix (25 mM each dNTP), 0.5 uL of RNase Block Ribonuclease Inhibitor (40 U/ul), and 1 uL of AffinityScript Multiple Temperature RT. Finally, the mixture was centrifuged for 5 sec at lower settings and placed onto the Px2 Thermal Cycler (Thermo Electron Corporation) to incubate at 25°C for 10 minutes, 42°C for 60 minute and 70ºC for 15 minutes. The synthetized cDNA was used immediately for qPCR, or stored at – 20°C.

3.3.7.2 cDNA for miRNA expression

The reverse transcription of cyRNA samples (separately in triplicate) was conducted using miRNA-specific stem-loop RT primers (see Table 4), which featured a 3′ overhang of 6 or 7 nucleotides complementary to the 3′ portion of the associated mature miRNA sequence [147]. We mix a pool of seven stem-loop RT primers that included one endogenous control at 10 nM, allowing simultaneously reverse transcriptions in one tube [148]. Thus, reverse transcriptase reactions contained 200 ng of cyRNA, stem-loop RT primer pool, and reagents from a TaqMan MicroRNA Reverse Transcription Kit (Thermo Fisher Scientific, Grand Island, NY, USA) based the manufacturer’s instructions. A negative control (no template) was included in all reactions.

First, the RT Reaction Mix is prepared by mixing 0.15 µL of 100mM dNTPs (with dTTP), 1.00 µL of MultiScribe™ Reverse Transcriptase (50 U/µL), 1.50 µL of 10× Reverse Transcription Buffer, 0.19 µL of RNase Inhibitor (20 U/µL), and 4.16 µL of nuclease-free water, which has a total volume of 7.00 µL. Next, mix 5uL of cyRNA, 3 uL of stem-loop RT primer pool and 7 uL of RT Reaction Mix. Finally, place the reaction tubes onto Px2 Thermal Cycler (Thermo Electron Corporation) and incubate using following settings:

Table 4. Cycling parameters for miRNA reverse transcription

Step	Temperature	Time
Primer extension	16ºC	30 min
Reverse transcription	42ªC	30 min
Stop reaction	85ªC	5 min
Hold	4ªC	Hold

3.3.8 Pre-amplification of cDNA for miRNA expression

Higher concentrations of total RNA are needed for hybridization techniques such as microarrays, RT-qPCR, sequencing, etc. Specifically, PCR-based techniques are able to detect low amount of individual miRNAs with high sensitivity and specificity on mature form of miRNAs [147]. The stem-loop RT-PCR can profile miRNA expression with few nanograms of total RNA or even single cells [147], [149], [150]. The use of cDNA pre-amplification increased the sensitivity of miRNA detection [151]. The protocol of pre-amplification was performed based [152], [153].

First, pre-amplification reactions were performed based on two miRNA primer pools (see Table 5). Both pools included miR-106a-5p as an endogenous control. For each reaction, 3 µL of cDNA (previously explained), 100 nM of the miRNA primer pool (forward primers), 12.5 µL of 2× Universal Master Mix with no UNG (Thermo Fisher Scientific, Grand Island, NY, USA), 1 uM of universal reverse primer, 1 µL of 5 U/µL

AmpliTaq Gold (Promega Corp, Madison, WI, USA), 0.5 µL of 100 mM dNTPs (Promega Corp, Madison, WI, USA), 0.5 µL of 100 mM MgCl2 (Promega Corp, Madison, WI, USA), and molecular grade water were used to achieve a final volume of 25 µL. Regarding the temperature profile of the reaction, incubation at 95 °C for 10 m, was followed by incubation at 55 °C for 2 m and 14 cycles of 95 °C for 1 s and 65 °C for 1 m. A negative pre-amplified control (no-cDNA) was included. Next, both pre-amplified cDNAs were diluted 10 times using molecular grade water and stored at −20 °C before further processing.

Table 5. Pools for pre-amplification of cDNA

Type	Pool-1	Pool-2
Testing miRNA	miR-1225-5p	miR-141-5p
Testing miRNA	miR-548ay-3p	miR-222-5p
Testing miRNA	miR-769-3p	miR-17-5p
Endogenous control	miR-106a-5p	miR-106a-5p

3.3.9 Quantitative real-time polymerase chain reaction (qPCR)

3.3.9.1 Assessment of qPCR assay

The qPCR efficiency is mainly affected by the performance of primers, due primers might produce large length of amplicons and secondary structures such as primer dimers. That´s why standard curve is generated to determine the efficiency, sensitivity, and reproducibility of the qPCR assay [154].

Once primers were designed and obtained, then they were resuspended in molecular grade water (1000 nM) and stored in aliquots at -20ºC. The concentration of primers (forward and reverse) for all qPCR assays was 200 nM. Next, the efficiency of each primer set was assessed by standard curves using the SYBR®Green dye.

The standard curve was carried out by 5 serial dilutions of a cDNA with known concentration. Each dilution was run by triplicate, plus triplicate non-template controls

(NTC). After performed qPCRs, the CT values were plotted on a semi-log10 plot. Amplification efficiency, E, is calculated from the slope of the straight line fitting of the data using the following formula:

$$E = 10 - 1/slope \quad (1)$$

The amount of PCR product is 2-fold increase in the number of copies with each cycle [155]. This corresponds to a reaction efficiency of 2. Using an E = 2 in the equation above indicates that the optimal slope of the standard curve will be –3.32. Primer sets with standard curve slope values ranging from -3.0 to -3.9 were accepted. Amplification efficiency is also frequently presented as a percentage:

$$\%\, Efficiency = (E - 1)\, x\, 100\% \quad (2)$$

The above formula allow to imply % Efficiency = (2 – 1) x 100% = 100%. An efficiency value close to 100% is the best indicator of a robust, reproducible assay. The target amplification efficiency of primers is always between 90–100%. Low reaction efficiencies may be caused by poor primer design or by suboptimal reaction conditions. Reaction efficiencies >100% may indicate pipetting error in serial dilutions or co-amplification of non-specific products, such as primer-dimers [155].

Finally, qPCR product can be evaluated using melting curve performed after run qPCRs. The shape of a melting curve is a function of the product length, GC/AT ratio and sequence. Melting curve can therefore be used to confirm the correct product and indicate the presence of multiple products, primer-dimers, and possible contamination.

3.3.9.2 Quantitative RT-qPCR for mRNA Expression

The qPCR reactions were carried out using the Applied Biosystems® StepOne™ Real-Time PCR System (Thermo Fisher Scientific, Grand Island, NY, USA). Each reaction was carried out in a reaction volume of 12µL loaded onto a MicroAmp® Fast 8-Tube strip with MicroAmp® Optical caps (Thermo Fisher Scientific, Grand Island, NY, USA). The reaction involved 20 ng of cDNA, 200 nM of forward and reverse primers for circadian clock genes, *BMAL1*, and *PER2*, and one rhythmic gene for MCF-7, SERPINB1, which we described in a previous study [141], 1X Brilliant II Fast SYBR® Green qPCR Master Mix (Agilent Technologies, Santa Clara, CA, USA), 300 nM passive reference dye, and molecular grade water to reach a final volume of 12 µL. The Brilliant qPCR master mixes contain enough Taq DNA polymerase, dNTPs, Mg2+, and its buffer is specially formulated for fast cycling. A NTC was also set up on each primer set to check for contamination.

The initial activation step was carried at 95 °C for 3 m, then a cycling program was begun, which involved denaturing at 95 °C for 6 s and annealing/extension at 60 °C for 12 s, and a melting curve analysis was performed to ensure the efficiency of the reaction.

3.3.9.3 Quantitative RT-qPCR for miRNA Expression

The qPCR reactions were carried out using the Applied Biosystems® StepOne™ Real-Time PCR System (Thermo Fisher Scientific, Grand Island, NY, USA). Seven miRNAs were profiled using 1X Brilliant II Fast SYBR® Green qPCR Master Mix (Agilent Technologies, Santa Clara, CA, USA). The reaction consisted of 1 µL of pre-amplified cDNA, 150 nM of forward and reverse primers (Table 3), 300 nM of passive reference dye, and molecular grade water to achieve a final volume of 12 µL. The following three-step cycling program was used: 95 °C for 3 min and 40 cycles of 95 °C for 6 s, 55 °C for 12 s, and 70 °C for 10 s. Melting curves were performed to ensure an efficient reaction. . A NTC was also set up on each primer set to check for contamination.

3.3.10 Data analysis

3.3.10.1 Data analysis of mRNA Expression

A preliminary data analysis was performed with Applied Biosystems® StepOne™ Software (Thermo Fisher Scientific, Grand Island, NY, USA). Next, CT values for each target gene's transcript were exported to Microsoft Excel. The relative expression in real-time PCR was calculated by Pfaffl equation [156]. The relative expression ratio (fold expression) of a target gene is calculated based on its efficiency (E) and the CT deviation of each time point versus the *t = 0* (control), and expressed in comparison to a reference gene:

$$Ratio = \frac{(E_{target})^{\Delta CP_{target}(control-sample)}}{(E_{reference})^{\Delta CP_{reference}(control-sample)}} \quad (3)$$

Equation 3 shows the ratio (R) of a target gene expressed in a sample versus a control in comparison to a reference gene. E_{target} is the real-time PCR efficiency of target gene transcript; E_{ref} is the real-time PCR efficiency of a reference gene transcript; ΔCP_{target} is the CT deviation of control – sample of the target gene transcript; ΔCP_{ref} = CP deviation of control – sample of reference gene transcript. The reference gene could be a stable and secure unregulated transcript, e.g. a housekeeping gene transcript. For the calculation of *R*, the individual real-time PCR efficiencies, and the CD deviation (ΔCP) of the investigated transcripts must be known. Real-time PCR efficiencies were calculated, according to $E = 10^{[-1/slope]}$[157].

The fold change of each biological replicate was calculated separately, then it was averaged, and a standard derivation was calculated for each time point. The relative expression results for each target gene were plotted versus the time in 4-h intervals.

3.3.10.2 Data analysis of miRNA Expression

A preliminary data analysis was performed with Applied Biosystems® StepOne™ Software (Thermo Fisher Scientific, Grand Island, NY, USA). Next, CT values for each

miRNA expression assay were exported to Microsoft Excel. The relative expression in real-time PCR was calculated by Pfaffl equation [156]. The relative expression ratio (fold expression) of a miRNA is calculated based on its efficiency (E) and the CT deviation of each time point versus the *t = 0* (control), and expressed in comparison to a reference gene, similar as Equation 1.

Equation 3 shows the ratio (R) of a target miRNA expressed in a sample versus a control in comparison to a reference miRNA. E_{target} is the real-time PCR efficiency of target miRNA transcript; E_{ref} is the real-time PCR efficiency of a reference miRNA transcript; ΔCP_{target} is the CT deviation of control – sample of the target miRNA transcript; ΔCP_{ref} = CP deviation of control – sample of reference miRNA transcript. The reference miRNA was miR-106a-5p because it keeps a stable expression [158]. For the calculation of *R*, the individual real-time PCR efficiencies, and the CD deviation (ΔCP) of the investigated transcripts must be known. Real-time PCR efficiencies were calculated, according to $E = 10^{[-1/slope]}$[157].

The level of expression of each biological replicate was calculated separately and averaged, and the SEM was calculated for each time point. The relative expression results of each miRNA were plotted over 48 h at 4 h intervals.

3.3.11 DNA microarray assays

3.3.11.1 DNA microarrays overview

DNA microarray technology allows measuring the expression levels of hundreds or thousands of targets in the same experiment. Specifically, for this research, technology of miRNA microarrays was used to identify human miRNAs. This technology contains miRNA probes (oligonucleotide sequences), which hybridize to target miRNAs. Probes are anchored to the glass slide surface by modified 5' end. Moreover, each probe contains 5' hairpin to increase target and size miRNA specificity. The miRNAs are fluorescently labeled and subsequently hybridized with sequence specific probes on the glass slide surface. Probes are anchored in the predetermined positions allowing analysis of the fluorescence signal and so determination of the presence and relative amounts of

miRNAs [159].

3.3.11.1 Microarray assays for miRNA expression - Workflow

Expression of miRNAs was temporally profiled using a Human miRNA Microarray 8 × 60 K Kit (Agilent Technologies, Santa Clara, CA, USA) which contained 2006 human miRNAs, based on miRBase Release 19.0 (http://www.mirbase.org/). In total, 100 ng of cyRNA and nuRNA samples (period within 12–40 h from 48 h study) were used for hybridization with miRNA complete labeling and the Hyb Kit (Agilent Technologies, Santa Clara, CA, USA). This period of 28 h belongs to the beginning of gene-sustained oscillations in living cells upon serum shock [129], [160]. Thus, we used two slides (eight arrays per slide). First slide was hybridized with cyRNA and nuRNA samples from MCF-10A cell lines and labeled with Cy3 and pCp (Cytidine-5′-phosphate-3′-(6-aminohexyl)phosphate)-Cy5 (277 µM) fluorochromes, respectively, according to [159]. Second slide was hybridized with cyRNA samples from MCF-7 and MDA-MB-231 and labeled with Cy3 and pCp (Cytidine-5′-phosphate-3′-(6-aminohexyl)phosphate)-Cy5 (277 µM) fluorochromes, respectively, according to [159]. Thus, microarray-processing workflow consisted of the following steps:

a. Sample preparation and labeling
b. Hybridization
c. Microarray wash
d. Scanning and Feature Extraction

3.3.11.2 Microarray assays for miRNA expression – Sample preparation and labeling

This step aimed to create fluorescently- labeled miRNA. The method involved the ligation of Cyanine 3-pCp and Cytidine 5-pCp to the 3' end of a RNA molecule. Below are displayed step-by-step procedures:

- Total RNA sample was diluted to 50 ng/µL in molecular grade water.
- 2 µL (100 ng) of the diluted total RNA was placed into 1.5 ml tubes and kept on ice.

- Prepare Calf Intestinal Alkaline Phosphatase (CIP) Master Mix.
- Dephosphorylation of the samples was performed using 2 µL of CIP Master mix added to 2 µL of each sample (100 ng), and then the total volume of dephosporylation reaction was 4 µL.
- Samples were incubated 30 min in thermal cycler at 37°C.
- Denaturation step was performed adding 2,8 µL of 100% DMSO to each sample.
- Samples were incubated at 100 °C in thermal cycler for 5 min.
- Samples were immediately transferred to ice-water bath to prevent the RNA from re-annealing.
- Ligation Master Mix was prepared separately for each fluorochrome and placed on ice without light fro 15 min. Both fluorochromes are light sensitive.
- 4.5 µL of the Ligation Master Mix was added to each sample tube for a total reaction volume of 11.3 µL. The reaction mix was mixed by pipetting and spinned gently.
- Tubes were incubated at 16°C for 2 hour in thermal-cycler.
- Samples were completely dried in vacuum concentrator (Thermo Fisher Scientific, Grand Island, NY, USA) at 50 °C for 55 min. Complete drying was important, because residual DMSO will adversely affect the hybridization results.

3.3.11.3 Microarray assays for miRNA expression – Hybridization

The microarray hybridization is one of key factors for targeting the labeled-molecule, miRNAs for this research. Below are displayed step-by-step procedures:

- Dried, labeled miRNA samples were resuspended in 18 µL of nuclease-free water.
- Hybridization mix for each sample was prepared by mixing 18 uL of sample, 4.5 uL of 10× Gene Expression Blocking Agent and 22.5 uL of 2× Hi-RPM Hybridization Buffer.
- Hybridization mixtures were vortexed gently and denatured at 100 °C for 5 min.
- Mixtures were immediately transferred to an ice water bath for 5 min and subsequently spinned.

- Slowly dispense all of the volume of hybridization sample onto the gasket well in a "drag and dispense" manner.
- Grip the slide on either end and slowly put the slide down.
- Assembled slide chambers were placed in rotisserie in a hybridization oven at 55°C. Hybridization rotator was set up at 20 RPM.
- Samples were hybridized at 55 °C for 20 hours.

3.3.11.4 Microarray assays for miRNA expression - Microarray wash

The microarray slides were washed according to the Agilent MiRNA Microarray System manual. GE Wash Buffer 1 and GE Wash Buffer 2 were used for this procedure according to manufacturer´s instructions.

3.3.11.5 Microarray assays for miRNA expression - Scanning and Feature Extraction

Microarray slides were scanned by GenePix® 4000B Microarray Scanner (Molecular Devices, Downingtown, PA, USA) with GenePix® Pro 6.0.1.25 Acquisition and Analysis Software (Molecular Devices, Downingtown, PA, USA). The GenePix® results (GPR) files were imported into the software R, version 2.12.2 (http://www.R-project.org) for further feature extraction.

The first process is to correct the overall measure of the intensity of the spots by background subtraction, for this procedure was used *backgroundCorrect* function of Linear Models for Microarray Data package (Limma, version 3.20.5, https://bioconductor.org/packages/limma/) [161], [162]. For two colors microarray data, normalization is usually applied to the log-ratios of the G channel signal and R channel signal, which are defined as M and A:

$$M = \log_2 R - \log_2 G \quad (4)$$

$$A = \frac{1}{2}(\log_2 R + \log_2 G) \quad (5)$$

The data contained an average of 30 replicates per probe sequence, with a total of 60,000 unique features and controls. Thus, data were normalized between arrays by

quantile normalization and log10 transformed, and the median was applied to the replicated probes [163]. The miRNA expression data contains one to four different probes associated with each miRNA, which were considered individually for further analysis.

3.3.12 Rhythmic expression analysis

3.3.12.1 Rhythmic expression analysis for microarray data

The determination of miRNAs rhythmic expression patterns was identified within 28 h period (containing since 12h – 40 h period from 48 h whole study) for MCF-10A, MCF-7, and MDA-MB-231 cell lines by using cosine-fitting algorithm. The first 12 h contains random biological process instead next 28 h display a robust rhythmicity [160]. The cosine function is defined as $g = \beta \times \cos(\omega \times t + \phi)$, where the cosine parameters β, ω, and ϕ were limited to [0, 30], [0, π], and [−2π, 2π], respectively. This function was used to evaluate distributions of the cosine correlations, periods, and phases in the experimental and randomized data. Afterward, restrictive values for amplitude, period, and cosine correlation were selected to identify rhythmic miRNAs. These values were $r >$ 0.82 for cosine correlation, 0.22–0.29 for period, and >0.045 for amplitude. The miRNAs that fulfilled those parameters were grouped using hierarchical clustering (ward agglomeration) to identify miRNAs with similar phases.

Next, miRNAs were selected for confirmation using RT-qPCR technology. They were chosen if they featured cosine-fitting correlation values of r were close to 1, a period of about 24 h, and a high amplitude value. Additionally, we restricted the selection of miRNAs for longer probe sequences, lengths of at least 15 nt, and/or high correlation among probes that belong to the selected miRNA. These parameters were used to ensure the reproducibility of the RT-qPCR assays [164].

3.3.12.1 Rhythmic expression analysis for qPCR data

The confirmation of miRNA rhythmic expression was performed on 48 h whole study for MCF-10A, MCF-7, MDA-MB-231, ZR-7530 and HCC-1954 cell lines by using MetaCycle package (version 1.0.0; https://github.com/gangwug/MetaCycleV100.git)

[165]. The miRNAs that exhibited *p*-values of less than 0.05 were considered rhythmic. All the statistical analyses were performed using R programming language.

3.3.13 Identification of Targeted mRNAs and Pathway Analysis

The MultiMiR package (version 1.0.1; http://multimir.ucdenver.edu/) was established to identify targeted miRNAs that were experimentally validated [166]. The Reactome pathway analysis tool was used to perform annotation enrichment analysis using lists of targeted mRNAs [167]

Chapter 4

Results and discussion

4.1 Entrainment of the circadian clock in human breast cell cultures

4.1.1 The Human breast clock

Scientists around the world are investigating the potential medical use of the 24-hour variations regarding human health-to-disease mechanisms [168]. However, although knowledge of circadian clock is expanding rapidly, translation into human studies require more research [169]. There are evidences regarding clock function can be species specific [170], [171] and even further tissue-cell specific [172], [173].

The circadian clock can be studied *in vitro*, considering that clock function is tissue specific. Initially, benign tissues such as the retinal and intestinal epithelium were commonly studied in order to know the clock physiology of cells [174], [175]. Over time, the theory of clock-regulated cell division has become more extensive, thus, clock disruption has been associated with deregulated cell-growth and an increased incidence of neoplasms [176]. Thus, scientific community also initiated studies in cancer cells in order to evaluate clock function, including breast cells [141], [177], [178].

In fact, breast cells have a highly proliferative nature that it is subject to abnormalities, which can result in tumorigenesis. Thus, some evidences report changes in clock genes/circadian rhythm in immortalized breast tumour cell lines [130], [141], [179] as well as in animal models, such as mouse where circadian clock maintains tissue stem cell population in mammary gland, being more specific, 600 genes possibly are under circadian control in mouse mammary gland [180]. However, there are not reports of changes in miRNAs/circadian rhythm in immortalized breast tumour cell lines. For this reason, to determine possible differences in oscillation of miRNAs in breast non-tumorigenic and tumorigenic cells, entrainment by serum shock, an approach known to synchronize rhythmic gene expression in mammalian cells grown in culture, was employed [129].

4.1.2 Optimization of gene expression protocol

To further understand the circadian clock at the molecular level, we sought to explore the expression changes of miRNAs by a 48 h time-course study after serum shock entrainment of human breast non-tumorigenic (MCF-10A) and tumorigenic (MCF-7, MDA-MB-231, HCC-1954, and ZR-75-30) cell lines. Thus, this optimization consisted of having controlled molecular assays, such as total RNA purification, RNA integrity, total RNA concentration, and primers efficiency:

4.1.2.1 Total RNA purification for microarray assays

The initial RNA samples contained large amount of impurities that certainly affect the microarray assays. Thus, total RNA extracted from cellular fractions needed purification to obtain appropriate RNA quality and quantity for hybridization of microarray assays. Particularly, the purified RNA samples obtained greater values of 260/280 and 260/230 ratios (see Figure 9). The purification process resulted an effective procedure for further processing.

4.1.2.2 RNA Integrity of samples for microarray assays

The RNA integrity Purified was assessed in cyRNA and nuRNA samples by peak areas 18S y 28S, internal reference ladder, and appropriate concentration of RNA (see Figure 10). Following a run, RQI was determined as indicator of quality for further processing. All samples achieved greater RQI value than 7.

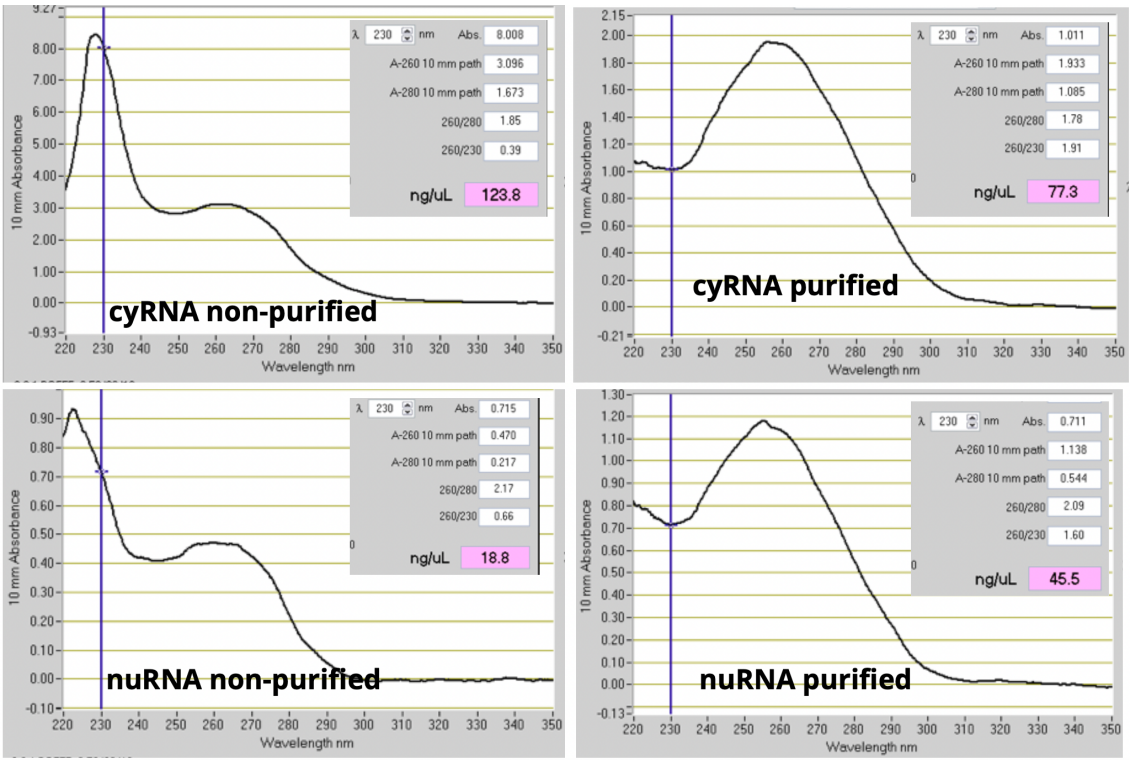

Figure 9. Comparison of total RNA from cellular fractions before and after purification. The purified RNA was used for microarray assays

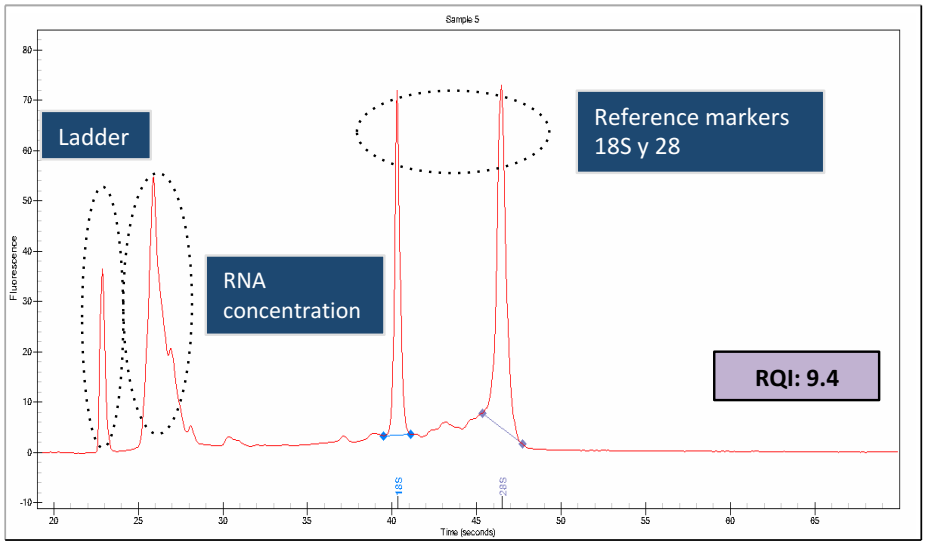

Figure 10. Electropherogram plot. This image depicts the parameters evaluated for evaluating RNA integrity. Markers 18S and 28S, and ladder are reference parameters.

4.1.2.3 Total RNA concentration for RT-qPCR assays

The RT-qPCR assays required the RNA samples with good quantity and quality. Thus, the RNA samples were purified and measured with MicroAmp® Fast 8-Tube strip. The batch for RT-qPCR assays consisted of 39 total RNA samples for each cell line (See Table 6 were illustrate the batch particularly for MCF-10A).

Table 6. RNA concentration and quality parameter of MCF-10A

Timepoint	RNA R1 (ng/ul)	260/280	RNA R2 (ng/ul)	260/280	RNA R3 (ng/ul)	260/280
T0	269.6	2.1	243.9	2.0	164.1	1.9
T1	175.1	1.9	177.0	1.9	65.2	2.1
T2	49.1	1.2	22.2	2.2	20.5	1.6
T3	65.5	1.9	141.5	2.2	105.0	2.7
T4	117.0	1.6	85.4	2.0	104.4	2.1
T5	155.7	2.1	113.5	2.2	184.7	1.9
T6	93.2	1.9	74.4	1.9	192.1	1.9
T7	76.7	1.7	69.2	2.3	129.6	2.0
T8	55.4	2.4	40.5	2.8	87.1	2.6
T9	125.2	1.9	228.9	2.3	102.3	2.1
T10	126.7	1.9	49.9	1.7	85.1	2.1
T11	58.8	2.1	70.9	1.7	64.8	1.7
T12	59.9	1.9	46.1	2.1	79.2	1.9

4.1.2.4 Efficiency of primers.

The expression levels of *BMAL1, PER2* and *SERPINB1* genes by RT-qPCR for assessing status of the circadian system in breast cell lines. The results were normalized using *GAPDH* as reference gene and the time = 0. These 4 genes were measured by using 4 sets of primers, which were previously evaluated by standard curves. These evaluations allow the optimization of qPCR conditions for performing robust assays. The four set of primers obtained efficiencies above 97%, see Table 7.

Table 7. Primers features

Set of Primers	Product size (Pb)	Efficiency (%)
BMAL1	141	99.87
PER2	149	97.41
SERPINB1	70	97.82
GAPDH	121	98.24

4.1.3 Rhythmic expression of clock genes displayed in MCF-10A cell lines

The MCF10A cell line is the most used non-tumorigenic human breast cell model, these cells were derived from benign proliferative breast tissue, and were spontaneously immortalized. Importantly, these cells are not tumorigenic and have not expression of estrogen receptor-*α* (ER*α*) [181]. Additionally, this cell line has molecular characteristics, which includes depletion of the chromosomal locus, containing p16 and p14ARF genes, both of which are critical in regulating senescence, and amplification of the Myc gene [181].

Based on non-tumorigenic characteristic of MCF-10A, cultured cells were entrained by serum shock, then we confirmed the pattern expression of *BMAL1* and *PER2* genes as prior studies showed [130], [141], [182], [183]. We obtained RT-qPCR data tracking the expression of *BMAL1* and *PER2* genes. Both transcripts were present and detectable (see Figure 11), having significant rhythmic patterns (*p-values* of 0.010 and 0.014, respectively using MetaCycle package) and showing periods of 24.15 and 20.40 h, respectively. In regards to the peaks of the patterns, *BMAL1* displayed peak expression levels at 12-h and 36-h, while PER2 displayed peak expression levels at 20-h and 40-h, disregarding first 12 hours, because this period belong initial synchronization process and does not have sustained rhythmicity [160]. Therefore, the phase difference between *BMAL1* and *PER2* was approximately 12 hours, and the two had expression profiles in opposition to one another, as expected [141].

Although, research about circadian clock identified many genes with rhythmic expression on diverse tissues [73]. However, two clock genes were selected due both has sustained rhythmic expression in human non-tumorigenic MCF-10A cells along

several studies, previously mentioned. The BMAL1 gene is a positive regulatory member of the circadian transcriptional complex [184], while PER2 gene is a negative regulatory member of the circadian transcriptional complex [184]. The sustained rhythmic expression given by BMAL1 and PER2 genes in MCF-10A cells are probably partial or non-dependent of circadian transcriptional complex, because this cell line has a lack of estrogen signaling, which triggers a lack of transactivation of PER2, however, apparently, this biological event does not affect PER2 rhythmic expression, as well as BMAL1 rhythmic expression [130].

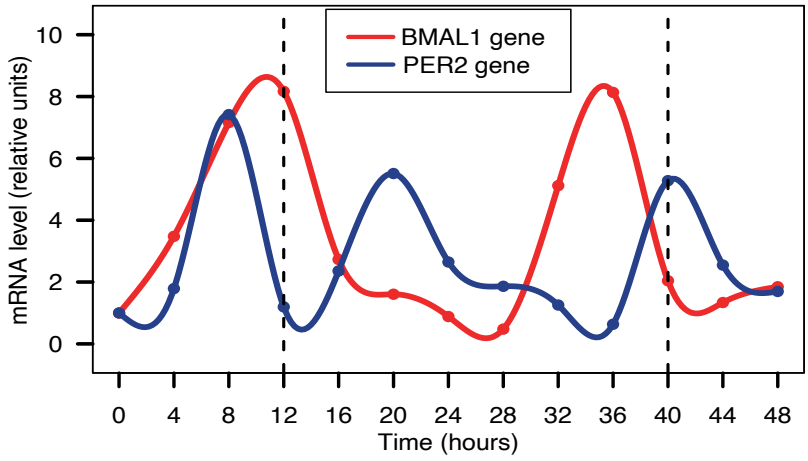

Figure 10. Temporal expression profiles of *BMAL1* and *PER2* genes in entrained human breast non-tumorigenic cell line, MCF-10A. The expression of *BMAL1* and *PER2* was measured by RT-qPCR assays. Samples were collected every 4-h for 48-h. Data points (mean of duplicates) were normalized using *GAPDH* gene, and corrected to the first time point (t = 0).

Although, ER*α* is essential for normal mammary gland physiology and also important as prognostic marker for the treatment of breast cancer [185]. MCF-10A a non-tumorigenic cell line with ERα non-expression displayed PER2 and BMAL1 rhythmic expression, which implies there are other mechanisms largely unknown involved to maintain rhythmic expression in mammary tissue.

4.1.4 Rhythmic expression of clock genes displayed on tumorigenic breast cell lines

Breast cancer is the most frequent malignancy in women around the world [186]. This disease represents a critical public health problem that requires further research at the molecular level in order to determine management strategies for prognosis and treatment prediction [187].

Breast cancer is known to be a complex and heterogeneous disease. This diversity is reflected in the underlying morphologic and molecular variation, with a spectrum of histologic features, such as tumour grade, lymph node status and the presence of predictive markers, ER, PR and HER2/neu markers. These are used for predicting clinical outcome for appropriately targeted therapies [188].

During last decades, gene expression profiling research has contributed significantly to understand the heterogeneity at a molecular level, sophisticated classification comprising luminal A, luminal B, basal-like, HER2-positive and normal subgroups [121], [189], [190]. Luminal subtypes are ER positive and express markers of the luminal epithelial layer of normal breast ducts cells. The HER2/neu subtypes are associated with amplification and overexpression of HER2 and adjacent genes on chromosome 17q12. Basal-like tumors share expression markers with the underlying myoepithelial layer of normal breast ducts, are ER negative, and are associated with an unfavorable outcome. TNBC are basal-like tumors and are defined as breast tumors that lack expression of ER, PR, and HER2 [191].

The extensive findings about molecular classifications of breast cancer now firmly established, researchers have turned their attention to breast cancer cell lines to determine whether the molecular profiles observed in breast carcinomas are reflected in cell line models of the disease. In general, several studies have shown molecular classifications in breast tumors can be distinguished in breast cancer cell lines [126], [192], [193]. Thus, our research performed with those breast cell lines provides good opportunities for the further study of miRNA expression phenotype, which will enhance our understanding of its biology. Our breast cancer cell lines represent most studied

molecular subtypes, MCF-7 (luminal), ZR-75-30 (luminal), MDA-MB-231 (basal-like) and HCC-1954 (HER2/neu) [126].

4.1.4.1 Temporal expression of BMAL1 and PER2 genes in MCF-7 cells

BMAL1 and *PER2* genes did not display circadian expression in MCF-7 cells. This non-rhythmicity might due that breast tumorigenic cell lines apparently have a disrupted inner clock [130], [141], [182]. Moreover, these clock genes showed lower amplitude (see Figure 12 and Table 8), compared with the expression displayed by MCF-10A cells. These findings might be related to the ER expression, due MCF-7 cells present an overexpression of it [194], and is a important feature for breast cancer development. Additionally, ER expression might a critical factor for downstream processes regarding circadian regulation as some investigations are mentioned in last decade [130], [182]. Indeed, there are earlier evidences that clock genes and estrogen receptor signaling appear to function in a bidirectional relationship [195].

Table 8. Circadian features of clock genes displayed in MCF-7 cells

Genes	P-value	Period	Amplitude
PER2	0.999	26.55	0.03
BMAL1	0.462	24.27	0.22

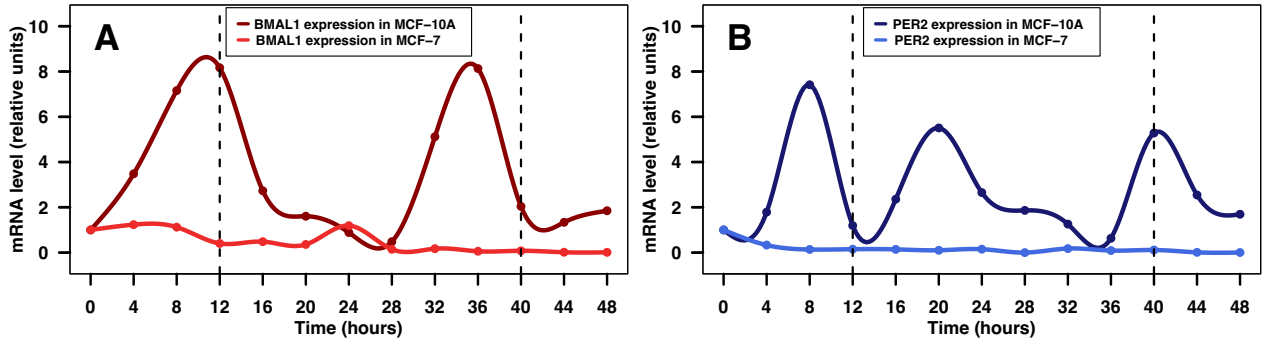

Figure 11 Temporal expression profiles of *BMAL1* and *PER2* genes in entrained MCF-7 cells. In addition, expression profiles in MCF10A cells are added for comparison purposes. The expression of *BMAL1* and *PER2* genes was measured by RT-qPCR assays. Samples were collected every 4-h for 48-h. Data points (mean of triplicates ± SEM) were normalized using GAPDH gene relative to the first time point (t = 0). Dotted gray lines at 12-h and 40h were added to show the period where profiles have robustness.

4.1.4.2 Temporal expression of BMAL1 and PER2 genes in MDA-MB-231 cells

The *BMAL1* and *PER2* genes did not displayed rhythmic fashion in serum shocked MDA-MB-231 cells (see p-values significance in Table 9). The expression of these genes through 48 hours was likely stable, non-rhythmic fashion, which was similar to previous investigations (see Figure 13) [130], [141], [196]. This cell line consists of invasive ductal/breast carcinoma cells, which is also known as triple-negative cell line, due it lacks ER and PR expression, as well as HER2/neu amplification [127], [128]. Thus, those pathological features of the cell line might affect some processes in rhythmic expression of clock genes. Particularly, *BMAL1* gene was reported that levels of expression of this gene might influence on the regulation of migration and invasion in MDA-MB-231 cells [117]. However, the rhythmicity displayed by this gene on breast non-tumorigenic cell lines was lost [196]. In regards to *PER2* gene, it has been linked with DNA damage responses, then PER2 expression results in potential downstream effects on both cell cycle and apoptotic targets, suggestive of a tumour suppressive role for breast cancer cells [179]. Nevertheless, *PER2* gene expression evidenced a lost rhythmicity in MDA-MB-231 cells [196].

Table 9 Circadian features of clock genes displayed in MDA-MB-231 cells

Genes	P-value	Period	Amplitude
BMAL1	0.999	28.46	0.30
PER2	0.417	26.57	0.06

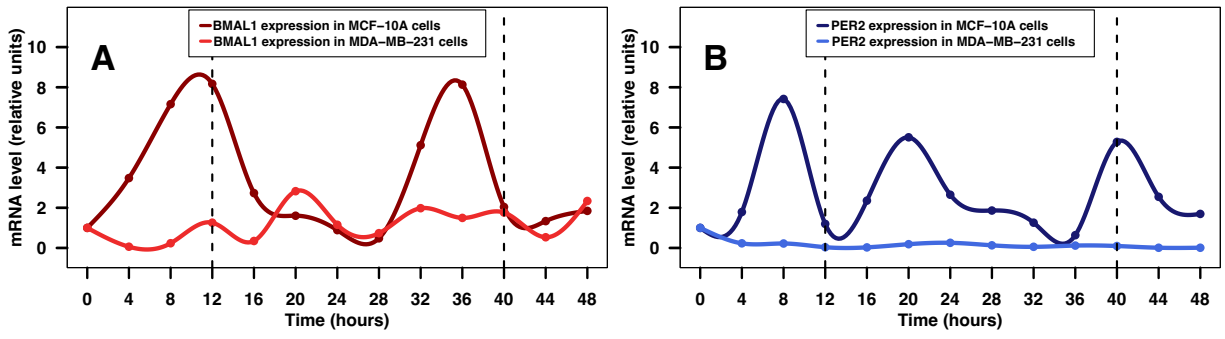

Figure 12 Temporal expression profiles of *BMAL1* and *PER2* genes in entrained MDA-MB-231 cells. In addition, expression profiles in MCF10A cells are added for comparison purposes. The expression of *BMAL1* and *PER2* gene was measured by RT-qPCR assays. Samples were collected

every 4-h for 48-h. Data points (mean of triplicates ± SEM) were normalized using GAPDH gene relative to the first time point (t = 0). Dotted gray lines at 12-h and 40h were added to show the period where profiles have robustness.

4.1.4.3 Temporal expression of BMAL1 and PER2 genes in ZR-7530 cells

The *BMAL1* and *PER2* genes did not displayed rhythmic fashion in serum shocked ZR-7530 cells (see p-values significance in Table 10). Particularly, BMAL1 gene displayed mild amplitude, while PER2 displayed a dampening expression, which was similar to previous investigation (see Figure 14) [141]. Noteworthy, ZR-7530 cells are well known as luminal B cells [128], and there are not much scientific progress linking those cells with circadian rhythm. Thus, those pathological features of this type of breast cancer might a critical factor for downstream processes regarding circadian regulation as some investigations are mentioned with other cell lines.

Table 10 Circadian features of clock genes displayed in ZR-7530 cells

Genes	P-value	Period	Amplitude
BMAL1	0.053	29.68	1.97
PER2	0.997	26.54	0.33

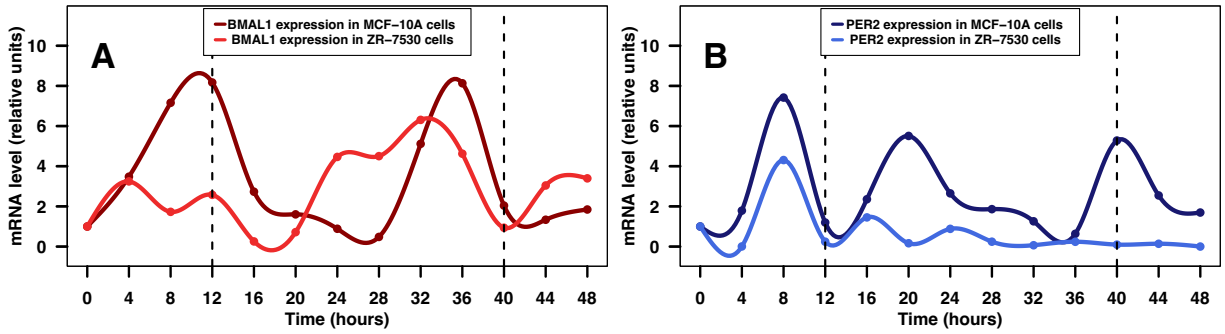

Figure 13 Temporal expression profiles of *BMAL1* and *PER2* genes in entrained ZR-7530 cells. In addition, expression profiles in MCF10A cells are added for comparison purposes. The expression of *BMAL1* and *PER2* genes was measured by RT-qPCR assays. Samples were collected every 4-h for 48-h. Data points (mean of triplicates ± SEM) were normalized using GAPDH gene relative to the first time point (t = 0). Dotted gray lines at 12-h and 40h were added to show the period where profiles have robustness.

4.1.4.4 Temporal expression of BMAL1 and PER2 genes in HCC-1954 cells

The *BMAL1* and *PER2* genes did not displayed rhythmic fashion in serum shocked HCC-1954 cells (see p-values significance in Table 11). The expression of BMAL1 gene through 40 hours was likely stable, except for last points where appeared an inconsistency expression level, whereas PER2 gene displayed multiple peaks, both patterns were similar to previous investigations (see Figure 15) [141]. In particular, HCC-1954 cell line was derived from a primary stage IIA, grade 3 invasive ductal carcinoma with non-lymph node metastases, which has not estrogen receptor, nor progesterone receptor, however, this cell is well-know due its overexpression of her2/neu [197]. Noteworthy, there has been reported lower expression of BMAL1 and PER2 gene in cells with overexpression of her2/neu [198], [199]. This lower expression might promotes the loss of rhythmicity, however, this phenomenon needs to be further studied.

Table 11 Circadian features of *BMAL1* and *PER2* genes displayed in HCC-1954 cells

Genes	P-value	Period	Amplitude
BMAL1	0.667	24.98	1.1
PER2	0.854	25.05	1.47

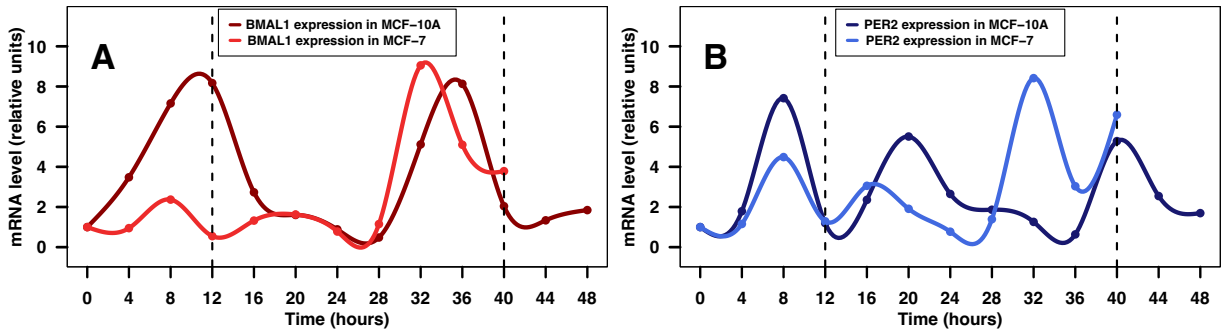

Figure 14 Temporal expression profiles of *BMAL1* and *PER2* genes in entrained HCC-1954 cells. In addition, expression profiles in MCF-10A cells are added for comparison purposes. The expression of *BMAL1* and *PER2* genes was measured by RT-qPCR assays. Samples were collected every 4-h for 48-h. Data points (mean of triplicates ± SEM) were normalized using GAPDH gene relative to the first time point (t = 0). Dotted gray lines at 12-h and 40h were added to show the period where profiles have robustness.

4.1.4.5 Temporal expression of SERPINB1 gene in MCF-7 cells

SERPINB1 gene displayed a particular rhythmic expression in MCF-7 cells (see Figure 16 and Table 12). This behavior expressed by *SERPINB1* gene was replicate from previous research [197], which was the first evidence about a supposed certain function in human circadian rhythm. Currently, there are evidences that human serpin proteins play important roles in diverse biological functions, the majority of which are involved in proteolytic cascades of blood clotting and anti-inflammatory responses [141], but evidences related to circadian are still being researched. Indeed, compelling evidence has shown that serpins proteins are closely linked to human diseases. Particularly, few studies suggested that SERPINB1 protein might suppress the migration and invasion of lung, liver, and breast cancers [200]. However, the possible connection of breast cancer with circadian behavior of SERPINB1 gene requires further investigation.

Table 12 Circadian features of *SERPINB1* gene displayed in MCF-7 cells

Genes	P-value	Period	Amplitude
SERPINB1	0.011	21.16	0.65

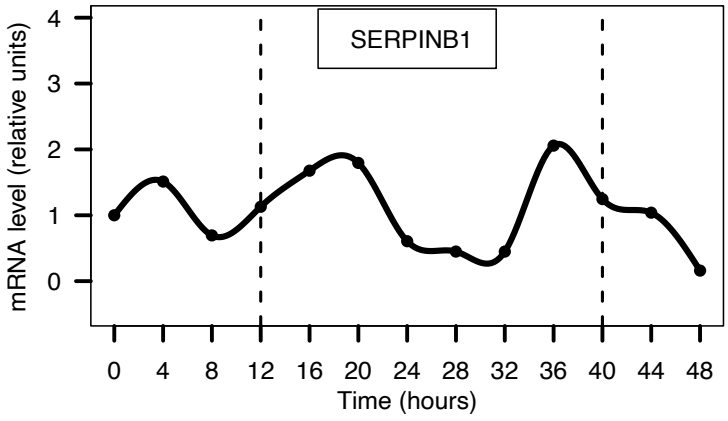

Figure 15. Temporal expression profile of *SERPINB1* gene in entrained MCF-7 cells. The profile expression of *SERPINB1* gene was done by RT-qPCR assays in serum-shocked MCF-7 cells during 48 hours (4-hour intervals). Data points (mean of triplicates ± SEM) were normalized using GAPDH gene relative to the first time point (t = 0). Dotted gray lines at 12-h and 40h were added to show the period where profiles have robustness.

4.2 Rhythmic expression of miRNAs displayed in human breast cell lines

In order to explore the expression of miRNAs through 8 time points (28 hours), then microarray assays were performed to test one non-tumorigenic breast MCF-10A cells and two tumorigenic cell lines, MCF-7 and MDA-MB-231.

4.2.1 Microarray assays for miRNA expression

Based on validation of entrainment of human breast cell lines. Thus, microarrays assays were performed for 4 groups: cyRNA from MCF-10A, nuRNA from MCF-10A, cyRNA from MCF-7, and cyRNA from MDA-MB-231.

The results of the microarrays evidenced that Cy5 hybridization in nuRNA samples presented lower signal intensities, which implies lower expression or bad hybridization procedure (See Figure 17). Thus, based on signal intensities the results from nuRNA samples were dropped in order to avoid unnecessary RT-qPCR assays and surely not reliable expression.

4.2.1 Statistical analysis of miRNA rhythmic profiles

The cosine-fitting function was used to identify potential rhythmic patterns expressed by miRNAs [201]. However, prior to this analysis, we evaluated the efficiency of the cosine-fitting function by testing it with diverse grades of data decomposition of experimental data.

The experimental data belonged to miRNA expression of MCF-10A, MCF-7, and MDA-MB-231 cells was decomposed by 5 five types of randomization methods, such as TL (time-label), RW (row-wise), CW (column-wise), RCW (row-column-wise), and RCWB (row-column-wise by blocks). Therefore, the features associative to rhythmicity, including cosine correlation, period, and phase of the experimental and randomized data for each miRNA were assessed. Thus, the evaluation identified that distributions are equivalent between cell lines from experimental data (see Figure 18).

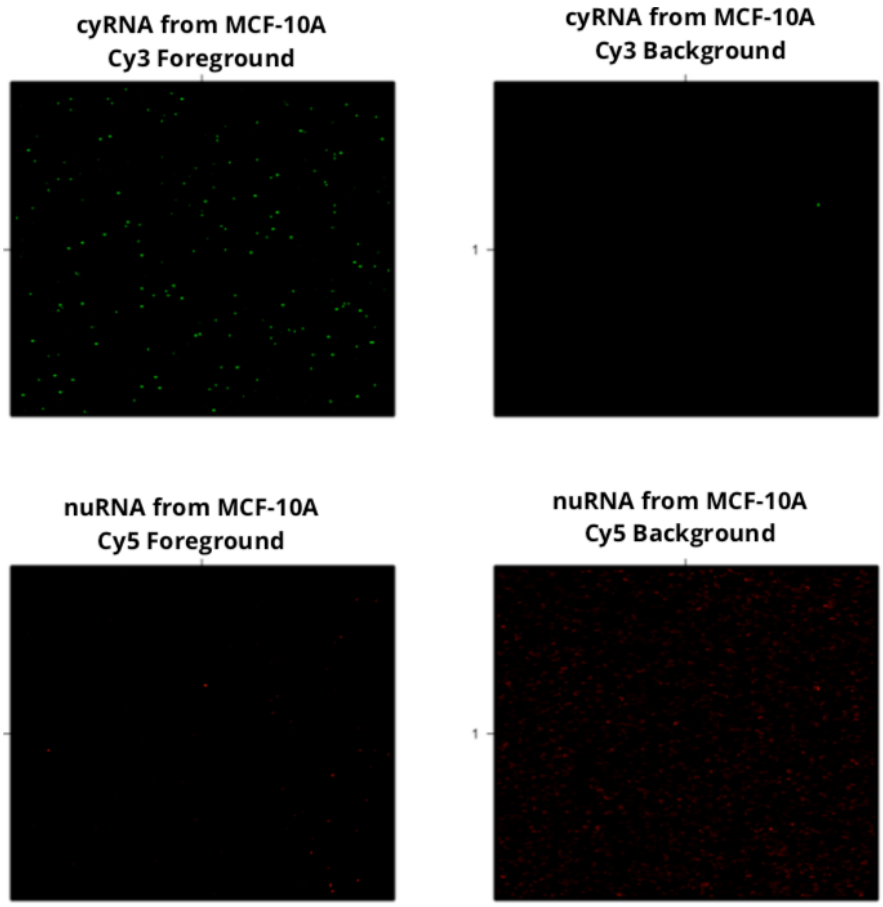

Figure 16 Comparison of background and foreground obtained from microarrays assays in MCF-10A. The foreground plot obtained from cyRNA samples has solid signal intensities (green) and background evidenced normal pattern. However, The foreground plot obtained from nuRNA samples has few dots and lower signal intensities (red) and background evidenced more dots and higher signal intensities.

The distributions of cosine correlation, period and phase features have been structured likely previous studies [202]–[204]. Particularly, there are evidences about some synchrony that follows clock gene expression in individual cells [205], [206]. However, clearly, such individual cells-synchronized must be coupled in the intact animals since otherwise they would rapidly lose synchrony under constant conditions and could therefore not drive coordinated rhythmic outputs of the circadian clock system [206]. Thus, these distributions that were obtained from cell line experiments that have some variations regarding distributions of peaks, which generate a possibly draw away of Gaussian distribution. These results might be due to those cell lines having been shocked by horse serum, but this chemical synchronization is just achieved through a short period,

then some miRNAs might experience changes of the expression, which trigger changes on distributions of cosine correlation, period, and phase features.

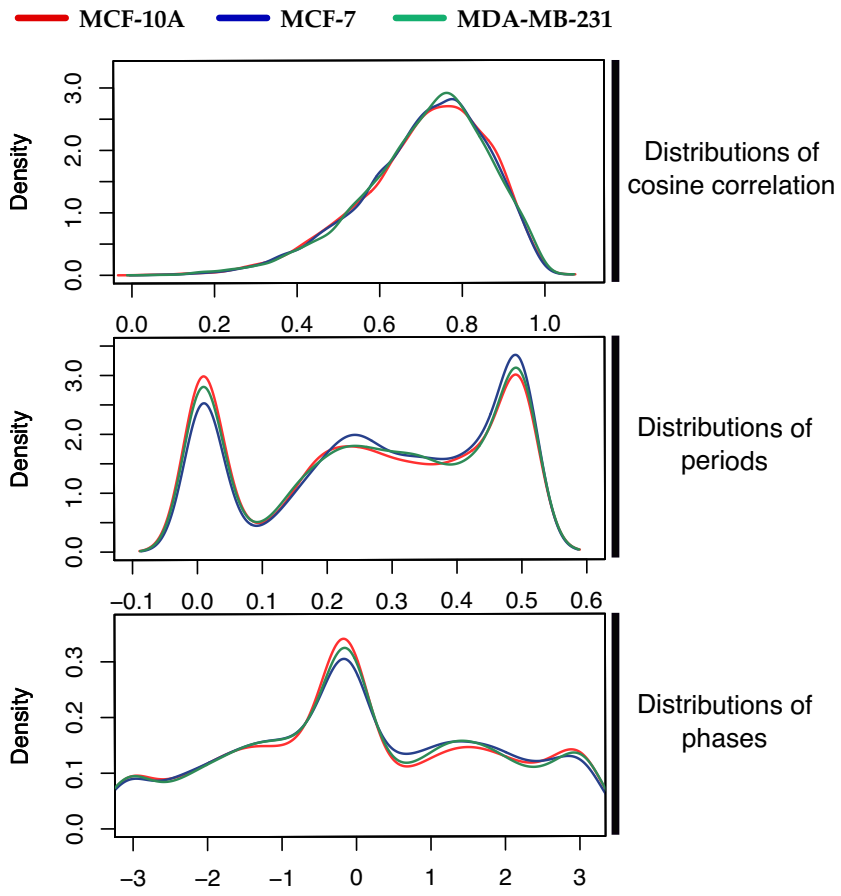

Figure 17. Distribution of cosine correlation, period and phase obtained from analyzing 28h temporal expression of 2006 miRNAs in MCF-10A, MCF-7 and MDA-MB-231 cells.

Furthermore, distributions obtained from experimental data were certainly different than randomized data. Particularly, distributions of circadian features obtained from data-decomposed by TL and RW methods had similar structures to experimental data (See Figure 18). Therefore, these results were what we expected, because the level of decomposition of data was minor, because the experimental data had 8 time-points, and there is still chance of not completely randomization [207]. Thus, these 2 methods of randomization are not recommended for evaluating decomposition of data, as well as evaluating efficiency of fitting-cosine function.

Additionally, distributions of periods obtained from data-decomposed by CW and RCW methods had similar pattern than the experimental data (See Figure 18). Particularly, this result was not expected, but it is evidence that period, as a circadian feature should be carefully evaluated; considering that experimental data has just 8 time-points [207]. Moreover, distributions of cosine correlations, and phases had different than the experimental data (See Figure 18). Particularly, this last result evidenced that CW and RCW methods are able to decompose data, which based on previous results, there is still a need to find an integral method for whole decomposing of data.

Finally, data obtained from RCWB method showed marked differences in structure compared with the experimental data, including different cosine correlations, periods, and phases (See Figure 18). Thus, cosine correlations and periods for experimental and randomized data were plotted (See Figure 19). We noted that data from RCWB method has a high proportion of transcripts with periods less than 0.22, which means they cannot be categorized as rhythmic transcript (periods close to 0.26) (see Figure 19D). We also compared periods between the experimental and randomized data, finding that the randomized data features have fewer rhythmic periods than from the experimental data (see Figure 19E).

The RCWB method changed noticeably the structure of the experimental data. The results can be explained by the simultaneous shuffling of columns and rows in two separate blocks to ensure a lack of intrinsic pattern in the data [208]. Biologically, it might be justified by the assumption that miRNAs feature diverse temporal patterns of expression [209], such as starting and ending expressions with slow peaks or dampened expression. Therefore, our results suggest that short time course data should be randomized using an appropriate method, such as RCWB, to achieve more accurate null distributions [208].

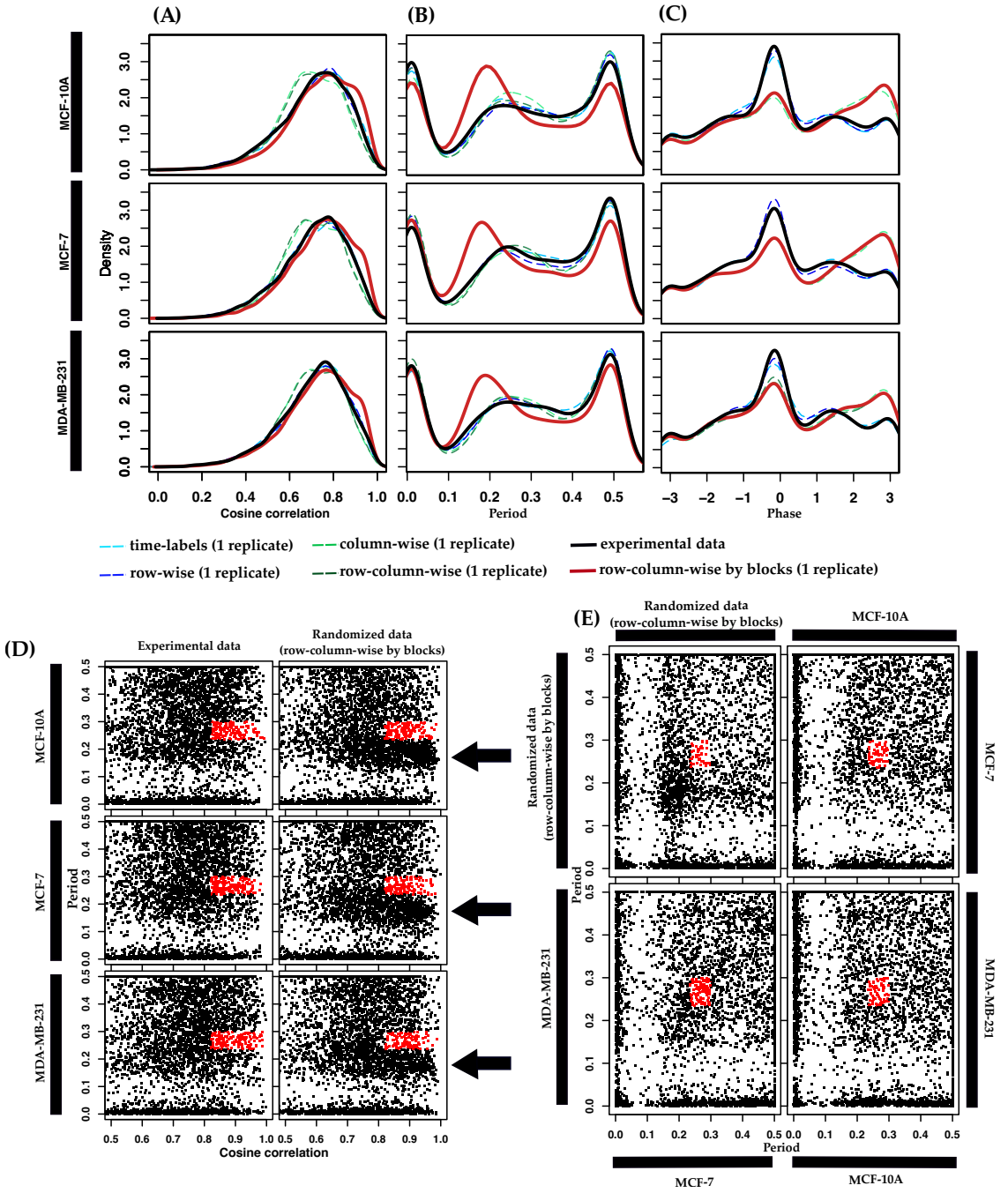

Figure 18 Evaluation of the cosine correlation, period and phase distributions in experimental and randomized data. Experimental data consisted of miRNA temporal expression in MCF- 10A, MCF-7 and MDA-MB-231 cells. Randomized data consisted of five types of data (by triplicate) decomposed from 5 types of randomization methods: TL, CW, RW, CRW and CRWB. Panel (A) shows the distributions of cosine correlation, panel (B) period, and panel (C) phase among experimental and randomized data. Panel (D) shows cosine correlation compared to the period for experimental and randomized (CRWB) data. An arrow mark regions in which miRNAs with large cosine correlation is highly associated to non-periodic values in randomized experiments whereas experimental data do not show such associations. Panel (E) shows plots of the period values in experimental and randomized (CRWB) data (two replicates). Red dots represent miRNAs fulfilling the selection criteria in correlation and period values.

In summary, when the structures of the experimental and randomized data show equivalents, then cosine fitting function calculate mathematical rhythmic features by chance, it is often observed when statistical analysis is performed in short temporal expression data [207]. However, our last results suggest that the RCWB method effectively randomize experimental data and removes the biological structure, which indicates that cosine fitting function can be used to calculate the circadian parameters of transcripts [208]. The current evaluation is consistent with our previous study [141]. Thus, we believe that our validation of miRNA profiles using RT-qPCR is the best evidence that microarray data are not random.

4.2.2 Determination of miRNAs with rhythmic expression

The miRNA profiles were analyzed by high-density Agilent microarrays, specific for 2006 human miRNAs in 3 human breast cell lines, such as MCF-10A, MCF-7, and MDA-MB-231 cells. To determine whether global miRNA profiling could distinguish molecular groups by phase measurement, clusters, then we performed an unsupervised analysis using conventional hierarchical agglomerative clustering, which revealed closely 6 clusters of miRNA profiles for each cell line (see Figure 20). The most striking finding was that MDA-MB-231 cells displayed miRNA profiles tightly clustered. The differences in phases displayed for temporal expression of miRNAs still need further research to have a clear biological meaning. Thus, this regulation might induce bistability, and oscillations, which suppose some variations on the phases displayed by miRNAs [210].

In addition, the analysis identified a total of 143 (7.12%) miRNAs with patterns of rhythmic expression in human breast non-tumorigenic cells, MCF-10A, while in tumorigenic cells, such as MCF-7 and MDA-MB-231 cells presented 183 (9.12%) and 147 (7.32%) rhythmic miRNAs, respectively. Thus, these results are comparable what has been found that at least 10% of transcriptome oscillate with circadian rhythmicity in many human tissues [211]. The majority of these miRNAs are tissue specific, indicating that the circadian clock is tightly coupled to key tissue specific functions [212], as well as might indicate differences according pathological condition [213].

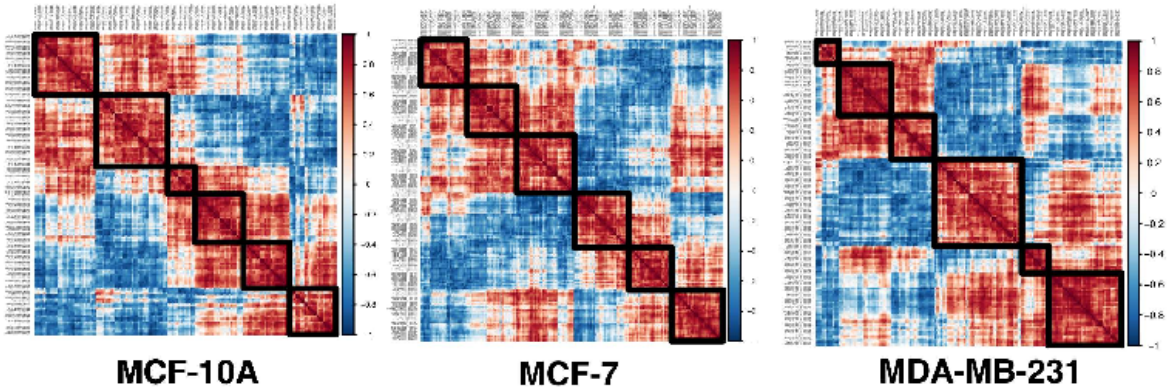

Figure 19 Correlations plots from miRNA profiling in breast cell lines. They illustrate the disposition of the clusters (based miRNA expression) identified for each breast cell line.

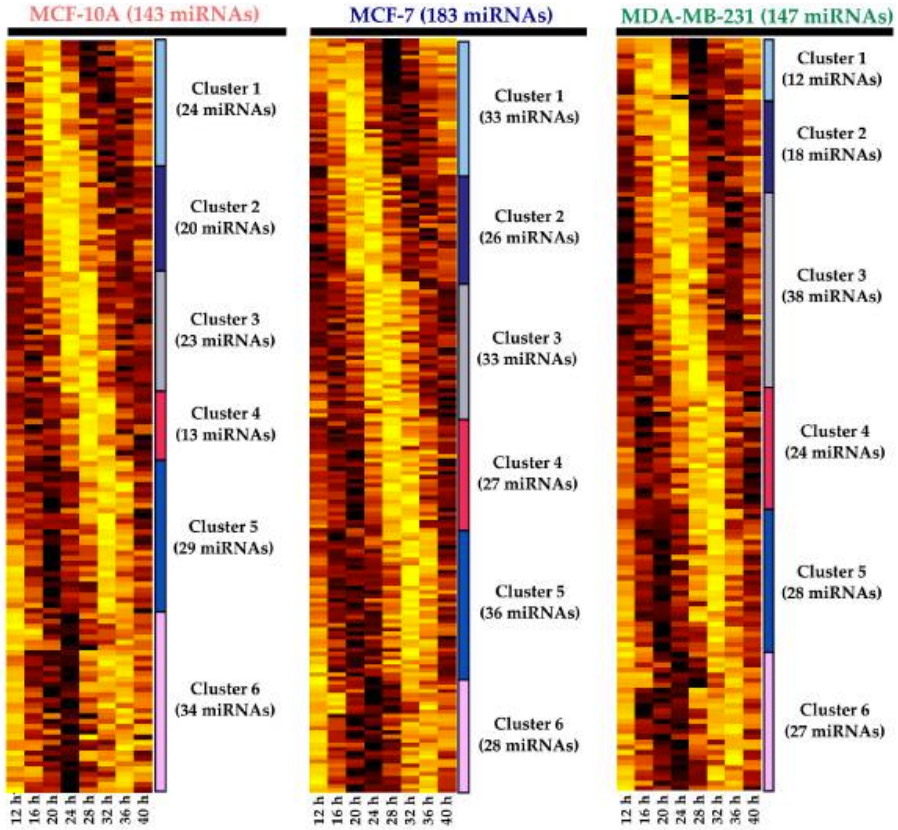

Figure 20. Heatmaps of temporal expression (28h) of miRNA profiling in breast cell lines. The heat maps depict the expression level of miRNAs over 28 h (between 12–40h) in MCF-10A, MCF-7 and MDA-MB-231 cells. Additionally, heat maps show 6 different clusters of miRNAs that depict marked phases. Brown colors represent higher expression values, while yellow colors represent lower expression values. Expression values are z-scaled relative to each cell line.

Subsequently, we determined potential miRNAs with rhythmicity between breast cell lines (see Figure 22). The comparison identified 9 common miRNAs between MCF-10A and MCF-7 cells, which was highly significant (*p-value* = 0.03, hypergeometric test). We also found that 11 miRNAs significantly overlapped across the tumorigenic cell lines MCF-7 and MDA-MB-231 (*p-value* = 0.007, hypergeometric test) and 8 miRNAs overlapped across MCF-10A and MDA-MB-231 cells (*p-value* = 0.02, hypergeometric test). Nevertheless, we identified 2 potential rhythmic miRNAs overlapped between the three breast cell lines. Thus, these results show a large component of specific rhythmic miRNAs and only small common component feature rhythmicity among the tested breast cell lines, which can be observed through cosine correlations, periods, and phases obtained from the cosine-fitting function, see Tables B1-3 in Appendix B.

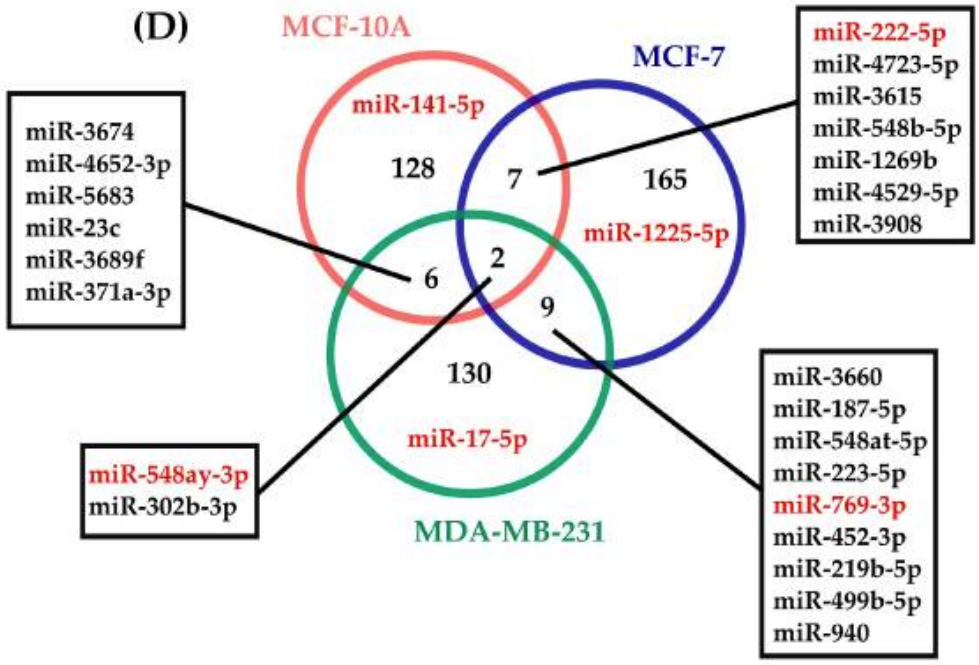

Figure 21. Venn diagram of 143, 183, and 147 miRNAs that exhibited rhythmic expression over 28 h in MCF-10A, MCF-7, and MDA-MB-231 cells. The diagram also shows miRNAs that exhibited rhythmicity across cell lines and were selected for RT-qPCR validation (red).

4.2.3 Validation of rhythmic expression profiles using RT-qPCR

For validation purposes, the selection of miRNAs was based on similar or opposite rhythmic patterns observed on 28h temporal expression from microarray results. We

selected one miRNA that displayed rhythmicity only for MCF-10A (miR-141-5p), MCF-7 (miR-1225-5p), and MDA-MB-231 (miR-17-5p). Additionally, we selected miR-769-3p because it shared a similar profile for MCF7 and MB-MDA-231, while miR-222-5p was selected because it had opposite profiles between MCF-10A and MCF-7, and finally, miR-548ay-3p was included due it exhibited rhythmic expression in MCF-10A, MCF-7, and MDA-MB-231. The selection was regarded on scientific findings, which declares that up-regulation of a set of miRNAs may also come from down-regulation of other miRNAs, in other words, read counts of a specific miRNA relative to all mapped reads, while miRNAs may have lower/higher absolute abundance depending of miRNA reference utilized for calculation of relative quantification [214].

Additionally, we measured the temporal expression of the selected miRNAs in two other tumorigenic breast cell lines, ZR-7530 and HCC-1954 (note that last two time points of HCC-1954 are missing due experimental issues). After comparing the miRNAs temporal expression between microarray and RT-qPCR results, we observed similar profiles, suggesting reproducibility among assays.

The significance of the rhythmicity of miRNAs was evaluated using MetaCycle ($p < 0.05$) [165]. In MCF-10A cells, the miR-141-5p displayed an expected significant rhythmicity (MetaCycle p-value = 0.023). Nevertheless, this miRNA also displayed significant rhythmicity in MCF-7 and HCC-1954 cells (MetaCycle p-values of 0.0011 and 0.041, respectively), which was not observed in microarray results (see Figure 23A). We additionally observed that miR-141-5p exhibited lower amplitude in MCF-7 than MCF-10A and HCC-1954. Based to our knowledge at this moment, there are not conclusive evidences about circadian behavior of miR-141-5p with breast pathophysiology. However, notably, one study reported that miR-141-5p showed circadian expression in rat enterocytes [15]. On other hand, there is one evidence about miR-141-5p related to progression of triple-negative breast cancer [215]. Although, there has also been this miRNA potentially proposed as biomarker for prostate cancer [216]. Finally, interestingly, the three breast cell lines where have been identified the rhythmicity of mir-141-5p have

different histopathological features which make hypothesize that ER, PR and Her2/neu might not related to circadian clock.

In particular, miR-1225-5p did not display significant rhythmicity in MCF-7 cells, but it did display rhythmicity in ZR-7530 and HCC-1954 (MetaCycle *p*-values of 0.0079 and 0.037, respectively). Nonetheless, it exhibited low amplitudes across five breast cell lines (see Figure 23B), suggesting randomness. At this moment, there are not conclusive evidence about circadian behavior of miR-1225-5p with breast pathophysiology. However, there are evidences that miRNA has potential biological function of tumour suppressor in diverse cancers, such as glioblastoma [217], non-small cell lung cancer [218], hepatocellular carcinoma [219], and osteosarcoma [220]. Nonetheless, there is evidence that miR-1225-5p has a possible oncogene function for progression of breast cancer [221], Based above evidences, we suspect that mir-1225-5p might have a specific role on breast pathophysiology, but there is still need more investigation to validate this assumption.

The miR-17-5p displayed the expected rhythmicity in MDA-MB-231 cells (MetaCycle *p*-value = 0.0018), and interestingly, it also exhibited rhythmicity in HCC-1954 cells (MetaCycle *p*-value = 0.037) (see Figure 23C). Interestingly, both cell lines are negative for ER and PR, but differ on ERBB2 (HER2/neu) expression. Thus, the rhythmicity exhibited in both cell lines appears to be beyond the biological function of the receptor tyrosine-kinase. Additionally, this miRNA is a member of the well-known miR-17/92 cluster, which is largely related to breast cancer as an oncogene and tumor suppressor [222], [223]. We also noted that miR-17-5p has potential 343 targeted mRNAs, five genes of which (*MEF2D*, *PPP1CA*, *NPAS2*, *PER1*, and *RPS27A*) are involved in the circadian clock pathway (*p* = 0.0027). Interestingly, a recent study found that miR-17-5p stabilizes the circadian clock period by inhibiting the translation of Clock and Npas2 in mice [224]. These results are encouraging and propose that the other miRNAs identified in the same way than mir-17-5p may play a potential role in rhythmicity. Nevertheless, further investigation is required to validate the remaining molecular associations.

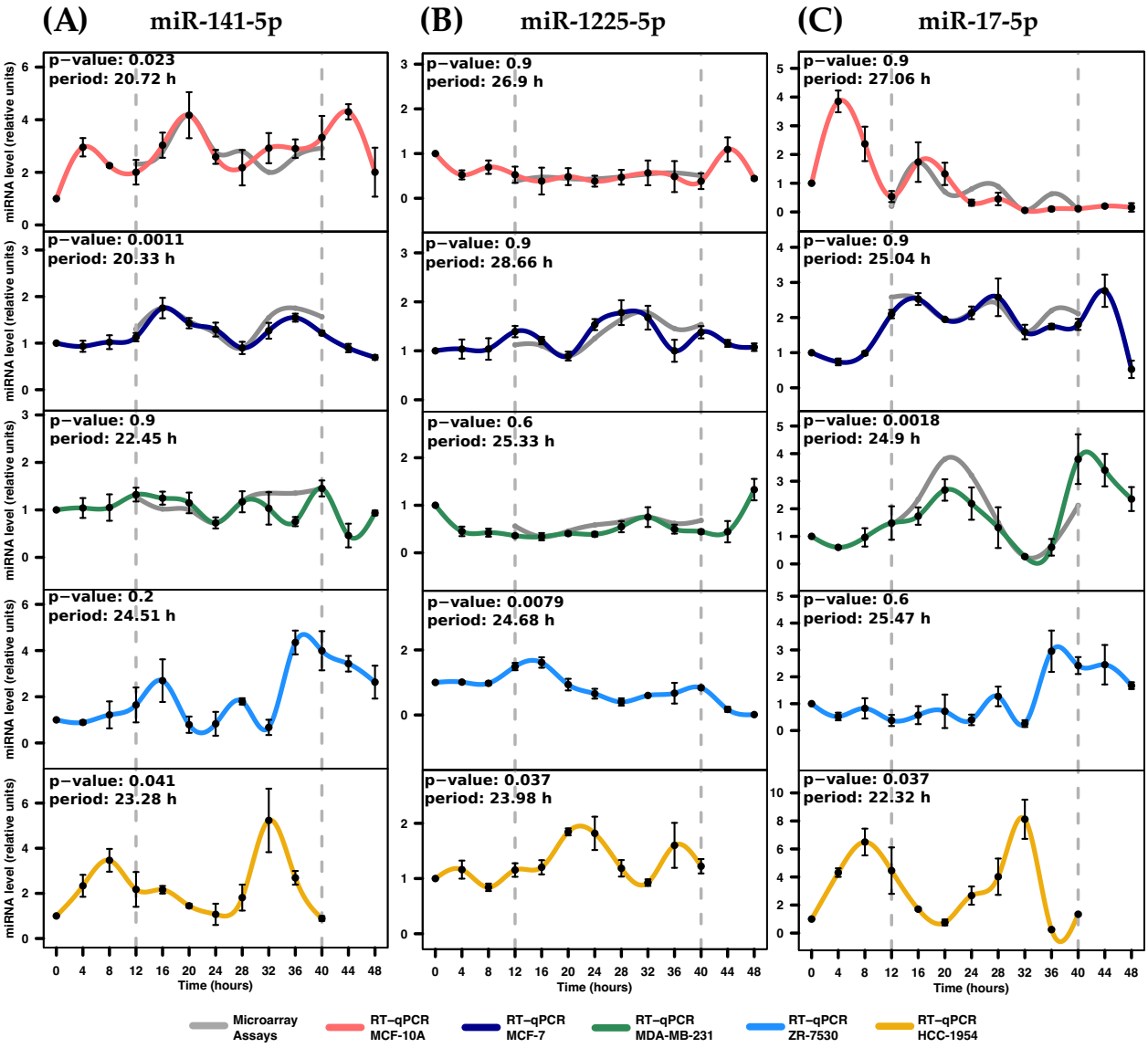

Figure 22. Expression profiles of miR-141-5p, miR-1225-5p, and miR-17-5p across breast cell lines. The rhythmic expression was evaluated by RT-qPCR assays in serum-shocked MCF-10A, MCF-7, MDA-MB-231, ZR-7530, and HCC-1954 cells over 48 h (4h intervals). (A) miR-141-5p exhibits rhythmic profiles in MCF-10A, MCF-7 and HCC-1954 cells; (B) miR-1225-5p exhibits rhythmic profiles in ZR-7530 and HCC-1954 cells; (C) miR-17-5p exhibits rhythmic profiles in MDA-MB-231 and HCC-1954 cells. Data points (means of three biological replicates ± standard error of the mean [SEM]) were normalized using miR-106a-5p relative to the first time point (*t* = 0). The *p*-value and period values of rhythmic profiles were obtained from the MetaCycle analysis and are illustrated at the top of each plot. Expression profiles with *p*-values less than 0.05 were considered rhythmic. For comparison purposes, the gray lines in the graphs concerning MCF-10A, MCF-7, and MDA-MB-231 illustrate the expression profiles obtained from the microarray data, which were scaled to the expression profile obtained from RT-qPCR assays. Dashed gray lines at 12 h and 40 h were added to show the period in which profiles were measured by microarray.

Furthermore, miR-769-3p displayed significant rhythmicity in MCF-7 and MDA-MB-231, both of which featured MetaCycle *p*-values close to 0.02 and demonstrated profiles consistent with those obtained from the microarray (see Figure 24A). Particularly, the temporal expression of this miRNA for MCF-7 exhibited lower amplitude. These results agreed with evidence showing that miRNA biogenesis is altered in cells with ERα over-expression [225]. In addition, one study evidenced that miR-769-3p can functionally regulate *NDRG1* upon reoxygenation in MCF-7 cells, thus, this evidence implies that miR-769-3p has a potential role in cancer cells were hypoxia is a cell condition [226]. While MDA-MB-231 are ERα-negative cells that presumably have different miRNA expression. Taken together, this evidence suggests that both cell lines share some inner mechanisms, despite the fact that they are distinct subtypes of breast cancer.

The miR-222-5p displayed rhythmicity in MCF-10A and MCF-7 cells with markedly distinct amplitudes (see Figure 24B). Previous studies reported that miR-222-5p plays a role in the regulation of ERα expression in breast cancer cells by promoting the transition from ER-positive to ER-negative tumors during the progression of cancer [227] and related to circadian clock outputs [228]. Taken together, this evidence suggests that miR-222-5p expression may participate in different mechanisms between both breast cell lines unknown as of yet.

The rhythmic expression of miR-548ay-3p was validated in MCF-10A and MDA-MB-231, but not in MCF-7 (see Figure 25). Interestingly, it also exhibited rhythmic patterns in ZR-7533 and HCC-1954. To date, no studies have investigated this miRNA because it was discovered only recently [229].

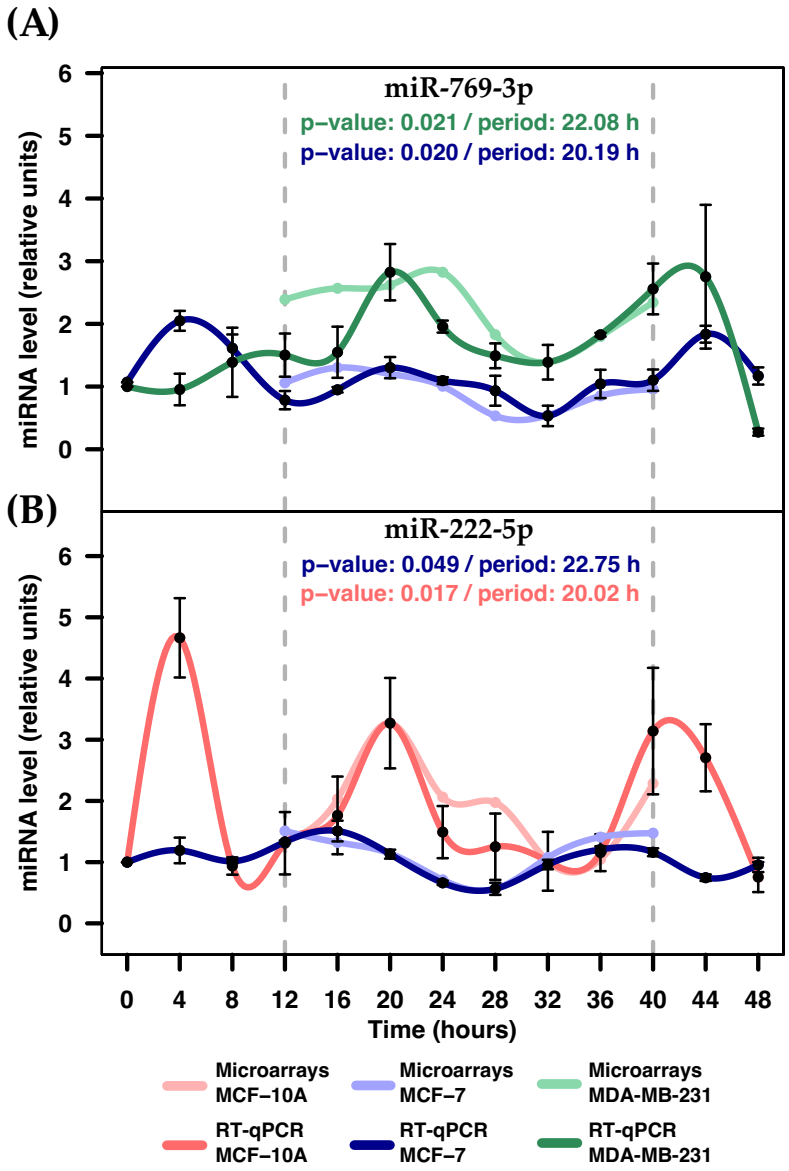

Figure 23 Expression profiles of miR-769-3p, miR-1225-5p, and miR-222-5p across MCF-10A, MCF-7 and MDA-MB-231 cells. The rhythmic expression was evaluated by RT-qPCR assays in serum-shocked MCF-10A, MCF-7, and MDA-MB-231 cells over 48 h (4 h intervals). (A) Rhythmic profiles of miR-769-3p exhibited in MCF-7 and MDA-MB-231 cells. (B) Rhythmic profiles of miR-222-5p exhibited in MCF-10A and MCF-7 cells. Data points (means of three biological replicates ± SEM) were normalized using miR-106a-5p relative to the first time point (*t* = 0). The *p*-values and period values of rhythmic profiles were obtained from MetaCycle analysis and are illustrated at the top of each plot. The *p*-values lesser than 0.05 were considered as rhythmic expression statistically significant. For comparison purposes, the more lightly colored lines illustrate the expression profiles obtained from microarray assays, which were scaled to the expression profiles obtained from RT-qPCR assays. Dashed gray lines at 12 and 40 h were added to show the periods in which the profiles were measured by microarrays.

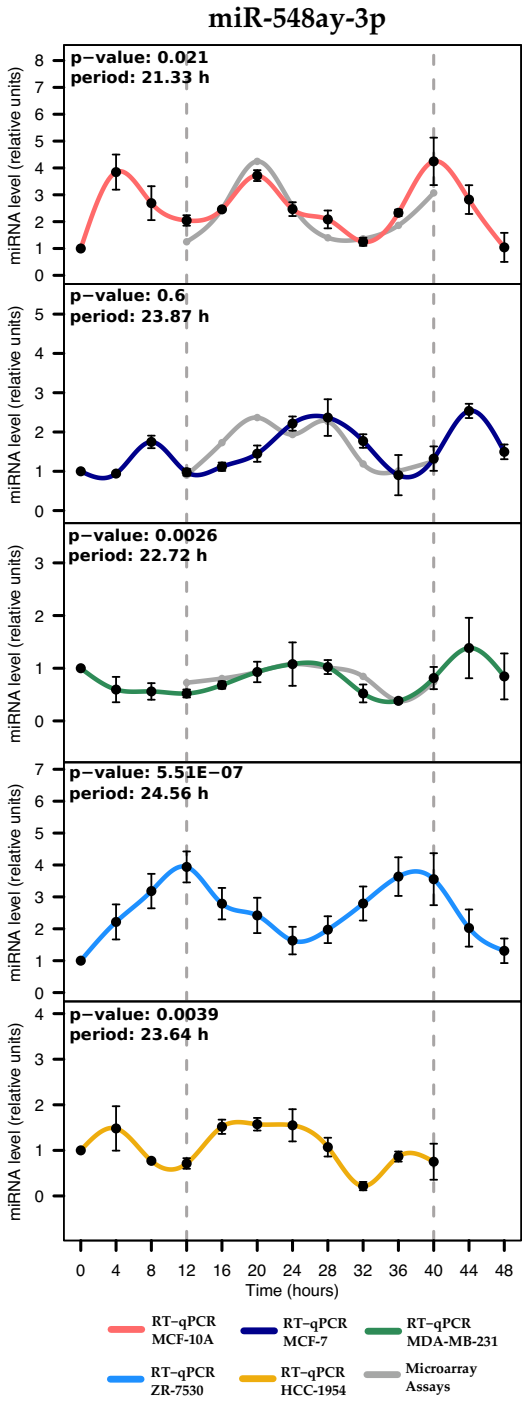

Figure 24 Expression profiles of miR-548ay-3p in MCF-10A, MCF-7, MDA-MB-231, ZR-7530 and HCC-1954 cells. The rhythmic expression was evaluated by RT-qPCR assays in serum-shocked 5 human breast cell lines over 48 h (4 h intervals). Data points (means of three biological replicates ± SEM) were normalized using miR-106a-5p relative to the first time point (*t* = 0). The *p*-values and period values of rhythmic profiles were obtained from MetaCycle analysis and are illustrated at the top of each plot. The *p*-values lesser than 0.05 were considered as rhythmic expression statistically significant. For comparison purposes, the more lightly colored lines illustrate the expression profiles obtained from microarray assays, which were scaled to the expression profiles obtained from RT-qPCR assays. Dashed gray lines at 12 and 40 h were added to show the periods in which the profiles were measured by microarrays.

4.3 Identification of the Target mRNAs in a Group of miRNAs

After the six miRNAs were validated, we sought their gene targets in multiMiR. It lists the gene targets that were experimentally validated for each miRNA. Of the six miRNAs, only miR-17-5p revealed targets (343 genes in total). We then performed an enrichment analysis using the Reactome enrichment tool, which identified 200 enriched pathways (see Appendix E). We observed the circadian clock pathways ($p = 0.0027$, FDR = 0.049, rank = 51) of five genes, MEF2D, PPP1CA, NPAS2, PER1, and RPS27A.

Chapter 5

Conclusions

Circadian rhythms of living organisms entrain to daily environmental cues such as light and dark. Thus, disruption between internal circadian rhythms in mammals and environmental cycles can induce physiological abnormalities, including, obesity, heart problems, cancer, etc. Light is a well-known stimulus for circadian entrainment where photic signals are transduced by a specific pathway to the transcriptional mechanism that can be mimicked by pharmacological manipulations or others. The findings presented in this dissertation consistently support the hypothesis that miRNAs present rhythmic expression among human breast cell lines, which were induced *in vitro* by horse serum. Although, there are several studies showing multiple significant miRNAs in breast cancer during last decades. However, this research support new evidence that miRNAs show different rhythmic expression pattern, and they need further research for understanding how them influence in breast tumorigenesis.

The rhythmic expression of miRNAs in breast cancer cell lines, representing the molecular breast cancer subtypes showed that each particular cell line responded differently to the horse serum shock stimulus. These findings suggest that mechanisms behind rhythmic expression might not be shared among breast cancer cells lines. That´s why, further investigation should be addressed to certainly identify how miRNAs act and influence in circadian clock. Additionally, new insights about this connection might support the research about the timing of drug, targeting molecular clock.

In conclusion, this research initiated with the cell synchronization, specifically, horse serum was the synchronizer agent, which set the inner circadian clock of human breast cultured cells. The results suggest that breast cells are able to respond to the synchronization stimulus might exert transcriptional control (induction) over genes and miRNAs (no limited to them) (see Figure 26), which further play roles in specific cell functions or as a feedback loop in the circadian system. The current research intents to

evidence that miRNAs might also present rhythmic behavior. It is unknown how this emerges, what is their contribution to tune specific cell functions, or their possible role in the feedback loop. This investigation intent to provide new insights that possibly supports the understanding of circadian mechanisms in breast cancer.

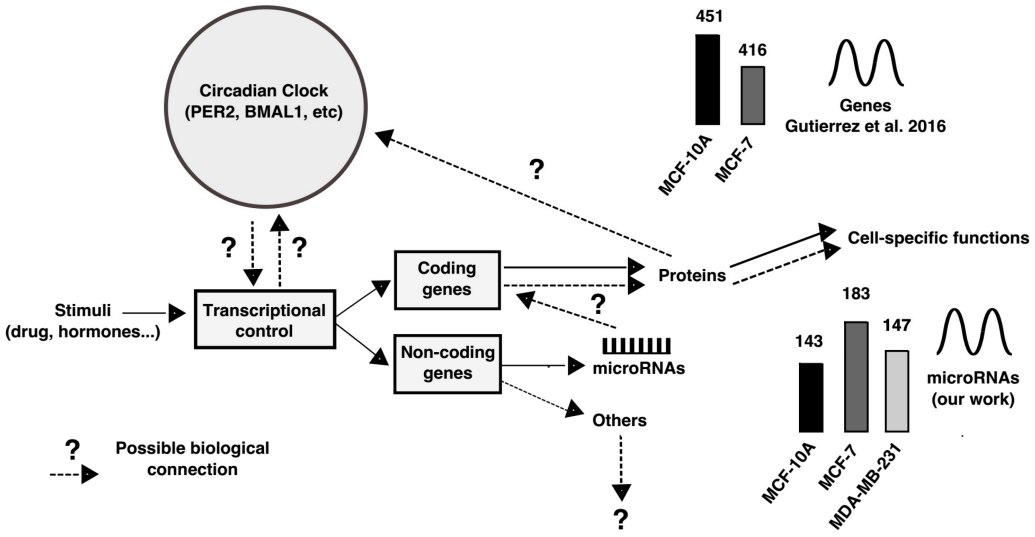

Figure 25. Overview of the interaction between circadian clock and miRNAs, specifically with rhythmicity. Continuous lines between concepts represent known facts. Dashed lines represent unknown information. Circadian control inspired in [230].

Possible future directions regarding this research are so many. Firstly, this research was an initiative for intending to evidence the multiple rhythmic expression patterns that can be found in miRNAs, specifically in human breast cell lines. The possible improvements can be divided according to objectives of the research:

The entrainment of human breast cell lines, this protocol used horse serum inducer, certainly, can be improved or even changed. Now, when research was performed, this procedure was a gold standard for initiative investigations about circadian expression of genes. We followed carefully the guidelines of previous PhD student, whom evidenced rhythmic expression of some genes in same cell lines. Thus, during next years, the scientific community demonstrated new roads for these kind investigations, such as luciferase assays, or even, in vivo studies. However, we strongly recommend studying

periods greater than 48 hours – we recommend 72 h -, as well as manage a group of people for achievement whole protocol.

Certainly, miRNA expression by microarrays was a valuable option in the moment when it was performed. However, during last years, emerged new technologies for screening whole miRNA expression, the RNAseq is valuable option, which limit some disadvantages of microarrays, even, appropriate costs. Additionally, it might provide better signal intensities, which was a technical issue that we found for nuRNA samples. At the moment, there are not many investigations about the understanding of potential rhythmic miRNAs from nuclear compartment. We encourage starting initiatives for this research line that could give more insights about miRNAs and circadian clock.

Additionally, the statistical procedure for analyzing rhythmic expression also require special attention. The use of cosine fitting function, or even any other related-method, needs to verify that function is appropriate for determining truly rhythmic expression, and not getting just random rhythmicity. Particularly, this research developed multiple decomposing data, which evidenced that cosine-fitting function are appropriate. However, we encourage in future investigations to having a parallel set control samples (experimentally), which means that our protocol for getting samples (cultured-cells) through a period should consider one set of samples that will be stimulated randomly or even, for each time point, thus, we can ensure those samples are correctly disturbed and will not have rhythmic expression.

Finally, the consideration of truly rhythmic expression needs to be mentioned carefully, because determined expression needs to be validated with other method, such as *in vivo* and validate these findings. One issue that we are aware is about amplitude of the temporal rhythmic patterns, since microarray to RT-qPCR, there is still a need to validate these kinds of findings.

Thus, based on previous recommendations, we presumably expect that our findings of this research will be replicated and confirmed, or even more, determined the understanding the behavior of miRNAs in breast cancer, and possible used for development of biomarkers.

Appendix A

Abbreviations and acronyms

Table A. 1 Abbreviations

Words	Description
TNBC	Triple Negative Breast Cancer
PER2	Period circadian clock 2
SERPINB1	Serpin family B member 1
ARNTL	Aryl hydrocarbon receptor nuclear translocator like
TL	Time-label
RW	Row-wise
CW	Column-wise
RCW	Row-column-wise
RCWB	Row-column-wise by blocks

Appendix B

mRNA expression performed in human breast cell lines

B 1 mRNA expression showed in MCF-10A cells

Time	CT (BMAL)	CT (GAPDH)	CT (PER2)	CT (GAPDH)
TIME-0	37.50	22.27	33.31	22.50
TIME-0	36.39	22.01	32.64	22.43
TIME-1	35.31	21.85	33.56	22.56
TIME-1	35.45	21.48	32.56	22.55
TIME-2	38.83	26.69	36.20	27.98
TIME-2	39.55	26.09	36.40	27.87
TIME-3	34.74	22.64	32.92	22.21
TIME-3	35.44	22.48	33.56	22.17
TIME-4	38.43	23.97	34.05	23.93
TIME-4	37.42	23.70	33.75	23.82
TIME-5	35.02	20.45	30.48	21.52
TIME-5	35.13	20.03	30.04	21.38
TIME-6	37.37	21.84	33.05	23.21
TIME-6	37.66	21.83	33.19	23.32
TIME-7	36.57	19.40	31.96	21.74
TIME-7	35.46	19.33	32.18	21.65
TIME-8	37.88	24.41	33.82	23.27
TIME-8	36.94	24.07	34.60	23.15
TIME-9	38.47	26.08	34.64	21.83
TIME-9	38.61	26.05	33.06	21.69
TIME-10	36.74	22.22	30.66	22.05
TIME-10	36.74	22.32	31.13	21.96
TIME-11	39.01	23.32	34.04	23.87
TIME-11	37.61	22.97	33.43	23.74
TIME-12	40.39	24.45	34.88	24.45
TIME-12	38.31	24.38	34.95	24.38
NC	Undetermined	Undetermined	Undetermined	Undetermined

B 2 mRNA expression showed in MCF-7 cells

Time	CT (BMAL)	CT (PER2)	CT (GAPDH)	CT (SERPINB1)	CT (GAPDH)
TIME-0	40.39	36.22	22.13	30.72	26.64
TIME-0	40.26	35.57	21.89	30.46	26.46
TIME-0	41.58	36.38	21.79	31.11	26.23
TIME-1	36.66	33.94	18.12	33.39	29.69
TIME-1	36.57	33.75	18.32	33.37	29.75
TIME-1	36.75	33.95	18.02	33.54	29.68
TIME-2	36.28	34.94	17.69	32.01	26.80
TIME-2	35.96	34.13	17.83	31.61	26.97
TIME-2	37.51	35.92	18.01	31.71	26.96
TIME-3	39.93	36.18	18.69	32.29	28.20
TIME-3	38.91	36.14	19.63	32.14	28.05
TIME-3	38.96	35.25	18.46	31.98	27.72
TIME-4	39.92	35.98	18.82	31.16	27.92
TIME-4	37.72	35.93	18.91	31.82	27.98
TIME-4	39.74	35.65	18.95	31.69	27.97
TIME-5	38.35	35.33	18.41	31.84	28.53
TIME-5	39.12	36.98	18.93	32.26	28.73
TIME-5	39.39	35.97	18.52	31.81	28.22
TIME-6	35.89	34.75	17.41	31.70	26.89
TIME-6	36.04	33.60	17.63	32.08	26.82
TIME-6	35.98	35.33	17.21	31.93	26.83
TIME-7	38.99	45.00	17.64	29.98	24.34
TIME-7	39.51	45.00	17.62	29.84	24.34
TIME-7	39.12	45.00	17.55	29.85	24.55
TIME-8	40.60	35.80	20.01	32.56	26.66
TIME-8	49.70	38.99	19.82	31.55	26.10
TIME-8	40.40	35.94	19.44	31.56	26.39
TIME-9	40.70	34.62	17.82	31.95	28.91
TIME-9	40.25	35.95	17.71	31.86	28.77
TIME-9	40.95	35.74	17.47	32.68	28.84
TIME-10	39.13	34.00	16.96	32.09	27.98
TIME-10	38.97	33.61	16.92	32.22	28.08
TIME-10	40.97	36.01	17.34	32.23	28.44
TIME-11	43.71	38.16	17.76	33.75	29.39
TIME-11	42.39	39.57	17.77	33.64	29.26
TIME-11	42.31	38.21	17.56	33.41	29.33

TIME-12	45.00	42.75	19.64	31.49	24.96
TIME-12	45.00	43.39	19.46	32.21	24.94
TIME-12	45.00	41.36	19.41	32.16	24.98
NC	Undetermined	Undetermined	Undetermined	Undetermined	Undetermined

B 3 mRNA expression showed in MDA-MB-231 cells

Time	CT (BMAL)	CT (GAPDH)	CT (PER2)	CT (GAPDH)
TIME-0	41.77	24.69	34.88	24.69
TIME-0	40.96	24.42	36.00	24.42
TIME-1	44.33	21.35	34.95	21.35
TIME-1	41.82	21.74	34.35	21.74
TIME-2	42.48	21.95	35.95	21.95
TIME-2	39.99	21.82	34.32	21.82
TIME-3	36.37	20.05	35.94	20.93
TIME-3	36.66	20.00	37.74	20.87
TIME-4	41.53	23.50	39.92	24.16
TIME-4	42.11	23.36	40.33	23.99
TIME-5	43.68	27.50	40.74	27.63
TIME-5	42.24	27.46	41.14	27.59
TIME-6	35.80	19.10	31.92	19.10
TIME-6	35.56	19.03	31.92	19.03
TIME-7	37.48	20.90	34.58	20.90
TIME-7	39.54	20.93	34.93	20.93
TIME-8	37.75	21.00	35.96	21.00
TIME-8	36.08	20.81	35.99	20.81
TIME-9	37.26	20.67	34.64	20.67
TIME-9	36.93	20.97	34.94	20.97
TIME-10	36.99	20.83	34.95	20.83
TIME-10	36.77	20.92	35.36	20.92
TIME-11	36.97	19.32	36.90	19.32
TIME-11	37.77	19.96	37.51	19.96
TIME-12	36.81	21.01	38.35	21.01
TIME-12	35.95	20.54	38.07	20.54
NC	Undetermined	Undetermined	Undetermined	Undetermined

B 4 mRNA expression showed in ZR-7530 cells

Time	CT (BMAL)	CT (GAPDH)	CT (PER2)	CT (GAPDH)
TIME-0	38.35	20.78	32.30	20.78
TIME-0	38.12	20.53	31.70	20.53
TIME-1	35.94	20.25	39.25	20.25
TIME-1	35.96	19.85	40.45	19.85
TIME-2	35.13	18.54	27.59	18.54
TIME-2	35.24	18.21	27.67	18.21
TIME-3	34.32	17.93	31.28	17.93
TIME-3	34.00	17.94	31.36	17.94
TIME-4	39.45	20.62	31.34	20.62
TIME-4	41.09	20.11	31.01	20.11
TIME-5	37.27	19.36	33.15	19.36
TIME-5	37.49	19.27	33.40	19.27
TIME-6	34.20	18.94	30.33	18.94
TIME-6	34.45	18.85	30.52	18.85
TIME-7	33.66	18.55	31.89	18.55
TIME-7	34.21	18.42	31.84	18.42
TIME-8	34.20	19.33	34.86	19.33
TIME-8	34.21	19.23	34.20	19.23
TIME-9	33.50	18.32	31.54	18.32
TIME-9	33.88	18.27	31.90	18.27
TIME-10	38.23	20.04	34.89	20.04
TIME-10	37.41	20.11	34.68	20.11
TIME-11	36.37	20.57	34.90	20.57
TIME-11	36.66	20.48	34.52	20.48
TIME-12	36.60	20.68	40.60	20.68
TIME-12	36.03	20.31	39.99	20.31
NC	Undetermined	Undetermined	Undetermined	Undetermined

B 5 mRNA expression showed in HC-1954 cells

Time	CT (BMAL)	CT (GAPDH)	CT (PER2)	CT (GAPDH)
TIME-0	37.99	22.85	38.08	22.85
TIME-0	38.91	22.58	37.52	22.58
TIME-1	35.56	19.87	35.95	19.87
TIME-1	35.93	19.96	34.19	19.96
TIME-2	33.98	18.59	31.87	18.59
TIME-2	32.88	18.93	31.57	18.93
TIME-3	34.94	18.87	33.27	18.87
TIME-3	35.91	18.44	33.58	18.44
TIME-4	34.96	19.69	33.75	19.69
TIME-4	35.40	20.00	33.06	20.00
TIME-5	34.94	19.35	33.71	19.35
TIME-5	34.61	19.96	33.93	19.96
TIME-6	35.93	18.60	34.95	18.60
TIME-6	35.44	19.99	34.91	19.99
TIME-7	34.58	18.91	33.66	18.91
TIME-7	33.93	18.52	32.99	18.52
TIME-8	31.96	19.30	31.50	19.30
TIME-8	31.79	19.31	31.17	19.31
TIME-9	32.93	19.30	33.18	19.30
TIME-9	32.58	19.39	32.56	19.39
TIME-10	33.94	19.46	32.39	19.46
TIME-10	33.83	20.46	32.42	20.46
NC	Undetermined	Undetermined	Undetermined	Undetermined

Appendix C

Circadian Features of miRNAs obtained from cosine-fitting function

C 6 Circadian features of the miRNA expression profiles from cosine-fitting function in MCF-10A.

miRNA	probe ID	cosine correlation	period	phase	amplitude	cluster
miR-1273e	A_25_P00016226	0.837	0.241	1.122	0.16	1
miR-191-3p	A_25_P00010878	0.883	0.237	1.104	0.19	1
miR-196b-3p	A_25_P00015383	0.867	0.283	1.475	0.07	1
miR-204-3p	A_25_P00017403	0.830	0.289	0.753	0.06	1
miR-20b-3p	A_25_P00013574	0.842	0.248	0.891	0.16	1
miR-23c	A_25_P00016198	0.875	0.276	1.928	0.06	1
miR-27b-5p	A_25_P00013377	0.846	0.235	0.988	0.16	1
miR-323b-5p	A_25_P00012440	0.849	0.286	1.195	0.11	1
miR-3622b-3p	A_25_P00016091	0.895	0.257	0.658	0.06	1
miR-3687	A_25_P00016033	0.823	0.237	1.654	0.08	1
miR-3689f	A_25_P00017126	0.821	0.233	2.284	0.06	1
miR-3908	A_25_P00015990	0.829	0.274	0.341	0.08	1
miR-4253	A_25_P00015539	0.830	0.269	0.149	0.08	1
miR-4456	A_25_P00016281	0.894	0.245	1.128	0.09	1
miR-4652-3p	A_25_P00017178	0.841	0.254	1.396	0.13	1
miR-4738-5p	A_25_P00016564	0.824	0.255	1.077	0.11	1
miR-548aa	A_25_P00016262	0.850	0.270	1.065	0.07	1
miR-548am-5p	A_25_P00012797	0.894	0.272	0.537	0.09	1
miR-548b-3p	A_25_P00010122	0.828	0.240	1.190	0.08	1
miR-552-3p	A_25_P00011479	0.851	0.240	1.323	0.11	1
miR-554	A_25_P00011289	0.916	0.249	0.834	0.08	1
miR-5572	A_25_P00017423	0.847	0.280	1.529	0.08	1
miR-5581-3p	A_25_P00017621	0.892	0.227	1.201	0.05	1
miR-760	A_25_P00013023	0.934	0.300	0.005	0.05	1
miR-10a-3p	A_25_P00013300	0.872	0.278	-0.176	0.08	2
miR-133a-3p	A_25_P00012167	0.830	0.239	0.496	0.06	2
miR-216b-5p	A_25_P00013029	0.835	0.232	0.740	0.08	2
miR-3147	A_25_P00015806	0.964	0.275	-0.068	0.07	2
miR-3169	A_25_P00015687	0.958	0.269	0.158	0.1	2
miR-34c-3p	A_25_P00012289	0.902	0.257	0.414	0.11	2
miR-3687	A_25_P00016032	0.881	0.232	0.792	0.05	2
miR-374b-3p	A_25_P00013680	0.909	0.270	-0.343	0.12	2

miR-4309	A_25_P00015857	0.931	0.229	0.102	0.11	2
miR-432-3p	A_25_P00010355	0.914	0.252	0.122	0.06	2
miR-4529-5p	A_25_P00017271	0.973	0.225	0.892	0.14	2
miR-4724-3p	A_25_P00016410	0.837	0.235	0.786	0.05	2
miR-4795-3p	A_25_P00016548	0.917	0.251	0.441	0.1	2
miR-503-5p	A_25_P00010658	0.844	0.282	-0.268	0.08	2
miR-519e-3p	A_25_P00012524	0.995	0.226	0.666	0.11	2
miR-5580-3p	A_25_P00017645	0.971	0.262	0.027	0.07	2
miR-5692b	A_25_P00017386	0.911	0.257	0.272	0.11	2
miR-6082	A_25_P00017900	0.852	0.252	0.302	0.05	2
miR-647	A_25_P00011370	0.930	0.296	-0.447	0.2	2
miR-873-5p	A_25_P00013008	0.837	0.289	0.008	0.19	2
miR-1271-5p	A_25_P00015043	0.928	0.242	-0.252	0.09	3
miR-150-5p	A_25_P00014847	0.884	0.299	-1.240	0.16	3
miR-20a-3p	A_25_P00013170	0.942	0.276	-0.940	0.06	3
miR-297	A_25_P00013108	0.970	0.258	-0.566	0.09	3
miR-3137	A_25_P00015538	0.969	0.248	-0.737	0.06	3
miR-3166	A_25_P00015802	0.882	0.290	-0.860	0.07	3
miR-3178	A_25_P00015670	0.845	0.229	0.148	0.09	3
miR-3617-5p	A_25_P00016108	0.860	0.274	-0.513	0.11	3
miR-383-5p	A_25_P00010384	0.838	0.280	-0.671	0.07	3
miR-4633-3p	A_25_P00017193	0.824	0.299	-1.091	0.06	3
miR-4652-5p	A_25_P00017075	0.854	0.259	-0.085	0.05	3
miR-4673	A_25_P00017120	0.906	0.278	-0.664	0.08	3
miR-4695-5p	A_25_P00016742	0.832	0.287	-0.659	0.08	3
miR-509-3p	A_25_P00012678	0.852	0.255	0.062	0.05	3
miR-548a-3p	A_25_P00014240	0.894	0.294	-1.183	0.18	3
miR-5683	A_25_P00017565	0.980	0.243	-0.068	0.08	3
miR-6072	A_25_P00017833	0.839	0.274	-0.872	0.05	3
miR-615-3p	A_25_P00012788	0.839	0.258	-0.444	0.16	3
miR-657	A_25_P00011359	0.842	0.296	-1.090	0.24	3
miR-888-3p	A_25_P00013661	0.885	0.296	-1.024	0.06	3
miR-888-5p	A_25_P00012939	0.892	0.268	-0.207	0.12	3
miR-9-5p	A_25_P00011003	0.846	0.253	-1.001	0.06	3
miR-942-5p	A_25_P00013097	0.919	0.280	-0.897	0.08	3
dmr_285		0.842	0.280	-1.603	0.06	4
miR-2277-5p	A_25_P00016164	0.833	0.293	-1.733	0.07	4
miR-27a-5p	A_25_P00013203	0.986	0.241	-0.945	0.16	4
miR-3607-3p	A_25_P00016097	0.822	0.275	-1.539	0.06	4
miR-3935	A_25_P00016203	0.881	0.239	-1.200	0.09	4

miR-450b-5p	A_25_P00012908	0.924	0.280	-1.607	0.07	4
miR-4746-3p	A_25_P00017145	0.872	0.295	-1.246	0.08	4
miR-548m	A_25_P00015184	0.847	0.241	-0.873	0.08	4
miR-589-5p	A_25_P00012761	0.860	0.272	-1.203	0.06	4
miR-6511a-5p	A_25_P00017819	0.956	0.291	-1.880	0.08	4
miR-6715b-5p	A_25_P00017971	0.853	0.254	-1.332	0.08	4
miR-889-3p	A_25_P00012949	0.835	0.239	-0.937	0.17	4
miR-944	A_25_P00013105	0.927	0.233	-1.170	0.16	4
let-7g-3p	A_25_P00013362	0.974	0.261	-2.109	0.07	5
miR-1269b	A_25_P00016688	0.821	0.261	-1.987	0.08	5
miR-140-3p	A_25_P00012176	0.914	0.260	-2.683	0.05	5
miR-141-5p	A_25_P00013414	0.826	0.266	-2.300	0.23	5
miR-193a-3p	A_25_P00012258	0.952	0.234	-1.737	0.12	5
miR-222-5p	A_25_P00013351	0.916	0.258	-2.284	0.08	5
miR-224-3p	A_25_P00015401	0.837	0.281	-2.386	0.09	5
miR-301a-5p	A_25_P00017444	0.830	0.252	-2.386	0.08	5
miR-302b-3p	A_25_P00010618	0.853	0.267	-2.071	0.16	5
miR-3129-3p	A_25_P00016905	0.829	0.263	-1.639	0.12	5
miR-3152-3p	A_25_P00015884	0.897	0.247	-1.536	0.05	5
miR-330-5p	A_25_P00012346	0.857	0.231	-1.614	0.05	5
miR-3615	A_25_P00016166	0.926	0.226	-1.627	0.06	5
miR-363-3p	A_25_P00010953	0.860	0.230	-1.793	0.06	5
miR-3681-5p	A_25_P00016174	0.853	0.257	-1.663	0.06	5
miR-3942-3p	A_25_P00016582	0.855	0.270	-2.587	0.11	5
miR-3973	A_25_P00016792	0.864	0.234	-1.318	0.06	5
miR-4286	A_25_P00015773	0.923	0.251	-2.734	0.27	5
miR-4511	A_25_P00016505	0.837	0.271	-2.782	0.07	5
miR-4697-5p	A_25_P00016630	0.904	0.279	-2.331	0.05	5
miR-4760-5p	A_25_P00016788	0.884	0.251	-2.418	0.13	5
miR-4766-5p	A_25_P00016303	0.840	0.291	-2.645	0.07	5
miR-4804-3p	A_25_P00017321	0.836	0.289	-2.540	0.07	5
miR-515-5p	A_25_P00010499	0.835	0.251	-2.071	0.12	5
miR-548ay-3p	A_25_P00017966	0.942	0.284	-2.360	0.05	5
miR-5572	A_25_P00017424	0.992	0.238	-1.505	0.05	5
miR-766-3p	A_25_P00011410	0.863	0.236	-1.501	0.11	5
miR-891a-5p	A_25_P00012881	0.831	0.266	-1.823	0.12	5
miR-921	A_25_P00013042	0.880	0.225	-1.570	0.08	5
miR-127-5p	A_25_P00012219	0.929	0.252	-2.529	0.07	6
miR-129-5p	A_25_P00013880	0.951	0.238	-2.271	0.06	6
miR-132-5p	A_25_P00013400	0.879	0.232	-1.832	0.05	6

miR-181b-5p	A_25_P00012089	0.821	0.225	-2.917	0.07	6
miR-200a-5p	A_25_P00011010	0.859	0.250	-2.114	0.07	6
miR-212-3p	A_25_P00010854	0.827	0.226	-2.944	0.12	6
miR-29a-5p	A_25_P00013209	0.871	0.285	3.142	0.05	6
miR-3177-5p	A_25_P00016485	0.860	0.245	-3.142	0.06	6
miR-3202	A_25_P00015596	0.888	0.278	-2.608	0.06	6
miR-324-5p	A_25_P00010153	0.863	0.264	-2.810	0.05	6
miR-34a-3p	A_25_P00013311	0.919	0.239	-2.585	0.09	6
miR-3612	A_25_P00016230	0.849	0.224	-3.142	0.12	6
miR-3619-5p	A_25_P00016183	0.957	0.235	-2.010	0.14	6
miR-367-3p	A_25_P00010985	0.902	0.238	-2.295	0.08	6
miR-3674	A_25_P00016190	0.872	0.260	-2.534	0.06	6
miR-371a-3p	A_25_P00013992	0.864	0.279	3.138	0.07	6
miR-3939	A_25_P00016163	0.821	0.270	2.929	0.05	6
miR-3978	A_25_P00016369	0.847	0.295	-2.352	0.09	6
miR-4254	A_25_P00015728	0.881	0.280	2.619	0.12	6
miR-4432	A_25_P00016498	0.885	0.289	-2.494	0.06	6
miR-4440	A_25_P00016616	0.832	0.290	2.781	0.06	6
miR-4498	A_25_P00016649	0.842	0.242	-2.719	0.05	6
miR-4652-3p	A_25_P00017179	0.866	0.248	-2.467	0.09	6
miR-4723-5p	A_25_P00017205	0.887	0.258	-2.245	0.05	6
miR-4803	A_25_P00017101	0.854	0.277	3.089	0.08	6
miR-5006-3p	A_25_P00017548	0.929	0.236	-3.142	0.07	6
miR-501-3p	A_25_P00012640	0.853	0.295	-3.075	0.09	6
miR-548au-5p	A_25_P00017584	0.836	0.254	-3.032	0.07	6
miR-548b-5p	A_25_P00012756	0.933	0.269	-2.969	0.11	6
miR-5588-3p	A_25_P00017615	0.852	0.256	-2.407	0.06	6
miR-646	A_25_P00011963	0.845	0.245	-2.894	0.18	6
miR-891a-5p	A_25_P00012882	0.936	0.262	-2.305	0.07	6
miR-943	A_25_P00013101	0.945	0.238	-1.906	0.06	6
miR-98-3p	A_25_P00017910	0.849	0.274	2.601	0.05	6

C 7 Circadian features of the miRNA expression profiles from cosine-fitting function in MCF-7.

11	agilent probe ID	cosine correlation	period	phase	amplitude	cluster

miR-10a-3p	A_25_P00013302	0.828	0.241	1.026	0.13	1
miR-1185-1-3p	A_25_P00017447	0.943	0.237	2.010	0.08	1
miR-1207-5p	A_25_P00015088	0.825	0.224	2.131	0.11	1
miR-1225-5p	A_25_P00014920	0.949	0.225	1.879	0.23	1
miR-1234-5p	A_25_P00017828	0.842	0.281	1.922	0.4	1
miR-1299	A_25_P00015122	0.863	0.275	0.921	0.08	1
miR-28-3p	A_25_P00012006	0.846	0.258	0.947	0.12	1
miR-3121-3p	A_25_P00015873	0.837	0.248	1.300	0.06	1
miR-3165	A_25_P00015847	0.888	0.265	1.253	0.07	1
miR-320e	A_25_P00015664	0.859	0.293	0.493	0.08	1
miR-3620-3p	A_25_P00016148	0.863	0.226	1.737	0.07	1
miR-378j	A_25_P00017982	0.847	0.281	1.183	0.09	1
miR-3928-3p	A_25_P00016175	0.880	0.253	2.115	0.05	1
miR-4294	A_25_P00015651	0.902	0.268	1.844	0.05	1
miR-4472	A_25_P00016275	0.877	0.253	1.407	0.09	1
miR-4507	A_25_P00016700	0.911	0.248	1.795	0.28	1
miR-4530	A_25_P00016774	0.921	0.224	2.208	0.38	1
miR-4534	A_25_P00016446	0.836	0.290	1.840	0.18	1
miR-4639-3p	A_25_P00016894	0.882	0.234	1.641	0.05	1
miR-4672	A_25_P00017202	0.831	0.237	1.962	0.44	1
miR-4699-3p	A_25_P00016970	0.826	0.261	2.418	0.09	1
miR-4701-3p	A_25_P00016366	0.922	0.243	1.161	0.05	1
miR-4712-3p	A_25_P00016524	0.952	0.281	1.734	0.09	1
miR-4725-5p	A_25_P00017000	0.894	0.297	0.678	0.05	1
miR-4764-3p	A_25_P00016695	0.861	0.243	1.425	0.06	1
miR-4787-5p	A_25_P00016992	0.831	0.274	1.320	0.07	1
miR-4793-5p	A_25_P00016728	0.864	0.239	0.989	0.06	1
miR-548b-5p	A_25_P00012756	0.840	0.266	1.278	0.12	1
miR-549a	A_25_P00010365	0.901	0.249	1.333	0.12	1
miR-562	A_25_P00011389	0.897	0.269	0.737	0.16	1
miR-6087	A_25_P00017892	0.837	0.255	2.388	0.49	1
miR-764	A_25_P00015440	0.834	0.262	1.129	0.07	1
miR-940	A_25_P00013090	0.833	0.299	0.606	0.05	1
miR-10a-3p	A_25_P00013301	0.898	0.253	0.326	0.08	2
miR-1206	A_25_P00015086	0.827	0.276	0.096	0.09	2
miR-1238-5p	A_25_P00017772	0.838	0.279	0.128	0.06	2
miR-127-5p	A_25_P00012221	0.865	0.299	-0.246	0.1	2
miR-1304-3p	A_25_P00017635	0.839	0.235	0.832	0.08	2
miR-188-5p	A_25_P00012246	0.852	0.294	0.406	0.07	2

miR-2116-3p	A_25_P00015463	0.832	0.261	0.565	0.11	2
miR-222-3p	A_25_P00012126	0.854	0.294	-0.450	0.19	2
miR-3185	A_25_P00015654	0.918	0.263	0.336	0.1	2
miR-335-3p	A_25_P00013557	0.948	0.275	0.138	0.05	2
miR-3944-5p	A_25_P00017159	0.829	0.254	0.206	0.07	2
miR-4313	A_25_P00015772	0.837	0.261	0.375	0.06	2
miR-452-3p	A_25_P00013583	0.890	0.235	0.323	0.07	2
miR-4520-2-3p	A_25_P00016398	0.890	0.287	-0.112	0.05	2
miR-4529-5p	A_25_P00017271	0.864	0.269	0.458	0.05	2
miR-4723-5p	A_25_P00017205	0.867	0.233	0.535	0.08	2
miR-5047	A_25_P00016399	0.845	0.253	0.567	0.1	2
miR-525-3p	A_25_P00012549	0.896	0.234	0.684	0.07	2
miR-548x-3p	A_25_P00016860	0.964	0.240	0.613	0.06	2
miR-550a-5p	A_25_P00012768	0.909	0.240	0.810	0.18	2
miR-554	A_25_P00011288	0.853	0.250	0.665	0.18	2
miR-5704	A_25_P00017598	0.870	0.256	0.662	0.08	2
miR-708-3p	A_25_P00013671	0.865	0.297	-0.090	0.09	2
miR-744-3p	A_25_P00013675	0.879	0.260	0.519	0.24	2
miR-876-5p	A_25_P00012961	0.831	0.234	1.041	0.12	2
miR-935	A_25_P00013071	0.825	0.285	-0.272	0.09	2
miR-1262	A_25_P00015178	0.950	0.233	-0.215	0.05	3
miR-129-1-3p	A_25_P00013277	0.893	0.262	-0.846	0.06	3
miR-1295b-3p	A_25_P00017728	0.891	0.300	-1.082	0.06	3
miR-181d-5p	A_25_P00012514	0.823	0.289	-0.820	0.11	3
miR-191-5p	A_25_P00012203	0.837	0.296	-1.556	0.08	3
miR-203b-3p	A_25_P00017122	0.939	0.243	-0.070	0.05	3
miR-219b-5p	A_25_P00016753	0.935	0.293	-0.609	0.08	3
miR-222-5p	A_25_P00013351	0.979	0.252	-0.427	0.07	3
miR-3123	A_25_P00015736	0.871	0.276	-1.069	0.05	3
miR-3182	A_25_P00015725	0.888	0.268	-0.476	0.09	3
miR-32-5p	A_25_P00012021	0.899	0.257	-1.006	0.12	3
miR-3622a-3p	A_25_P00016014	0.854	0.245	-0.612	0.08	3
miR-367-3p	A_25_P00010984	0.867	0.284	-1.240	0.07	3
miR-412-3p	A_25_P00010266	0.869	0.252	-0.311	0.16	3
miR-4427	A_25_P00016416	0.938	0.281	-1.257	0.08	3
miR-4429	A_25_P00016765	0.923	0.283	-1.753	0.07	3
miR-4433-5p	A_25_P00017390	0.866	0.273	-0.553	0.05	3
miR-4441	A_25_P00017055	0.987	0.234	-0.543	0.05	3
miR-4643	A_25_P00017260	0.827	0.274	-0.635	0.08	3

miR-4743-5p	A_25_P00016575	0.884	0.260	-0.490	0.08	3
miR-4764-5p	A_25_P00016450	0.821	0.282	-1.015	0.11	3
miR-4769-3p	A_25_P00017011	0.836	0.273	-1.318	0.1	3
miR-4786-5p	A_25_P00016997	0.924	0.300	-1.906	0.05	3
miR-499b-5p	A_25_P00017168	0.862	0.290	-0.732	0.08	3
miR-542-5p	A_25_P00012858	0.879	0.293	-0.878	0.07	3
miR-548az-5p	A_25_P00017868	0.951	0.280	-0.900	0.08	3
miR-551a	A_25_P00011473	0.941	0.239	-0.694	0.07	3
miR-551a	A_25_P00011638	0.953	0.254	-0.527	0.09	3
miR-553	A_25_P00011219	0.825	0.294	-1.794	0.12	3
miR-556-3p	A_25_P00012717	0.919	0.266	-0.864	0.08	3
miR-614	A_25_P00010535	0.867	0.223	-0.231	0.09	3
miR-628-5p	A_25_P00012814	0.838	0.297	-1.093	0.07	3
miR-6505-3p	A_25_P00017858	0.930	0.256	-0.853	0.1	3
miR-106b-3p	A_25_P00013479	0.846	0.281	-1.044	0.13	4
miR-1184	A_25_P00015066	0.910	0.276	-1.799	0.06	4
miR-1225-3p	A_25_P00014924	0.884	0.245	-0.967	0.1	4
miR-1236-3p	A_25_P00014955	0.955	0.267	-1.833	0.09	4
miR-1236-3p	A_25_P00014956	0.879	0.261	-1.480	0.09	4
miR-155-3p	A_25_P00013471	0.899	0.262	-1.900	0.07	4
miR-16-1-3p	A_25_P00013145	0.890	0.270	-1.836	0.07	4
miR-191-5p	A_25_P00012202	0.883	0.269	-1.784	0.17	4
miR-223-5p	A_25_P00013355	0.834	0.224	-0.963	0.08	4
miR-302d-5p	A_25_P00013516	0.853	0.279	-1.706	0.13	4
miR-30b-3p	A_25_P00013381	0.832	0.280	-1.961	0.06	4
miR-30c-2-3p	A_25_P00013287	0.919	0.297	-2.394	0.05	4
miR-32-3p	A_25_P00013217	0.958	0.241	-1.072	0.08	4
miR-363-5p	A_25_P00010043	0.922	0.263	-1.348	0.09	4
miR-3908	A_25_P00015990	0.877	0.253	-0.824	0.08	4
miR-4419a	A_25_P00017190	0.830	0.231	-1.450	0.07	4
miR-4537	A_25_P00016657	0.908	0.253	-1.535	0.14	4
miR-4663	A_25_P00016419	0.878	0.256	-1.388	0.06	4
miR-5089-5p	A_25_P00017582	0.827	0.228	-1.517	0.1	4
miR-518c-5p	A_25_P00012559	0.948	0.245	-0.972	0.06	4
miR-548ae-3p	A_25_P00017682	0.879	0.280	-1.601	0.11	4
miR-548at-5p	A_25_P00017425	0.929	0.266	-1.833	0.09	4
miR-5584-3p	A_25_P00017368	0.955	0.257	-1.430	0.05	4
miR-610	A_25_P00011025	0.836	0.255	-1.451	0.13	4
miR-620	A_25_P00010450	0.854	0.236	-0.977	0.06	4

miR-769-3p	A_25_P00011231	0.962	0.223	-1.144	0.16	4
miR-892c-3p	A_25_P00017937	0.923	0.269	-1.593	0.11	4
miR-105-5p	A_25_P00012041	0.847	0.246	-1.730	0.09	5
miR-1273c	A_25_P00015723	0.830	0.223	-1.123	0.1	5
miR-138-1-3p	A_25_P00013440	0.892	0.240	-1.702	0.16	5
miR-152-3p	A_25_P00012196	0.880	0.249	-2.018	0.07	5
miR-187-5p	A_25_P00013327	0.929	0.235	-1.825	0.09	5
miR-193b-5p	A_25_P00013597	0.899	0.262	-2.359	0.08	5
miR-202-3p	A_25_P00014864	0.825	0.224	-1.848	0.05	5
miR-206	A_25_P00010528	0.928	0.236	-1.863	0.07	5
miR-27b-5p	A_25_P00013378	0.861	0.235	-1.484	0.21	5
miR-302b-3p	A_25_P00010618	0.925	0.249	-1.929	0.07	5
miR-3132	A_25_P00015821	0.822	0.238	-1.781	0.07	5
miR-320a	A_25_P00012262	0.926	0.254	-2.209	0.05	5
miR-3622b-5p	A_25_P00016219	0.837	0.235	-1.291	0.06	5
miR-3650	A_25_P00016185	0.860	0.281	-2.343	0.05	5
miR-3654	A_25_P00016268	0.864	0.227	-1.210	0.05	5
miR-3660	A_25_P00016217	0.824	0.235	-1.818	0.09	5
miR-3688-3p	A_25_P00016048	0.870	0.226	-1.298	0.1	5
miR-4262	A_25_P00015626	0.892	0.241	-1.559	0.05	5
miR-4304	A_25_P00015850	0.928	0.226	-1.853	0.1	5
miR-4447	A_25_P00016283	0.916	0.265	-1.676	0.06	5
miR-4483	A_25_P00016607	0.824	0.295	-2.363	0.09	5
miR-4499	A_25_P00017132	0.831	0.233	-1.811	0.06	5
miR-4724-5p	A_25_P00016749	0.854	0.256	-2.459	0.08	5
miR-4758-5p	A_25_P00016654	0.847	0.243	-2.269	0.06	5
miR-4774-5p	A_25_P00017266	0.874	0.227	-1.906	0.08	5
miR-4789-5p	A_25_P00016661	0.846	0.277	-2.067	0.14	5
miR-488-5p	A_25_P00014633	0.950	0.248	-2.090	0.05	5
miR-548ab	A_25_P00016460	0.894	0.241	-1.904	0.09	5
miR-548ae-3p	A_25_P00017681	0.842	0.252	-2.102	0.16	5
miR-551b-5p	A_25_P00013620	0.914	0.268	-2.335	0.05	5
miR-5588-5p	A_25_P00017336	0.902	0.270	-2.352	0.05	5
miR-569	A_25_P00010313	0.882	0.227	-1.268	0.09	5
miR-6499-5p	A_25_P00017751	0.861	0.266	-1.897	0.06	5
miR-660-5p	A_25_P00010459	0.855	0.293	-2.955	0.09	5
miR-664a-3p	A_25_P00015251	0.887	0.291	-2.336	0.06	5
miR-99a-5p	A_25_P00010471	0.913	0.273	-2.390	0.07	5
miR-1179	A_25_P00015056	0.899	0.263	-2.990	0.05	6

miR-1228-5p	A_25_P00015006	0.910	0.240	-2.358	0.07	6
miR-1269b	A_25_P00016688	0.982	0.273	-2.827	0.05	6
miR-1468-5p	A_25_P00015296	0.905	0.271	-3.142	0.05	6
miR-148a-5p	A_25_P00013281	0.942	0.273	-2.902	0.06	6
miR-3115	A_25_P00015534	0.831	0.244	-2.415	0.06	6
miR-3156-3p	A_25_P00016435	0.882	0.249	-2.723	0.05	6
miR-3615	A_25_P00016166	0.859	0.248	-3.065	0.07	6
miR-363-5p	A_25_P00010041	0.838	0.263	-3.003	0.08	6
miR-4804-3p	A_25_P00017320	0.860	0.300	2.979	0.1	6
miR-483-5p	A_25_P00012459	0.858	0.277	2.279	0.05	6
miR-5190	A_25_P00017704	0.926	0.224	-2.994	0.06	6
miR-5197-3p	A_25_P00017465	0.926	0.232	-2.150	0.05	6
miR-526b-3p	A_25_P00010784	0.835	0.237	-2.798	0.08	6
miR-548at-5p	A_25_P00017427	0.890	0.247	-2.477	0.09	6
miR-548ay-3p	A_25_P00017966	0.916	0.234	-2.554	0.07	6
miR-548h-3p	A_25_P00016243	0.841	0.268	3.142	0.05	6
miR-548i	A_25_P00015225	0.937	0.277	-2.788	0.07	6
miR-5586-5p	A_25_P00017601	0.840	0.299	2.702	0.08	6
miR-570-3p	A_25_P00012721	0.891	0.225	-2.360	0.07	6
miR-580-3p	A_25_P00011353	0.877	0.297	2.246	0.08	6
miR-581	A_25_P00011283	0.839	0.256	-2.931	0.06	6
miR-6083	A_25_P00017802	0.926	0.292	2.390	0.07	6
miR-6128	A_25_P00017984	0.896	0.261	-2.655	0.09	6
miR-617	A_25_P00010772	0.836	0.294	3.142	0.1	6
miR-626	A_25_P00011235	0.945	0.291	2.518	0.1	6
miR-6500-3p	A_25_P00017878	0.878	0.292	2.543	0.06	6
miR-759	A_25_P00015466	0.930	0.262	-2.663	0.06	6

C 8 Circadian features of the miRNA expression profiles from cosine-fitting function in MDA-MB-231.

miRNA	agilent-code	cosine correlation	period	phase	amplitude	cluster
miR-3674	A_25_P00016190	0.856	0.238	1.670	0.11	1
miR-3910	A_25_P00016263	0.841	0.262	1.549	0.06	1
miR-4300	A_25_P00015719	0.832	0.296	0.634	0.09	1
miR-4654	A_25_P00016684	0.844	0.232	1.540	0.09	1
miR-4697-5p	A_25_P00016631	0.875	0.251	1.603	0.1	1
miR-4724-3p	A_25_P00016409	0.953	0.300	1.758	0.07	1

miR-503-5p	A_25_P00010657	0.913	0.283	1.904	0.07	1
miR-544b	A_25_P00015881	0.934	0.278	1.400	0.06	1
miR-548b-3p	A_25_P00010124	0.883	0.226	-3.142	0.07	1
miR-5583-5p	A_25_P00017479	0.871	0.233	1.240	0.14	1
miR-5688	A_25_P00017617	0.822	0.294	1.647	0.05	1
miR-6515-5p	A_25_P00017867	0.835	0.242	1.629	0.06	1
let-7b-3p	A_25_P00013118	0.957	0.278	0.435	0.1	2
miR-124-5p	A_25_P00013389	0.857	0.259	0.552	0.07	2
miR-142-3p	A_25_P00013937	0.827	0.230	1.382	0.05	2
miR-150-5p	A_25_P00010490	0.849	0.257	1.395	0.05	2
miR-23a-5p	A_25_P00013182	0.897	0.229	0.697	0.12	2
miR-28-3p	A_25_P00012007	0.886	0.279	0.669	0.16	2
miR-3195	A_25_P00015499	0.921	0.228	1.634	0.05	2
miR-325	A_25_P00010180	0.862	0.299	0.498	0.12	2
miR-3656	A_25_P00016105	0.906	0.280	0.423	0.06	2
miR-376a-2-5p	A_25_P00017745	0.866	0.260	0.806	0.09	2
miR-4252	A_25_P00015871	0.896	0.255	0.965	0.1	2
miR-4467	A_25_P00016337	0.942	0.295	-0.013	0.09	2
miR-4693-3p	A_25_P00016299	0.837	0.240	1.195	0.07	2
miR-4786-3p	A_25_P00016918	0.845	0.241	1.000	0.05	2
miR-520a-3p	A_25_P00014113	0.857	0.245	1.089	0.05	2
miR-611	A_25_P00010903	0.853	0.272	0.468	0.11	2
miR-615-5p	A_25_P00012787	0.825	0.286	0.357	0.14	2
miR-658	A_25_P00011946	0.887	0.239	0.757	0.09	2
dmr_316		0.951	0.271	-0.389	0.06	3
mr_1		0.919	0.290	-0.184	0.13	3
miR-1-3p	A_25_P00012150	0.982	0.287	-0.624	0.09	3
miR-101-5p	A_25_P00013250	0.842	0.272	-0.858	0.09	3
miR-1237-5p	A_25_P00017824	0.950	0.234	0.600	0.09	3
miR-182-3p	A_25_P00010966	0.925	0.273	0.045	0.06	3
miR-183-3p	A_25_P00013323	0.858	0.248	0.523	0.14	3
miR-185-3p	A_25_P00013457	0.952	0.297	-1.154	0.18	3
miR-1976	A_25_P00015365	0.910	0.277	-1.279	0.06	3
miR-219b-5p	A_25_P00016753	0.911	0.244	0.464	0.08	3
miR-2276-3p	A_25_P00015447	0.948	0.294	-0.442	0.08	3
miR-2277-3p	A_25_P00015459	0.969	0.274	-0.013	0.1	3
miR-23a-5p	A_25_P00013181	0.941	0.290	-0.847	0.11	3
miR-25-5p	A_25_P00013191	0.827	0.236	-0.139	0.11	3
miR-2681-3p	A_25_P00017021	0.964	0.280	0.119	0.07	3

miR-3120-3p	A_25_P00015853	0.857	0.297	-0.398	0.07	3
miR-3171	A_25_P00015735	0.946	0.249	0.068	0.08	3
miR-3194-3p	A_25_P00016421	0.878	0.272	-0.491	0.05	3
miR-33b-3p	A_25_P00013651	0.957	0.295	-0.861	0.05	3
miR-376c-3p	A_25_P00012316	0.889	0.299	-0.232	0.07	3
miR-3974	A_25_P00016911	0.874	0.282	-0.255	0.07	3
miR-4659b-3p	A_25_P00016492	0.874	0.263	0.039	0.12	3
miR-4744	A_25_P00016662	0.917	0.269	-0.427	0.07	3
miR-491-3p	A_25_P00012485	0.832	0.228	0.747	0.08	3
miR-499b-5p	A_25_P00017168	0.930	0.269	-1.066	0.08	3
miR-502-3p	A_25_P00012647	0.924	0.273	-0.442	0.07	3
miR-5093	A_25_P00017613	0.827	0.274	0.133	0.08	3
miR-541-5p	A_25_P00013667	0.886	0.276	-0.136	0.1	3
miR-548h-5p	A_25_P00015208	0.873	0.266	-0.006	0.06	3
miR-564	A_25_P00010786	0.893	0.282	-0.112	0.07	3
miR-5683	A_25_P00017565	0.885	0.230	0.964	0.09	3
miR-5685	A_25_P00017506	0.923	0.236	0.169	0.06	3
miR-5686	A_25_P00017376	0.833	0.290	-1.201	0.11	3
miR-573	A_25_P00011618	0.921	0.252	0.238	0.05	3
miR-607	A_25_P00010935	0.863	0.235	0.534	0.11	3
miR-6501-3p	A_25_P00017756	0.840	0.268	-0.938	0.16	3
miR-892b	A_25_P00012942	0.872	0.279	-0.093	0.1	3
miR-940	A_25_P00013090	0.913	0.283	-0.254	0.15	3
miR-1204	A_25_P00015082	0.923	0.275	-1.211	0.08	4
miR-1258	A_25_P00015167	0.950	0.254	-1.360	0.12	4
miR-1273a	A_25_P00015203	0.914	0.270	-1.739	0.07	4
miR-141-5p	A_25_P00013413	0.875	0.299	-1.577	0.08	4
miR-187-5p	A_25_P00013327	0.824	0.261	-1.404	0.13	4
miR-223-5p	A_25_P00013355	0.839	0.253	-1.416	0.22	4
miR-3157-5p	A_25_P00015563	0.826	0.231	-1.140	0.08	4
miR-33b-5p	A_25_P00012824	0.852	0.281	-1.534	0.07	4
miR-362-5p	A_25_P00013984	0.870	0.229	-1.220	0.06	4
miR-3660	A_25_P00016217	0.922	0.285	-1.845	0.07	4
miR-3925-5p	A_25_P00016056	0.824	0.259	-1.008	0.14	4
miR-4423-5p	A_25_P00016909	0.862	0.277	-1.804	0.07	4
miR-449b-5p	A_25_P00010776	0.932	0.293	-1.502	0.12	4
miR-4652-3p	A_25_P00017179	0.943	0.238	-0.728	0.07	4
miR-4725-3p	A_25_P00016713	0.862	0.258	-1.695	0.06	4
miR-4742-3p	A_25_P00016821	0.853	0.283	-1.502	0.08	4

miR-4787-3p	A_25_P00016945	0.944	0.262	-1.616	0.12	4
miR-4802-5p	A_25_P00016308	0.872	0.248	-0.937	0.1	4
miR-495-3p	A_25_P00012507	0.961	0.287	-1.767	0.1	4
miR-499a-3p	A_25_P00012626	0.843	0.240	-1.120	0.1	4
miR-505-3p	A_25_P00012654	0.875	0.238	-1.241	0.06	4
miR-512-3p	A_25_P00010710	0.924	0.272	-1.640	0.05	4
miR-567	A_25_P00010942	0.914	0.272	-1.688	0.07	4
miR-590-5p	A_25_P00014257	0.855	0.244	-1.025	0.1	4
miR-101-5p	A_25_P00014977	0.853	0.234	-1.844	0.13	5
miR-124-3p	A_25_P00014839	0.979	0.267	-2.116	0.06	5
miR-17-5p	A_25_P00011991	0.987	0.247	-2.122	0.17	5
miR-193b-3p	A_25_P00012512	0.848	0.277	-2.529	0.09	5
miR-196a-5p	A_25_P00012052	0.849	0.279	-2.288	0.08	5
miR-19b-2-5p	A_25_P00013164	0.828	0.248	-1.705	0.12	5
miR-30c-5p	A_25_P00013883	0.821	0.284	-2.177	0.17	5
miR-3119	A_25_P00015746	0.968	0.249	-1.737	0.15	5
miR-3675-5p	A_25_P00016157	0.895	0.255	-2.528	0.05	5
miR-3689f	A_25_P00017126	0.932	0.258	-2.472	0.08	5
miR-4308	A_25_P00015502	0.857	0.287	-2.148	0.06	5
miR-452-3p	A_25_P00013583	0.954	0.231	-1.965	0.07	5
miR-4520-5p	A_25_P00017309	0.847	0.265	-2.470	0.06	5
miR-4531	A_25_P00017111	0.828	0.258	-2.300	0.07	5
miR-4684-5p	A_25_P00017088	0.823	0.274	-1.832	0.1	5
miR-4700-3p	A_25_P00016640	0.922	0.251	-1.639	0.06	5
miR-4768-3p	A_25_P00016594	0.979	0.282	-2.164	0.08	5
miR-486-3p	A_25_P00012469	0.846	0.272	-2.130	0.07	5
miR-532-5p	A_25_P00014179	0.911	0.284	-2.879	0.07	5
miR-548at-5p	A_25_P00017425	0.861	0.266	-2.005	0.14	5
miR-5584-5p	A_25_P00017674	0.946	0.243	-1.872	0.05	5
miR-571	A_25_P00010633	0.933	0.274	-2.086	0.1	5
miR-6081	A_25_P00017906	0.868	0.252	-1.631	0.09	5
miR-6128	A_25_P00017983	0.912	0.261	-1.958	0.06	5
miR-6165	A_25_P00017841	0.962	0.267	-2.139	0.08	5
miR-619-3p	A_25_P00011293	0.891	0.260	-2.039	0.12	5
miR-769-3p	A_25_P00011231	0.915	0.229	-1.591	0.12	5
miR-942-5p	A_25_P00013098	0.856	0.261	-1.641	0.1	5
miR-106b-5p	A_25_P00010434	0.828	0.260	-2.722	0.29	6
miR-130b-5p	A_25_P00013503	0.946	0.283	-2.981	0.09	6
miR-18a-3p	A_25_P00013155	0.848	0.291	3.142	0.16	6

miR-196b-5p	A_25_P00012412	0.821	0.262	-2.662	0.06	6
miR-21-3p	A_25_P00013173	0.931	0.291	3.021	0.12	6
miR-23c	A_25_P00016198	0.837	0.227	-2.583	0.06	6
miR-302b-3p	A_25_P00010618	0.823	0.235	-2.131	0.06	6
miR-302d-3p	A_25_P00010163	0.902	0.271	-2.998	0.1	6
miR-3074-5p	A_25_P00016835	0.866	0.230	-2.038	0.06	6
miR-3622a-5p	A_25_P00016140	0.854	0.251	-2.221	0.13	6
miR-3714	A_25_P00016015	0.922	0.275	-3.142	0.05	6
miR-371a-3p	A_25_P00013992	0.921	0.239	-2.155	0.07	6
miR-423-3p	A_25_P00012422	0.844	0.286	2.788	0.11	6
miR-4325	A_25_P00015808	0.835	0.299	-3.018	0.06	6
miR-455-3p	A_25_P00012698	0.839	0.227	-2.203	0.08	6
miR-4667-5p	A_25_P00017004	0.914	0.254	-1.953	0.05	6
miR-4704-5p	A_25_P00016353	0.863	0.264	2.917	0.06	6
miR-4715-3p	A_25_P00016596	0.828	0.233	-1.833	0.05	6
miR-548as-3p	A_25_P00017374	0.926	0.292	2.495	0.05	6
miR-548ay-3p	A_25_P00017966	0.862	0.250	-3.027	0.08	6
miR-5582-3p	A_25_P00017509	0.937	0.231	-2.320	0.07	6
miR-636	A_25_P00012829	0.985	0.285	2.307	0.07	6
miR-655-3p	A_25_P00011229	0.897	0.262	-2.210	0.11	6
miR-885-3p	A_25_P00012992	0.951	0.239	-1.945	0.13	6
miR-92a-2-5p	A_25_P00013230	0.823	0.243	-2.642	0.07	6
miR-92a-3p	A_25_P00012031	0.848	0.297	2.828	0.25	6
miR-938	A_25_P00013083	0.868	0.283	-2.982	0.05	6

Appendix D

Circadian Features of validated miRNAs obtained from MetaCycle

D 1 Circadian features of validated miRNAs obtained from MetaCycle in MCF-10A cells

miRNAs	MetaCycle P-value	Period	Phase	Amplitude
miR-222-5p	0.017	20.020	0.397	1.283
miR-769-3p	0.944	25.333	6.785	0.028
miR-141-5p	0.024	20.722	19.967	0.829
miR-1225-3p	0.990	26.906	9.116	0.043
miR-17-5p	0.966	27.060	4.730	0.006
miR-548ay-3p	0.022	21.333	20.563	1.106

D 2 Circadian features of validated miRNAs obtained from MetaCycle in MCF-7 cells

miRNAs	MetaCycle P-value	Period	Phase	Amplitude
miR-222-5p-	0.049	22.755	13.955	0.251
miR-769-3p-	0.020	20.192	2.260	0.348
miR-141-5p-	0.001	20.337	17.880	0.344
miR-1225-3p-	0.953	28.667	1.532	0.186
miR-17-5p-	0.905	25.038	19.807	0.340
miR-548ay-3p	0.669	23.874	1.992	0.391

D 3 Circadian features of validated miRNAs obtained from MetaCycle in MDA-MB-231 cells

miRNAs	Metacycle P-value	Period	Phase	Amplitude
miR-222-5p	0.765	25.802	7.366	0.096
miR-769-3p	0.021	22.088	19.904	0.735
miR-141-5p	0.937	22.460	13.758	0.140
miR-1225-3p	0.684	25.333	4.721	0.144
miR-17-5p	0.002	24.903	20.159	1.138
miR-548ay-3p	0.003	22.728	1.091	0.273

D 4 Circadian features of validated miRNAs obtained from MetaCycle in ZR-7530 cells

miRNAs	MetaCycle P-value	Period	Phase	Amplitude
miR-222-5p	0.190	27.150	7.894	0.323
miR-769-3p	0.966	28.667	14.215	0.244
miR-141-5p	0.236	24.517	15.422	0.928
miR-1225-3p	0.008	24.686	13.186	0.350
miR-17-5p	0.669	25.472	16.145	0.249
miR-548ay-3p	0.000	24.562	12.471	1.075

D 5 Circadian features of validated miRNAs obtained from MetaCycle in HCC-1954 cells

miRNAs	MetaCycle P-value	Period	Phase	Amplitude
miR-222-5p	0.991	28.667	7.650	0.835
miR-769-3p	0.961	21.333	18.464	0.466
miR-141-5p	0.041	23.282	9.515	1.437
miR-1225-3p	0.037	23.988	21.858	0.361
miR-17-5p	0.038	22.323	8.135	2.838
miR-548ay-3p	0.004	23.643	21.328	0.555

Appendix E

Pathways related to targeted genes of validated miRNAs

E 1 Pathways related to targeted genes of miR-15-5p.

	Pathway identifier	Pathway name	N genes found	Total genes	p-Value	FDR
1	R-HSA-69236	G1 Phase	12	42	1.6E-08	9.9E-06
2	R-HSA-69231	Cyclin D associated events in G1	12	42	1.6E-08	9.9E-06
3	R-HSA-3247509	Chromatin modifying enzymes	24	247	1.7E-06	5.4E-04
4	R-HSA-4839726	Chromatin organization	24	247	1.7E-06	5.4E-04
5	R-HSA-2173789	TGF-beta receptor signaling activates SMADs	9	36	2.9E-06	6.9E-04
6	R-HSA-3214847	HATs acetylate histones	15	110	3.3E-06	6.9E-04
7	R-HSA-170834	Signaling by TGF-beta Receptor Complex	13	84	3.9E-06	7.0E-04

8	R-HSA-2173788	Downregulation of TGF-beta receptor signaling	7	28	3.7E-05	4.3E-03
9	R-HSA-157118	Signaling by NOTCH	16	153	4.0E-05	4.3E-03
10	R-HSA-3214815	HDACs deacetylate histones	10	63	4.1E-05	4.3E-03
11	R-HSA-2173796	SMAD2/SMAD3:SMAD4 heterotrimer regulates transcription	8	39	4.2E-05	4.3E-03
12	R-HSA-3214858	RMTs methylate histone arginines	9	51	4.5E-05	4.3E-03
13	R-HSA-1912408	Pre-NOTCH Transcription and Translation	9	52	5.2E-05	4.6E-03
14	R-HSA-201722	Formation of the beta-catenin:TCF transactivating complex	10	66	6.0E-05	5.0E-03
15	R-HSA-453279	Mitotic G1-G1/S phases	15	143	6.7E-05	5.1E-03
16	R-HSA-3214842	HDMs demethylate histones	7	31	7.0E-05	5.1E-03
17	R-HSA-5689901	Metalloprotease DUBs	7	32	8.5E-05	5.9E-03
18	R-HSA-3700989	Transcriptional Regulation by TP53	31	476	1.4E-04	8.1E-03

19	R-HSA-2559582	Senescence-Associated Secretory Phenotype (SASP)	11	89	1.6E-04	8.1E-03
20	R-HSA-937039	IRAK1 recruits IKK complex	5	16	1.8E-04	8.1E-03
21	R-HSA-975144	IRAK1 recruits IKK complex upon TLR7/8 or 9 stimulation	5	16	1.8E-04	8.1E-03
22	R-HSA-1912422	Pre-NOTCH Expression and Processing	10	76	1.9E-04	8.2E-03
23	R-HSA-2559583	Cellular Senescence	17	194	1.9E-04	8.2E-03
24	R-HSA-73854	RNA Polymerase I Promoter Clearance	10	83	3.7E-04	1.5E-02
25	R-HSA-6804116	TP53 Regulates Transcription of Genes Involved in G1 Cell Cycle Arrest	5	19	3.9E-04	1.5E-02
26	R-HSA-2173793	Transcriptional activity of SMAD2/SMAD3:SMAD4 heterotrimer	8	55	4.3E-04	1.6E-02
27	R-HSA-5675482	Regulation of necroptotic cell death	5	20	4.9E-04	1.7E-02

28	R-HSA-73864	RNA Polymerase I Transcription	10	86	4.9E-04	1.7E-02
29	R-HSA-69202	Cyclin E associated events during G1/S transition	9	73	6.2E-04	2.1E-02
30	R-HSA-2559580	Oxidative Stress Induced Senescence	11	109	8.3E-04	2.7E-02
31	R-HSA-8866911	TFAP2 (AP-2) family regulates transcription of cell cycle factors	3	6	9.8E-04	3.0E-02
32	R-HSA-69895	Transcriptional activation of cell cycle inhibitor p21	3	6	9.8E-04	3.0E-02
33	R-HSA-69560	Transcriptional activation of p53 responsive genes	3	6	9.8E-04	3.0E-02
34	R-HSA-5689880	Ub-specific processing proteases	16	206	1.0E-03	3.1E-02
35	R-HSA-427389	ERCC6 (CSB) and EHMT2 (G9a) positively regulate rRNA expression	7	49	1.1E-03	3.1E-02
36	R-HSA-912631	Regulation of signaling by CBL	5	24	1.1E-03	3.2E-02
37	R-HSA-69298	Association of licensing factors with the pre-replicative complex	4	15	1.4E-03	3.8E-02

38	R-HSA-5637815	Signaling by Ligand-Responsive EGFR Variants in Cancer	6	38	1.5E-03	3.8E-02
39	R-HSA-1236382	Constitutive Signaling by Ligand-Responsive EGFR Cancer Variants	6	38	1.5E-03	3.8E-02
40	R-HSA-1643713	Signaling by EGFR in Cancer	6	38	1.5E-03	3.8E-02
41	R-HSA-69278	Cell Cycle, Mitotic	30	526	1.5E-03	3.8E-02
42	R-HSA-201681	TCF dependent signaling in response to WNT	16	215	1.6E-03	3.8E-02
43	R-HSA-69206	G1/S Transition	11	119	1.7E-03	4.0E-02
44	R-HSA-209543	p75NTR recruits signalling complexes	4	16	1.8E-03	4.2E-02
45	R-HSA-5218859	Regulated Necrosis	5	27	1.8E-03	4.2E-02
46	R-HSA-5213460	RIPK1-mediated regulated necrosis	5	27	1.8E-03	4.2E-02
47	R-HSA-195721	Signaling by Wnt	21	329	2.1E-03	4.5E-02
48	R-HSA-453274	Mitotic G2-G2/M phases	15	201	2.2E-03	4.5E-02
49	R-HSA-1295596	Spry regulation of FGF signaling	4	17	2.2E-03	4.5E-02

50	R-HSA-69656	Cyclin A:Cdk2-associated events at S phase entry	8	74	2.7E-03	5.0E-02
51	R-HSA-400253	Circadian Clock	9	91	2.8E-03	5.0E-02
52	R-HSA-975871	MyD88 cascade initiated on plasma membrane	9	91	2.8E-03	5.0E-02
53	R-HSA-168176	Toll Like Receptor 5 (TLR5) Cascade	9	91	2.8E-03	5.0E-02
54	R-HSA-168142	Toll Like Receptor 10 (TLR10) Cascade	9	91	2.8E-03	5.0E-02
55	R-HSA-2565942	Regulation of PLK1 Activity at G2/M Transition	9	92	3.0E-03	5.2E-02
56	R-HSA-3769402	Deactivation of the beta-catenin transactivating complex	6	44	3.0E-03	5.2E-02
57	R-HSA-3304349	Loss of Function of SMAD2/3 in Cancer	3	9	3.1E-03	5.2E-02
58	R-HSA-3315487	SMAD2/3 MH2 Domain Mutants in Cancer	3	9	3.1E-03	5.2E-02
59	R-HSA-4411364	Binding of TCF/LEF:CTNNB1 to target gene promoters	3	9	3.1E-03	5.2E-02
60	R-HSA-975138	TRAF6 mediated induction of NFkB and MAP kinases upon TLR7/8 or 9 activation	9	93	3.2E-03	5.3E-02
61	R-HSA-193639	p75NTR signals via NF-kB	4	19	3.3E-03	5.3E-02

62	R-HSA-73777	RNA Polymerase I Chain Elongation	7	61	3.6E-03	5.6E-02
63	R-HSA-975155	MyD88 dependent cascade initiated on endosome	9	95	3.6E-03	5.6E-02
64	R-HSA-168181	Toll Like Receptor 7/8 (TLR7/8) Cascade	9	95	3.6E-03	5.6E-02
65	R-HSA-380994	ATF4 activates genes	5	32	3.8E-03	5.6E-02
66	R-HSA-3304351	Signaling by TGF-beta Receptor Complex in Cancer	3	10	4.1E-03	6.2E-02
67	R-HSA-3311021	SMAD4 MH2 Domain Mutants in Cancer	2	3	4.2E-03	6.3E-02
68	R-HSA-3304347	Loss of Function of SMAD4 in Cancer	2	3	4.2E-03	6.3E-02
69	R-HSA-168138	Toll Like Receptor 9 (TLR9) Cascade	9	98	4.4E-03	6.3E-02
70	R-HSA-109581	Apoptosis	13	176	4.5E-03	6.3E-02
71	R-HSA-446652	Interleukin-1 signaling	6	48	4.6E-03	6.3E-02
72	R-HSA-6791312	TP53 Regulates Transcription of Cell Cycle Genes	7	64	4.7E-03	6.3E-02
73	R-HSA-427413	NoRC negatively regulates rRNA expression	8	81	4.7E-03	6.3E-02
74	R-HSA-5250913	Positive epigenetic regulation of rRNA expression	8	81	4.7E-03	6.3E-02
75	R-HSA-5688426	Deubiquitination	18	285	4.8E-03	6.3E-02

76	R-HSA-73728	RNA Polymerase I Promoter Opening	5	34	4.8E-03	6.3E-02
77	R-HSA-8849469	PTK6 Regulates RTKs and Their Effectors AKT1 and DOK1	3	11	5.4E-03	7.0E-02
78	R-HSA-2979096	NOTCH2 Activation and Transmission of Signal to the Nucleus	4	22	5.5E-03	7.2E-02
79	R-HSA-212165	Epigenetic regulation of gene expression	11	140	5.6E-03	7.2E-02
80	R-HSA-5357801	Programmed Cell Death	13	184	6.4E-03	8.2E-02
81	R-HSA-504046	RNA Polymerase I, RNA Polymerase III, and Mitochondrial Transcription	10	124	6.8E-03	8.2E-02
82	R-HSA-113501	Inhibition of replication initiation of damaged DNA by RB1/E2F1	3	12	6.8E-03	8.2E-02
83	R-HSA-5687128	MAPK6/MAPK4 signaling	9	105	6.8E-03	8.2E-02
84	R-HSA-5334118	DNA methylation	5	37	6.8E-03	8.2E-02

85	R-HSA-1640170	Cell Cycle	32	638	7.3E-03	8.2E-02
86	R-HSA-450321	JNK (c-Jun kinases) phosphorylation and activation mediated by activated human TAK1	4	24	7.5E-03	8.2E-02
87	R-HSA-381042	PERK regulates gene expression	5	38	7.6E-03	8.3E-02
88	R-HSA-166058	MyD88:Mal cascade initiated on plasma membrane	9	107	7.7E-03	8.3E-02
89	R-HSA-168188	Toll Like Receptor TLR6:TLR2 Cascade	9	107	7.7E-03	8.3E-02
90	R-HSA-166054	Activated TLR4 signalling	10	128	8.3E-03	8.3E-02
91	R-HSA-350054	Notch-HLH transcription pathway	3	13	8.4E-03	8.4E-02
92	R-HSA-2559585	Oncogene Induced Senescence	5	39	8.5E-03	8.5E-02
93	R-HSA-5250941	Negative epigenetic regulation of rRNA expression	8	90	8.6E-03	8.6E-02
94	R-HSA-1227986	Signaling by ERBB2	6	55	8.6E-03	8.6E-02
95	R-HSA-168179	Toll Like Receptor TLR1:TLR2 Cascade	9	110	9.1E-03	9.1E-02
96	R-HSA-181438	Toll Like Receptor 2 (TLR2) Cascade	9	110	9.1E-03	9.1E-02
97	R-HSA-2122947	NOTCH1 Intracellular Domain Regulates Transcription	6	56	9.4E-03	9.3E-02

98	R-HSA-5637812	Signaling by EGFRvIII in Cancer	4	26	9.8E-03	9.3E-02
99	R-HSA-5637810	Constitutive Signaling by EGFRvIII	4	26	9.8E-03	9.3E-02
100	R-HSA-174490	Membrane binding and targetting of GAG proteins	3	14	1.0E-02	9.3E-02
101	R-HSA-901042	Calnexin/calreticulin cycle	5	41	1.0E-02	9.3E-02
102	R-HSA-2173795	Downregulation of SMAD2/3:SMAD4 transcriptional activity	4	27	1.1E-02	1.0E-01
103	R-HSA-3214841	PKMTs methylate histone lysines	5	42	1.1E-02	1.0E-01
104	R-HSA-69275	G2/M Transition	13	199	1.2E-02	1.1E-01
105	R-HSA-209560	NF-kB is activated and signals survival	3	15	1.2E-02	1.1E-01
106	R-HSA-174495	Synthesis And Processing Of GAG, GAGPOL Polyproteins	3	15	1.2E-02	1.1E-01
107	R-HSA-182971	EGFR downregulation	4	28	1.3E-02	1.1E-01
108	R-HSA-5689603	UCH proteinases	8	98	1.4E-02	1.2E-01
109	R-HSA-977225	Amyloid fiber formation	7	80	1.5E-02	1.2E-01
110	R-HSA-5250924	B-WICH complex positively regulates rRNA expression	6	62	1.5E-02	1.2E-01

111	R-HSA-212300	PRC2 methylates histones and DNA	5	45	1.5E-02	1.2E-01
112	R-HSA-166016	Toll Like Receptor 4 (TLR4) Cascade	10	141	1.5E-02	1.2E-01
113	R-HSA-5578749	Transcriptional regulation by small RNAs	7	81	1.5E-02	1.2E-01
114	R-HSA-2262752	Cellular responses to stress	24	470	1.6E-02	1.2E-01
115	R-HSA-427359	SIRT1 negatively regulates rRNA Expression	5	46	1.6E-02	1.2E-01
116	R-HSA-1169410	Antiviral mechanism by IFN-stimulated genes	7	83	1.7E-02	1.2E-01
117	R-HSA-1169408	ISG15 antiviral mechanism	7	83	1.7E-02	1.2E-01
118	R-HSA-5654695	PI-3K cascade:FGFR2	10	144	1.8E-02	1.2E-01
119	R-HSA-5654710	PI-3K cascade:FGFR3	10	144	1.8E-02	1.2E-01
120	R-HSA-5654720	PI-3K cascade:FGFR4	10	144	1.8E-02	1.2E-01
121	R-HSA-5654689	PI-3K cascade:FGFR1	10	144	1.8E-02	1.2E-01
122	R-HSA-1250342	PI3K events in ERBB4 signaling	10	144	1.8E-02	1.2E-01
123	R-HSA-1257604	PIP3 activates AKT signaling	10	144	1.8E-02	1.2E-01

124	R-HSA-5696395	Formation of Incision Complex in GG-NER	5	47	1.8E-02	1.2E-01
125	R-HSA-212436	Generic Transcription Pathway	45	1032	1.8E-02	1.2E-01
126	R-HSA-5628897	TP53 Regulates Metabolic Genes	9	125	1.9E-02	1.2E-01
127	R-HSA-450294	MAP kinase activation in TLR cascade	6	66	1.9E-02	1.2E-01
128	R-HSA-180292	GAB1 signalosome	10	147	2.0E-02	1.2E-01
129	R-HSA-198203	PI3K/AKT activation	10	147	2.0E-02	1.2E-01
130	R-HSA-391160	Signal regulatory protein (SIRP) family interactions	3	18	2.0E-02	1.2E-01
131	R-HSA-5684264	MAP3K8 (TPL2)-dependent MAPK1/3 activation	3	18	2.0E-02	1.2E-01
132	R-HSA-2173791	TGF-beta receptor signaling in EMT (epithelial to mesenchymal transition)	3	18	2.0E-02	1.2E-01
133	R-HSA-6803211	TP53 Regulates Transcription of Death Receptors and Ligands	3	18	2.0E-02	1.2E-01
134	R-HSA-5625886	Activated PKN1 stimulates transcription of AR (androgen receptor) regulated genes KLK2 and KLK3	5	49	2.1E-02	1.2E-01
135	R-HSA-8864260	Transcriptional regulation by the AP-2 (TFAP2) family of transcription factors	5	49	2.1E-02	1.2E-01

136	R-HSA-2894862	Constitutive Signaling by NOTCH1 HD+PEST Domain Mutants	6	67	2.1E-02	1.2E-01
137	R-HSA-2644602	Signaling by NOTCH1 PEST Domain Mutants in Cancer	6	67	2.1E-02	1.2E-01
138	R-HSA-2894858	Signaling by NOTCH1 HD+PEST Domain Mutants in Cancer	6	67	2.1E-02	1.2E-01
139	R-HSA-2644606	Constitutive Signaling by NOTCH1 PEST Domain Mutants	6	67	2.1E-02	1.2E-01
140	R-HSA-2644603	Signaling by NOTCH1 in Cancer	6	67	2.1E-02	1.2E-01
141	R-HSA-75158	TRAIL signaling	2	7	2.1E-02	1.2E-01
142	R-HSA-3304356	SMAD2/3 Phosphorylation Motif Mutants in Cancer	2	7	2.1E-02	1.2E-01
143	R-HSA-68911	G2 Phase	2	7	2.1E-02	1.2E-01
144	R-HSA-5663202	Diseases of signal transduction	20	384	2.1E-02	1.2E-01
145	R-HSA-73762	RNA Polymerase I Transcription Initiation	5	50	2.2E-02	1.2E-01
146	R-HSA-937061	TRIF-mediated TLR3/TLR4 signaling	8	108	2.3E-02	1.2E-01
147	R-HSA-166166	MyD88-independent TLR3/TLR4 cascade	8	108	2.3E-02	1.2E-01
148	R-HSA-168164	Toll Like Receptor 3 (TLR3) Cascade	8	108	2.3E-02	1.2E-01
149	R-HSA-975110	TRAF6 mediated IRF7 activation in TLR7/8 or 9 signaling	3	19	2.3E-02	1.2E-01
150	R-HSA-5654732	Negative regulation of FGFR3 signaling	4	34	2.4E-02	1.2E-01
151	R-HSA-2262749	Cellular response to hypoxia	4	34	2.4E-02	1.2E-01

152	R-HSA-1234174	Regulation of Hypoxia-inducible Factor (HIF) by oxygen	4	34	2.4E-02	1.2E-01
153	R-HSA-392451	G beta:gamma signalling through PI3Kgamma	5	52	2.6E-02	1.3E-01
154	R-HSA-5654733	Negative regulation of FGFR4 signaling	4	35	2.6E-02	1.3E-01
155	R-HSA-1266695	Interleukin-7 signaling	3	20	2.6E-02	1.3E-01
156	R-HSA-380284	Loss of proteins required for interphase microtubule organizationåÊfrom the centrosome	6	71	2.7E-02	1.3E-01
157	R-HSA-380259	Loss of Nlp from mitotic centrosomes	6	71	2.7E-02	1.3E-01
158	R-HSA-111453	BH3-only proteins associate with and inactivate anti-apoptotic BCL-2 members	2	8	2.7E-02	1.3E-01
159	R-HSA-426496	Post-transcriptional silencing by small RNAs	2	8	2.7E-02	1.3E-01
160	R-HSA-2559586	DNA Damage/Telomere Stress Induced Senescence	6	72	2.8E-02	1.4E-01
161	R-HSA-1980145	Signaling by NOTCH2	4	37	3.1E-02	1.5E-01
162	R-HSA-445989	TAK1 activates NFkB by phosphorylation and activation of IKKs complex	4	37	3.1E-02	1.5E-01

163	R-HSA-211000	Gene Silencing by RNA	8	115	3.1E-02	1.6E-01
164	R-HSA-8854518	AURKA Activation by TPX2	6	74	3.2E-02	1.6E-01
165	R-HSA-2299718	Condensation of Prophase Chromosomes	5	55	3.2E-02	1.6E-01
166	R-HSA-936964	Activation of IRF3/IRF7 mediated by TBK1/IKK epsilon	3	22	3.3E-02	1.6E-01
167	R-HSA-392851	Prostacyclin signalling through prostacyclin receptor	3	22	3.3E-02	1.6E-01
168	R-HSA-3656534	Loss of Function of TGFBR1 in Cancer	2	9	3.3E-02	1.6E-01
169	R-HSA-3656532	TGFBR1 KD Mutants in Cancer	2	9	3.3E-02	1.6E-01
170	R-HSA-6781823	Formation of TC-NER Pre-Incision Complex	5	56	3.4E-02	1.6E-01
171	R-HSA-397795	G-protein beta:gamma signalling	5	57	3.6E-02	1.6E-01
172	R-HSA-532668	N-glycan trimming in the ER and Calnexin/Calreticulin cycle	5	57	3.6E-02	1.6E-01
173	R-HSA-5654726	Negative regulation of FGFR1 signaling	4	39	3.6E-02	1.6E-01
174	R-HSA-389356	CD28 co-stimulation	4	39	3.6E-02	1.6E-01
175	R-HSA-174048	APC/C:Cdc20 mediated degradation of Cyclin B	3	23	3.7E-02	1.6E-01

176	R-HSA-6804760	Regulation of TP53 Activity through Methylation	3	23	3.7E-02	1.6E-01
177	R-HSA-73887	Death Receptor Signalling	5	58	3.8E-02	1.6E-01
178	R-HSA-69304	Regulation of DNA replication	6	78	3.9E-02	1.6E-01
179	R-HSA-5696394	DNA Damage Recognition in GG-NER	4	40	3.9E-02	1.6E-01
180	R-HSA-156902	Peptide chain elongation	7	99	4.0E-02	1.6E-01
181	R-HSA-1253288	Downregulation of ERBB4 signaling	2	10	4.0E-02	1.6E-01
182	R-HSA-3371378	Regulation by c-FLIP	2	10	4.0E-02	1.6E-01
183	R-HSA-69416	Dimerization of procaspase-8	2	10	4.0E-02	1.6E-01
184	R-HSA-5625740	RHO GTPases activate PKNs	6	79	4.1E-02	1.6E-01
185	R-HSA-175474	Assembly Of The HIV Virion	3	24	4.1E-02	1.7E-01
186	R-HSA-5654727	Negative regulation of FGFR2 signaling	4	41	4.2E-02	1.7E-01
187	R-HSA-8868766	rRNA processing in the mitochondrion	4	41	4.2E-02	1.7E-01
188	R-HSA-927802	Nonsense-Mediated Decay (NMD)	8	123	4.4E-02	1.7E-01
189	R-HSA-975957	Nonsense Mediated Decay (NMD) enhanced by the Exon Junction Complex (EJC)	8	123	4.4E-02	1.7E-01
190	R-HSA-5633007	Regulation of TP53 Activity	10	169	4.4E-02	1.8E-01

191	R-HSA-975956	Nonsense Mediated Decay (NMD) independent of the Exon Junction Complex (EJC)	7	102	4.5E-02	1.8E-01
192	R-HSA-6804757	Regulation of TP53 Degradation	4	42	4.5E-02	1.8E-01
193	R-HSA-179409	APC-Cdc20 mediated degradation of Nek2A	3	25	4.6E-02	1.8E-01
194	R-HSA-450302	activated TAK1 mediates p38 MAPK activation	3	25	4.6E-02	1.8E-01
195	R-HSA-8852276	The role of GTSE1 in G2/M progression after G2 checkpoint	6	82	4.8E-02	1.9E-01
196	R-HSA-1980143	Signaling by NOTCH1	6	82	4.8E-02	1.9E-01
197	R-HSA-426486	Small interfering RNA (siRNA) biogenesis	2	11	4.8E-02	1.9E-01
198	R-HSA-68689	CDC6 association with the ORC:origin complex	2	11	4.8E-02	1.9E-01
199	R-HSA-156842	Eukaryotic Translation Elongation	7	104	4.9E-02	2.0E-01
200	R-HSA-1168372	Downstream signaling events of B Cell Receptor (BCR)	12	220	4.9E-02	2.0E-01

Bibliography

[1] D. A. Golombek and R. E. Rosenstein, “Physiology of Circadian Entrainment,” *Physiol. Rev.*, vol. 90, no. 3, pp. 1063–1102, Jul. 2010.

[2] R. M. Grippo and A. D. Güler, “Dopamine signaling in circadian photoentrainment: Consequences of desynchrony,” *Yale Journal of Biology and Medicine*, vol. 92, no. 2. Yale Journal of Biology and Medicine Inc., pp. 271–281, 2019.

[3] S. Rana and S. Mahmood, “Circadian rhythm and its role in malignancy,” *J. Circadian Rhythms*, vol. 8, no. 1, pp. 1–13, Dec. 2010.

[4] K. Maiese, “Moving to the Rhythm with Clock (Circadian) Genes, Autophagy, mTOR, and SIRT1 in Degenerative Disease and Cancer,” *Curr. Neurovasc. Res.*, vol. 14, no. 3, Aug. 2017.

[5] E. Garbarino-Pico and C. B. Green, “Posttranscriptional Regulation of Mammalian Circadian Clock Output,” *Cold Spring Harb. Symp. Quant. Biol.*, vol. 72, pp. 145–156, Jan. 2007.

[6] Y. Wang, X. Ni, J. Yan, and L. Yang, “Modeling transcriptional co-regulation of mammalian circadian clock,” in *Mathematical Biosciences and Engineering*, 2017, vol. 14, no. 5–6, pp. 1447–1462.

[7] J. S. Takahashi, “Transcriptional architecture of the mammalian circadian clock,” *Nat. Rev. Genet.*, 2016.

[8] V. Pilorz, C. Helfrich-Förster, and H. Oster, “The role of the circadian clock system in physiology,” *Pflugers Archiv European Journal of Physiology*, vol. 470, no. 2. Springer Verlag, pp. 227–239, 01-Feb-2018.

[9] S. Kojima and C. B. Green, “Circadian Genomics Reveal a Role for Post-transcriptional Regulation in Mammals,” *Biochemistry*, vol. 54, no. 2, pp. 124–133, Jan. 2015.

[10] L. He and G. J. Hannon, “MicroRNAs: small RNAs with a big role in gene regulation,” *Nat. Rev. Genet.*, vol. 5, no. 7, pp. 522–531, Jul. 2004.

[11] C. Catalanotto, C. Cogoni, and G. Zardo, “MicroRNA in Control of Gene Expression: An Overview of Nuclear Functions,” *Int. J. Mol. Sci.*, vol. 17, no. 10, p. 1712, Oct.

2016.

[12] A. B. Reddy *et al.*, “Circadian Orchestration of the Hepatic Proteome,” *Curr. Biol.*, vol. 16, no. 11, pp. 1107–1115, Jun. 2006.

[13] K. H. Lee *et al.*, “MicroRNA-185 oscillation controls circadian amplitude of mouse Cryptochrome 1 via translational regulation,” *Mol. Biol. Cell*, vol. 24, no. 14, pp. 2248–2255, Jul. 2013.

[14] W. Zhang, P. Wang, S. Chen, Z. Zhang, T. Liang, and C. Liu, “Rhythmic expression of miR-27b-3p targets the clock gene Bmal1 at the posttranscriptional level in the mouse liver,” *FASEB J.*, 2016.

[15] A. Balakrishnan *et al.*, “MicroRNA mir-16 is anti-proliferative in enterocytes and exhibits diurnal rhythmicity in intestinal crypts,” *Exp. Cell Res.*, vol. 316, no. 20, pp. 3512–3521, Dec. 2010.

[16] Q. Wang, S. N. Bozack, Y. Yan, M. E. Boulton, M. B. Grant, and J. V. Busik, “Regulation of retinal inflammation by rhythmic expression of miR-146a in diabetic Retina,” *Investig. Ophthalmol. Vis. Sci.*, vol. 55, no. 6, pp. 3986–3994, May 2014.

[17] L. F. Sempere *et al.*, “Altered MicroRNA Expression Confined to Specific Epithelial Cell Subpopulations in Breast Cancer,” *Cancer Res.*, vol. 67, no. 24, pp. 11612–11620, Dec. 2007.

[18] L. Mulrane, S. F. McGee, W. M. Gallagher, and D. P. O’Connor, “miRNA Dysregulation in Breast Cancer,” *Cancer Res.*, vol. 73, no. 22, pp. 6554–6562, Nov. 2013.

[19] D. Z. Kochan, Y. Ilnytskyy, A. Golubov, S. H. Deibel, R. J. McDonald, and O. Kovalchuk, “Circadian disruption-induced microRNAome deregulation in rat mammary gland tissues,” *Oncoscience*, vol. 2, no. 4, pp. 428–442, Apr. 2015.

[20] T. Hamilton, “Influence of environmental light and melatonin upon mammary tumour induction.,” *Br. J. Surg.*, vol. 56, no. 10, pp. 764–6, Oct. 1969.

[21] H. H. Lin and M. E. Farkas, “Altered Circadian rhythms and breast cancer: From the human to the molecular level,” *Frontiers in Endocrinology*, vol. 9, no. MAY. Frontiers Media S.A., 04-May-2018.

[22] C. D. Mallet De Lima and A. Göndör, “Circadian organization of the genome,” *Science*, vol. 359, no. 6381. American Association for the Advancement of Science, pp. 1212–1213, 16-Mar-2018.

[23] L. Perrin *et al.*, “Transcriptomic analyses reveal rhythmic and CLOCK-driven pathways in human skeletal muscle,” *Elife*, vol. 7, Apr. 2018.

[24] Y. Wang *et al.*, “A proteomics landscape of circadian clock in mouse liver,” *Nat. Commun.*, vol. 9, no. 1, Dec. 2018.

[25] K. A. Dyar and K. L. Eckel-Mahan, “Circadian metabolomics in time and space,” *Frontiers in Neuroscience*, vol. 11, no. JUL. Frontiers Media S.A., 11-Jul-2017.

[26] A. E. Rosselot, C. I. Hong, and S. R. Moore, “Rhythm and bugs: Circadian clocks, gut microbiota, and enteric infections,” *Current Opinion in Gastroenterology*, vol. 32, no. 1. Lippincott Williams and Wilkins, 01-Jan-2016.

[27] C. R. Marinac *et al.*, “Prolonged nightly fasting and breast cancer prognosis,” *JAMA Oncol.*, vol. 2, no. 8, pp. 1049–1055, Aug. 2016.

[28] D. Z. Kochan and O. Kovalchuk, “Circadian disruption-induced breast cancer – knowns and unknowns,” *Cell Cycle*, vol. 15, no. 5. Taylor and Francis Inc., pp. 613–614, 03-Mar-2016.

[29] L. Xiao *et al.*, “Induction of the CLOCK Gene by E2-ERα Signaling Promotes the Proliferation of Breast Cancer Cells,” *PLoS One*, vol. 9, no. 5, p. e95878, May 2014.

[30] L. Chi *et al.*, “TIMELESS contributes to the progression of breast cancer through activation of MYC,” *Breast Cancer Res.*, vol. 19, no. 1, p. 53, Dec. 2017.

[31] A. McGuire, J. A. L. Brown, and M. J. Kerin, “Metastatic breast cancer: the potential of miRNA for diagnosis and treatment monitoring,” *Cancer Metastasis Rev.*, vol. 34, no. 1, pp. 145–155, 2015.

[32] M. Adhami, A. A. Haghdoost, B. Sadeghi, and R. Malekpour Afshar, “Candidate miRNAs in human breast cancer biomarkers: a systematic review,” *Breast Cancer*, vol. 25, no. 2, pp. 198–205, Mar. 2018.

[33] R. Benca, M. J. Duncan, E. Frank, C. McClung, R. J. Nelson, and A. Vicentic, “Biological rhythms, higher brain function, and behavior: Gaps, opportunities, and

challenges," *Brain Res. Rev.*, vol. 62, no. 1, pp. 57–70, Dec. 2009.

[34] M. Moser, R. Penter, M. Fruehwirth, and T. Kenner, "Why Life Oscillates - Biological Rhythms and Health," in *2006 International Conference of the IEEE Engineering in Medicine and Biology Society*, 2006, pp. 424–428.

[35] R. Saini, M. Jaskolski, and S. J. Davis, "Circadian oscillator proteins across the kingdoms of life: Structural aspects," *BMC Biology*, vol. 17, no. 1. BioMed Central Ltd., 18-Feb-2019.

[36] R. A. Hut and D. G. M. Beersma, "Evolution of time-keeping mechanisms: early emergence and adaptation to photoperiod.," *Philos. Trans. R. Soc. Lond. B. Biol. Sci.*, vol. 366, no. 1574, pp. 2141–54, Jul. 2011.

[37] D. A. Paranjpe and V. Sharma, "Evolution of temporal order in living organisms," *J. Circadian Rhythms*, vol. 3, no. 1, p. 7, May 2005.

[38] Z. Gerhart-Hines and M. A. Lazar, "Circadian metabolism in the light of evolution.," *Endocr. Rev.*, vol. 36, no. 3, pp. 289–304, Jun. 2015.

[39] A. Sancar, L. A. Lindsey-Boltz, T.-H. Kang, J. T. Reardon, J. H. Lee, and N. Ozturk, "Circadian clock control of the cellular response to DNA damage.," *FEBS Lett.*, vol. 584, no. 12, pp. 2618–25, Jun. 2010.

[40] W. J. M. Hrushesky, B. Lester, and D. Lannin, "Circadian coordination of cancer growth and metastatic spread," *Int. J. Cancer*, vol. 83, no. 3, pp. 365–373, Oct. 1999.

[41] C. Savvidis and M. Koutsilieris, "Circadian rhythm disruption in cancer biology.," *Mol. Med.*, vol. 18, no. 1, pp. 1249–60, Dec. 2012.

[42] C. Feillet, G. T. J. van der Horst, F. Levi, D. A. Rand, and F. Delaunay, "Coupling between the Circadian Clock and Cell Cycle Oscillators: Implication for Healthy Cells and Malignant Growth.," *Front. Neurol.*, vol. 6, p. 96, 2015.

[43] A. Shostak, "Circadian Clock, Cell Division, and Cancer: From Molecules to Organism.," *Int. J. Mol. Sci.*, vol. 18, no. 4, Apr. 2017.

[44] S. A. Rivkees, "The Development of Circadian Rhythms: From Animals To Humans.," *Sleep Med. Clin.*, vol. 2, no. 3, pp. 331–341, Sep. 2007.

[45] T. Mori and C. H. Johnson, "Independence of circadian timing from cell division in

cyanobacteria.," *J. Bacteriol.*, vol. 183, no. 8, pp. 2439–44, Apr. 2001.

[46] J. C. Dunlap, J. N. Stevens, E. U. Selker, and I. Morzycka-Wroblewska, "Closely watched clocks: molecular analysis of circadian rhythms in Neurospora and Drosophila.," *Trends Genet.*, vol. 6, no. 5, pp. 159–65, May 1990.

[47] E. M. Farré, "The regulation of plant growth by the circadian clock," *Plant Biol.*, vol. 14, no. 3, pp. 401–410, May 2012.

[48] R. Y. Moore MD, "CIRCADIAN RHYTHMS: Basic Neurobiology and Clinical Applications," *Annu. Rev. Med.*, vol. 48, no. 1, pp. 253–266, Feb. 1997.

[49] M. W. Young, "Life's 24-hour clock: molecular control of circadian rhythms in animal cells.," *Trends Biochem. Sci.*, vol. 25, no. 12, pp. 601–6, Dec. 2000.

[50] M. H. Hastings, A. B. Reddy, and E. S. Maywood, "A clockwork web: circadian timing in brain and periphery, in health and disease," *Nat. Rev. Neurosci.*, vol. 4, no. 8, pp. 649–661, Aug. 2003.

[51] S. M. Abbott, K. J. Reid, and P. C. Zee, "Circadian Rhythm Sleep-Wake Disorders," *Psychiatric Clinics of North America*, vol. 38, no. 4. W.B. Saunders, pp. 805–823, 01-Dec-2015.

[52] E. N. C. Manoogian and S. Panda, "Circadian rhythms, time-restricted feeding, and healthy aging," *Ageing Research Reviews*, vol. 39. Elsevier Ireland Ltd, pp. 59–67, 01-Oct-2017.

[53] I. Guisle *et al.*, "Circadian and sleep/wake-dependent variations in tau phosphorylation are driven by temperature," *Sleep*, Nov. 2019.

[54] C. J. Morris, D. Aeschbach, and F. A. J. L. Scheer, "Circadian system, sleep and endocrinology," *Molecular and Cellular Endocrinology*, vol. 349, no. 1. pp. 91–104, 05-Feb-2012.

[55] S. Crnko, B. C. Du Pré, J. P. G. Sluijter, and L. W. Van Laake, "Circadian rhythms and the molecular clock in cardiovascular biology and disease," *Nature Reviews Cardiology*, vol. 16, no. 7. Nature Publishing Group, pp. 437–447, 01-Jul-2019.

[56] S. Panda, "Circadian physiology of metabolism," *Science*, vol. 354, no. 6315. American Association for the Advancement of Science, pp. 1008–1015, 25-Nov-

2016.

[57] N. Labrecque and N. Cermakian, “Circadian Clocks in the Immune System.,” *J. Biol. Rhythms*, vol. 30, no. 4, pp. 277–90, Aug. 2015.

[58] C. A. Thaiss, M. Levy, and E. Elinav, “Chronobiomics: The Biological Clock as a New Principle in Host–Microbial Interactions,” *PLOS Pathog.*, vol. 11, no. 10, p. e1005113, Oct. 2015.

[59] J. C. Dunlap *et al.*, “Molecular bases for circadian clocks.,” *Cell*, vol. 96, no. 2, pp. 271–90, Jan. 1999.

[60] C. L. Partch, C. B. Green, and J. S. Takahashi, “Molecular architecture of the mammalian circadian clock,” *Trends Cell Biol.*, vol. 24, no. 2, pp. 90–99, Feb. 2014.

[61] E. D. Buhr and J. S. Takahashi, “Molecular components of the Mammalian circadian clock,” *Handb. Exp. Pharmacol.*, no. 217, pp. 3–27, 2013.

[62] D. Bell-Pedersen *et al.*, “Circadian rhythms from multiple oscillators: lessons from diverse organisms,” *Nat. Rev. Genet.*, vol. 6, no. 7, pp. 544–556, Jul. 2005.

[63] A. C. Liu, W. G. Lewis, and S. A. Kay, “Mammalian circadian signaling networks and therapeutic targets,” *Nature Chemical Biology*, vol. 3, no. 10. Nature Publishing Group, pp. 630–639, 20-Oct-2007.

[64] E. Slat, G. M. Freeman, and E. D. Herzog, “The Clock in the Brain: Neurons, Glia, and Networks in Daily Rhythms,” Springer, Berlin, Heidelberg, 2013, pp. 105–123.

[65] Y. Tahara and S. Shibata, “Circadian rhythms of liver physiology and disease: experimental and clinical evidence,” *Nat. Rev. Gastroenterol. Hepatol.*, vol. 13, no. 4, pp. 217–226, Feb. 2016.

[66] P. L. Lowrey and J. S. Takahashi, “Genetics of Circadian Rhythms in Mammalian Model Organisms,” 2011, pp. 175–230.

[67] E. D. Buhr and J. S. Takahashi, “Molecular components of the Mammalian circadian clock.,” *Handb. Exp. Pharmacol.*, no. 217, pp. 3–27, 2013.

[68] S. Masri and P. Sassone-Corsi, “Plasticity and specificity of the circadian epigenome.,” *Nat. Neurosci.*, vol. 13, no. 11, pp. 1324–9, Nov. 2010.

[69] J. E. Baggs and J. B. Hogenesch, “Genomics and systems approaches in the

mammalian circadian clock.," *Curr. Opin. Genet. Dev.*, vol. 20, no. 6, pp. 581–7, Dec. 2010.

[70] G. J. Menger, K. Lu, T. Thomas, V. M. Cassone, and D. J. Earnest, "Circadian profiling of the transcriptome in immortalized rat SCN cells," *Physiol. Genomics*, vol. 21, no. 3, pp. 370–381, May 2005.

[71] S. Panda *et al.*, "Coordinated transcription of key pathways in the mouse by the circadian clock.," *Cell*, vol. 109, no. 3, pp. 307–20, May 2002.

[72] A. Korenčič, R. Košir, G. Bordyugov, R. Lehmann, D. Rozman, and H. Herzel, "Timing of circadian genes in mammalian tissues.," *Sci. Rep.*, vol. 4, p. 5782, 2014.

[73] R. Zhang, N. F. Lahens, H. I. Ballance, M. E. Hughes, and J. B. Hogenesch, "A circadian gene expression atlas in mammals: implications for biology and medicine.," *Proc. Natl. Acad. Sci. U. S. A.*, vol. 111, no. 45, pp. 16219–24, Nov. 2014.

[74] C. Saini, S. A. Brown, and C. Dibner, "Human Peripheral Clocks: Applications for Studying Circadian Phenotypes in Physiology and Pathophysiology," *Front. Neurol.*, vol. 6, p. 95, May 2015.

[75] C. Lim and R. Allada, "Emerging roles for post-transcriptional regulation in circadian clocks," *Nat. Neurosci.*, vol. 16, no. 11, pp. 1544–50, 2013.

[76] S. Kojima, D. L. Shingle, and C. B. Green, "Post-transcriptional control of circadian rhythms," *J. Cell Sci.*, vol. 124, no. 3, 2011.

[77] M. Preußner and F. Heyd, "Post-transcriptional control of the mammalian circadian clock: implications for health and disease.," *Pflugers Arch.*, vol. 468, no. 6, pp. 983–91, Jun. 2016.

[78] Y. Umemura *et al.*, "Involvement of posttranscriptional regulation of Clock in the emergence of circadian clock oscillation during mouse development.," *Proc. Natl. Acad. Sci. U. S. A.*, p. 201703170, Aug. 2017.

[79] I. G. Cannell, Y. W. Kong, and M. Bushell, "How do microRNAs regulate gene expression?," *Biochemical Society Transactions*, vol. 36, no. 6. pp. 1224–1231, 2008.

[80] A. F. Olena and J. G. Patton, "Genomic organization of microRNAs," *J. Cell. Physiol.*,

p. n/a-n/a, 2009.

[81] J. Alles *et al.*, “An estimate of the total number of true human miRNAs,” *Nucleic Acids Res.*, vol. 47, no. 7, pp. 3353–3364, Apr. 2019.

[82] S. Lin and R. I. Gregory, “MicroRNA biogenesis pathways in cancer,” *Nature Reviews Cancer*, vol. 15, no. 6. Nature Publishing Group, pp. 321–333, 22-May-2015.

[83] H. Siomi and M. C. Siomi, “Posttranscriptional Regulation of MicroRNA Biogenesis in Animals,” *Molecular Cell*, vol. 38, no. 3. pp. 323–332, 14-May-2010.

[84] D. Lee and C. Shin, “Emerging roles of DROSHA beyond primary microRNA processing,” *RNA Biology*, vol. 15, no. 2. Taylor and Francis Inc., pp. 186–193, 01-Feb-2018.

[85] E. Lund, S. Güttinger, A. Calado, J. E. Dahlberg, and U. Kutay, “Nuclear Export of MicroRNA Precursors,” *Science (80-.).*, vol. 303, no. 5654, pp. 95–98, Jan. 2004.

[86] P. D. Zamore, T. Tuschl, P. A. Sharp, and D. P. Bartel, “RNAi: Double-stranded RNA directs the ATP-dependent cleavage of mRNA at 21 to 23 nucleotide intervals,” *Cell*, vol. 101, no. 1, pp. 25–33, Mar. 2000.

[87] T. P. Chendrimada *et al.*, “TRBP recruits the Dicer complex to Ago2 for microRNA processing and gene silencing,” *Nature*, vol. 436, no. 7051, pp. 740–744, Aug. 2005.

[88] L. Ding and M. Han, “GW182 family proteins are crucial for microRNA-mediated gene silencing,” *Trends in Cell Biology*, vol. 17, no. 8. pp. 411–416, Aug-2007.

[89] R. Parker and U. Sheth, “P Bodies and the Control of mRNA Translation and Degradation,” *Molecular Cell*, vol. 25, no. 5. pp. 635–646, 09-Mar-2007.

[90] R. C. Lee and V. Ambros, “An extensive class of small RNAs in Caenorhabditis elegans,” *Science (80-.).*, vol. 294, no. 5543, pp. 862–864, Oct. 2001.

[91] C. Llave, K. D. Kasschau, M. A. Rector, and J. C. Carrington, “Endogenous and silencing-associated small RNAs in plants,” *Plant Cell*, vol. 14, no. 7, pp. 1605–1619, Jul. 2002.

[92] S. Griffiths-Jones, “The microRNA Registry,” *Nucleic Acids Res.*, 2004.

[93] A. Kozomara and S. Griffiths-Jones, “MiRBase: Annotating high confidence

microRNAs using deep sequencing data," *Nucleic Acids Res.*, 2014.

[94] G. A. Calin *et al.*, "Frequent deletions and down-regulation of micro-RNA genes miR15 and miR16 at 13q14 in chronic lymphocytic leukemia," *Proc. Natl. Acad. Sci. U. S. A.*, vol. 99, no. 24, pp. 15524–15529, Nov. 2002.

[95] Y. Peng and C. M. Croce, "The role of microRNAs in human cancer," *Signal Transduction and Targeted Therapy*, vol. 1, no. 1. Springer Nature, pp. 1–9, 28-Jan-2016.

[96] Z. Yang *et al.*, "DbDEMC: A database of differentially expressed miRNAs in human cancers," *BMC Genomics*, 2010.

[97] D. Niveditha *et al.*, "Common and Unique microRNAs in Multiple Carcinomas Regulate Similar Network of Pathways to Mediate Cancer Progression," *Sci. Rep.*, vol. 10, no. 1, pp. 1–11, Dec. 2020.

[98] D. Hanahan and R. A. Weinberg, "Hallmarks of cancer: The next generation," *Cell*, vol. 144, no. 5. Elsevier, pp. 646–674, 04-Mar-2011.

[99] S. A. Ross and C. D. Davis, "MicroRNA, Nutrition, and Cancer Prevention," *Adv. Nutr.*, vol. 2, no. 6, pp. 472–485, Nov. 2011.

[100] B. Zhang, X. Pan, G. P. Cobb, and T. A. Anderson, "microRNAs as oncogenes and tumor suppressors," *Developmental Biology*, vol. 302, no. 1. Academic Press Inc., pp. 1–12, 01-Feb-2007.

[101] C. J. Cheng and F. J. Slack, "The Duality of OncomiR Addiction in the Maintenance and Treatment of Cancer," *Cancer J.*, vol. 18, no. 3, pp. 232–237, May 2012.

[102] A. A. Svoronos, D. M. Engelman, and F. J. Slack, "OncomiR or tumor suppressor? The duplicity of MicroRNAs in cancer," *Cancer Research*, vol. 76, no. 13. American Association for Cancer Research Inc., pp. 3666–3670, 01-Jul-2016.

[103] C. Fitzmaurice *et al.*, "Global, regional, and national cancer incidence, mortality, years of life lost, years lived with disability, and disability-Adjusted life-years for 29 cancer groups, 1990 to 2017: A systematic analysis for the global burden of disease study," *JAMA Oncol.*, vol. 5, no. 12, pp. 1749–1768, Dec. 2019.

[104] M. Dieterich, J. Stubert, T. Reimer, N. Erickson, and A. Berling, "Influence of Lifestyle

Factors on Breast Cancer Risk," *Breast Care*, vol. 9, no. 6, pp. 4–4, Jan. 2014.

[105] A. Antoniou *et al.*, "Average risks of breast and ovarian cancer associated with BRCA1 or BRCA2 mutations detected in case series unselected for family history: A combined analysis of 22 studies," *Am. J. Hum. Genet.*, vol. 72, no. 5, pp. 1117–1130, May 2003.

[106] H. Y. Loh, B. P. Norman, K. S. Lai, N. M. A. N. A. Rahman, N. B. M. Alitheen, and M. A. Osman, "The regulatory role of microRNAs in breast cancer," *International Journal of Molecular Sciences*, vol. 20, no. 19. MDPI AG, p. 4940, 01-Oct-2019.

[107] D. T. Ramsay, J. C. Kent, R. A. Hartmann, and P. E. Hartmann, "Anatomy of the lactating human breast redefined with ultrasound imaging," *J. Anat.*, vol. 206, no. 6, pp. 525–534, Jun. 2005.

[108] K. P. McGuire, "Breast Anatomy and Physiology," in *Breast Disease: Diagnosis and Pathology*, vol. 1, Springer International Publishing, 2015, pp. 1–14.

[109] J. Muschler and C. H. Streuli, "Cell-matrix interactions in mammary gland development and breast cancer.," *Cold Spring Harbor perspectives in biology*. 2010.

[110] S. H. Yoo *et al.*, "PERIOD2::LUCIFERASE real-time reporting of circadian dynamics reveals persistent circadian oscillations in mouse peripheral tissues," *Proc. Natl. Acad. Sci. U. S. A.*, 2004.

[111] N. Cermakian, L. Monaco, M. P. Pando, A. Dierich, and P. Sassone-Corsi, "Altered behavioral rhythms and clock gene expression in mice with a targeted mutation in the Period1 gene," *EMBO J.*, 2001.

[112] N. Park *et al.*, "A novel Bmal1 mutant mouse reveals essential roles of the C-terminal domain on circadian rhythms," *PLoS One*, 2015.

[113] M. P. Antoch *et al.*, "Disruption of the circadian clock due to the Clock mutation has discrete effects on aging and carcinogenesis," *Cell Cycle*, 2008.

[114] S. Gaddameedhi, J. T. Reardon, R. Ye, N. Ozturk, and A. Sancar, "Effect of circadian clock mutations on DNA damage response in mammalian cells," *Cell Cycle*, 2012.

[115] A. Sultan, A. Parganiha, T. Sultan, V. Choudhary, and A. K. Pati, "Circadian clock, cell cycle, and breast cancer: an updated review," *Biological Rhythm Research*.

2017.

[116] S. T. Chen, K. B. Choo, M. F. Hou, K. T. Yeh, S. J. Kuo, and J. G. Chang, "Deregulated expression of the PER1, PER2 and PER3 genes in breast cancers," *Carcinogenesis*, 2005.

[117] J. Wang *et al.*, "Circadian protein BMAL1 promotes breast cancer cell invasion and metastasis by up-regulating matrix metalloproteinase9 expression," *Cancer Cell Int.*, 2019.

[118] S. Volinia *et al.*, "A microRNA expression signature of human solid tumors defines cancer gene targets," *Proc. Natl. Acad. Sci. U. S. A.*, 2006.

[119] D. Serpico, L. Molino, and S. Di Cosimo, "MicroRNAs in breast cancer development and treatment," *Cancer Treatment Reviews*. 2014.

[120] A. J. Lowery *et al.*, "MicroRNA signatures predict oestrogen receptor, progesterone receptor and HER2/neu receptor status in breast cancer," *Breast Cancer Res.*, 2009.

[121] C. M. Perou *et al.*, "Molecular portraits of human breast tumours," *Nature*, vol. 406, no. 6797, pp. 747–752, Aug. 2000.

[122] T. Sørlie, "Molecular portraits of breast cancer: tumour subtypes as distinct disease entities," *Eur. J. Cancer*, vol. 40, no. 18, pp. 2667–2675, Dec. 2004.

[123] A. Prat *et al.*, "Phenotypic and molecular characterization of the claudin-low intrinsic subtype of breast cancer," *Breast Cancer Res.*, vol. 12, p. R68, 2010.

[124] R. Sandhu, J. S. Parker, W. D. Jones, C. A. Livasy, and W. B. Coleman, "Microarray-Based Gene Expression Profiling for Molecular Classification of Breast Cancer and Identification of New Targets for Therapy," *Lab. Med.*, vol. 41, no. 6, pp. 364–372, Jun. 2010.

[125] G. K. Malhotra, X. Zhao, H. Band, and V. Band, "Histological, molecular and functional subtypes of breast cancers," *Cancer Biol. Ther.*, vol. 10, no. 10, pp. 955–960, Nov. 2010.

[126] R. M. Neve *et al.*, "A collection of breast cancer cell lines for the study of functionally distinct cancer subtypes," *Cancer Cell*, vol. 10, no. 6, pp. 515–527, Dec. 2006.

[127] K. Subik *et al.*, "The Expression Patterns of ER, PR, HER2, CK5/6, EGFR, Ki-67

and AR by Immunohistochemical Analysis in Breast Cancer Cell Lines," *Breast Cancer (Auckl).*, vol. 4, pp. 35–41, May 2010.

[128] D. L. Holliday and V. Speirs, "Choosing the right cell line for breast cancer research," *Breast Cancer Res.*, vol. 13, p. 215, 2011.

[129] A. Balsalobre, F. Damiola, and U. Schibler, "A Serum Shock Induces Circadian Gene Expression in Mammalian Tissue Culture Cells," *Cell*, vol. 93, no. 6, pp. 929–937, Jun. 1998.

[130] S. Rossetti, J. Esposito, F. Corlazzoli, A. Gregorski, and N. Sacchi, "Entrainment of breast (cancer) epithelial cells detects distinct circadian oscillation patterns for clock and hormone receptor genes," *Cell Cycle*, vol. 11, no. 2, pp. 350–360, Jan. 2012.

[131] B. Chen, B. Zhang, H. Luo, J. Yuan, G. Skogerbø, and R. Chen, "Distinct MicroRNA Subcellular Size and Expression Patterns in Human Cancer Cells," *Int. J. Cell Biol.*, vol. 2012, Feb. 2012.

[132] T. A. Turunen *et al.*, "Changes in nuclear and cytoplasmic microRNA distribution in response to hypoxic stress," *Sci. Rep.*, vol. 9, no. 1, pp. 1–12, Dec. 2019.

[133] B. W. Solnestam *et al.*, "Comparison of total and cytoplasmic mRNA reveals global regulation by nuclear retention and miRNAs," *BMC Genomics*, vol. 13, no. 1, p. 574, Oct. 2012.

[134] C. D. Jeffries, H. M. Fried, and D. O. Perkins, "Nuclear and cytoplasmic localization of neural stem cell microRNAs," *RNA*, 2011.

[135] D. C. Rio, M. Ares, G. J. Hannon, and T. W. Nilsen, "Purification of RNA using TRIzol (TRI Reagent)," *Cold Spring Harb. Protoc.*, vol. 5, no. 6, Jun. 2010.

[136] Y. Guo, A. Bosompem, X. Zhong, T. Clark, Y. Shyr, and A. S. Kim, "A comparison of microRNA sequencing reproducibility and noise reduction using mirVana and TRIzol isolation methods," in *International Journal of Computational Biology and Drug Design*, 2014, vol. 7, no. 2–3, pp. 102–112.

[137] K. Deepa *et al.*, "A simple and efficient protocol for isolation of high quality functional RNA from different tissues of turmeric (Curcuma longa L.)," *Physiol. Mol. Biol. Plants*, vol. 20, no. 2, pp. 263–271, Apr. 2014.

[138] K. Wright, K. de Silva, A. C. Purdie, and K. M. Plain, “Comparison of methods for miRNA isolation and quantification from ovine plasma,” *Sci. Rep.*, vol. 10, no. 1, pp. 1–11, Dec. 2020.

[139] I. Riedmaier, M. Bergmaier, and M. W. Pfaffl, “Comparison of two available platforms for determination of RNA quality,” *Biotechnol. Biotechnol. Equip.*, vol. 24, no. 4, pp. 2154–2159, 2010.

[140] J. Kuang, X. Yan, A. J. Genders, C. Granata, and D. J. Bishop, “An overview of technical considerations when using quantitative real-time PCR analysis of gene expression in human exercise research,” *PLoS One*, vol. 13, no. 5, p. e0196438, May 2018.

[141] M. A. Gutiérrez-Monreal, V. Treviño, J. E. Moreno-Cuevas, and S.-P. Scott, “Identification of circadian-related gene expression profiles in entrained breast cancer cell lines,” *Chronobiol. Int.*, vol. 33, no. 4, pp. 392–405, Apr. 2016.

[142] A. Untergasser *et al.*, “Primer3-new capabilities and interfaces,” *Nucleic Acids Res.*, 2012.

[143] J. Ye, G. Coulouris, I. Zaretskaya, I. Cutcutache, S. Rozen, and T. L. Madden, “Primer-BLAST: a tool to design target-specific primers for polymerase chain reaction.,” *BMC Bioinformatics*, vol. 13, no. 1, p. 134, Dec. 2012.

[144] Z. Czimmerer *et al.*, “A Versatile Method to Design Stem-Loop Primer-Based Quantitative PCR Assays for Detecting Small Regulatory RNA Molecules,” *PLoS One*, vol. 8, no. 1, p. e55168, Jan. 2013.

[145] L. Yang *et al.*, “Universal Stem-Loop Primer Method for Screening and Quantification of MicroRNA,” *PLoS One*, vol. 9, no. 12, p. e115293, Dec. 2014.

[146] I. Balcells, S. Cirera, and P. K. Busk, “Specific and sensitive quantitative RT-PCR of miRNAs with DNA primers,” *BMC Biotechnol.*, vol. 11, no. 1, p. 70, Jun. 2011.

[147] C. Chen *et al.*, “Real-time quantification of microRNAs by stem–loop RT–PCR,” *Nucleic Acids Res.*, vol. 33, no. 20, pp. e179–e179, Jan. 2005.

[148] P. Mestdagh *et al.*, “High-throughput stem-loop RT-qPCR miRNA expression profiling using minute amounts of input RNA,” *Nucleic Acids Res.*, vol. 36, no. 21,

pp. e143–e143, Dec. 2008.

[149] F. Tang, P. Hajkova, S. C. Barton, K. Lao, and M. A. Surani, “MicroRNA expression profiling of single whole embryonic stem cells,” *Nucleic Acids Res.*, 2006.

[150] Y. Chen and R. L. Stallings, “Differential patterns of microRNA expression in neuroblastoma are correlated with prognosis, differentiation, and apoptosis,” *Cancer Res.*, vol. 67, no. 3, pp. 976–983, Feb. 2007.

[151] Y. Chen, J. A. L. Gelfond, L. M. McManus, and P. K. Shireman, “Reproducibility of quantitative RT-PCR array in miRNA expression profiling and comparison with microarray analysis,” *BMC Genomics*, vol. 10, no. 1, p. 407, Aug. 2009.

[152] K. Lao, N. L. Xu, V. Yeung, C. Chen, K. J. Livak, and N. A. Straus, “Multiplexing RT-PCR for the detection of multiple miRNA species in small samples,” *Biochem. Biophys. Res. Commun.*, vol. 343, no. 1, pp. 85–89, Apr. 2006.

[153] M. G. Pezzolesi, E. Satake, K. P. McDonnell, M. Major, A. M. Smiles, and A. S. Krolewski, “Circulating TGF-β1–Regulated miRNAs and the Risk of Rapid Progression to ESRD in Type 1 Diabetes,” *Diabetes*, vol. 64, no. 9, pp. 3285–3293, Sep. 2015.

[154] M. R. Green and J. Sambrook, “Optimizing primer and probe concentrations for use in real-time polymerase chain reaction (Pcr) assays,” *Cold Spring Harb. Protoc.*, vol. 2018, no. 10, pp. 825–835, Oct. 2018.

[155] D. Svec, A. Tichopad, V. Novosadova, M. W. Pfaffl, and M. Kubista, “How good is a PCR efficiency estimate: Recommendations for precise and robust qPCR efficiency assessments,” *Biomol. Detect. Quantif.*, vol. 3, pp. 9–16, Mar. 2015.

[156] M. W. Pfaffl, “A new mathematical model for relative quantification in real-time RT-PCR,” *Nucleic Acids Res.*, 2001.

[157] R. Rasmussen, “Quantification on the LightCycler,” in *Rapid Cycle Real-Time PCR*, Springer Berlin Heidelberg, 2001, pp. 21–34.

[158] K. H. Lee *et al.*, “MicroRNA-185 oscillation controls circadian amplitude of mouse Cryptochrome 1 via translational regulation,” *Mol. Biol. Cell*, vol. 24, no. 14, pp. 2248–2255, Jul. 2013.

[159] H. Wang, R. A. Ach, and B. Curry, “Direct and sensitive miRNA profiling from low-input total RNA,” *RNA*, vol. 13, no. 1, pp. 151–159, Jan. 2007.

[160] M. Izumo, T. R. Sato, M. Straume, and C. H. Johnson, “Quantitative analyses of circadian gene expression in mammalian cell cultures,” *PLoS Comput. Biol.*, vol. 2, no. 10, pp. 1248–1261, Oct. 2006.

[161] M. E. Ritchie *et al.*, “A comparison of background correction methods for two-colour microarrays.,” *Bioinformatics*, vol. 23, no. 20, pp. 2700–2707, Oct. 2007.

[162] G. K. Smyth and T. Speed, “Normalization of cDNA microarray data.,” *Methods*, vol. 31, no. 4, pp. 265–273, Dec. 2003.

[163] P. López-Romero, M. A. González, S. Callejas, A. Dopazo, and R. A. Irizarry, “Processing of Agilent microRNA array data,” *BMC Res. Notes*, vol. 3, p. 18, 2010.

[164] C.-C. Chou, C.-H. Chen, T.-T. Lee, and K. Peck, “Optimization of probe length and the number of probes per gene for optimal microarray analysis of gene expression,” *Nucleic Acids Res.*, vol. 32, no. 12, pp. e99–e99, Jan. 2004.

[165] G. Wu, R. C. Anafi, M. E. Hughes, K. Kornacker, and J. B. Hogenesch, “MetaCycle: an integrated R package to evaluate periodicity in large scale data,” *Bioinformatics*, vol. 32, no. 21, pp. 3351–3353, Nov. 2016.

[166] Y. Ru *et al.*, “The multiMiR R package and database: integration of microRNA–target interactions along with their disease and drug associations,” *Nucleic Acids Res.*, vol. 42, no. 17, pp. e133–e133, Sep. 2014.

[167] A. Fabregat *et al.*, “The Reactome pathway Knowledgebase,” *Nucleic Acids Res.*, vol. 44, no. D1, pp. D481–D487, Jan. 2016.

[168] J. T. Bass, “The circadian clock system’s influence in health and disease,” *Genome Medicine*, vol. 9, no. 1. BioMed Central Ltd., p. 94, 31-Oct-2017.

[169] J. S. Takahashi, H. K. Hong, C. H. Ko, and E. L. McDearmon, “The genetics of mammalian circadian order and disorder: Implications for physiology and disease,” *Nature Reviews Genetics*, vol. 9, no. 10. Nature Publishing Group, pp. 764–775, Oct-2008.

[170] W. Yu and P. E. Hardin, “Circadian oscillators of Drosophila and mammals,” *J. Cell*

Sci., vol. 119, no. 23, pp. 4793–4795, Dec. 2006.

[171] V. Meyer and A. Lerchl, “Evidence for species-specific clock gene expression patterns in hamster peripheral tissues,” *Gene*, vol. 548, no. 1, pp. 101–111, Sep. 2014.

[172] J. S. Menet and P. E. Hardin, “Circadian clocks: The tissue is the issue,” *Current Biology*, vol. 24, no. 1. Cell Press, pp. R25–R27, 06-Jan-2014.

[173] M. D. Ruben *et al.*, “A database of tissue-specific rhythmically expressed human genes has potential applications in circadian medicine,” *Sci. Transl. Med.*, vol. 10, no. 458, Sep. 2018.

[174] A. Yoshikawa *et al.*, “Establishment of human cell lines showing circadian rhythms of bioluminescence,” *Neurosci. Lett.*, vol. 446, no. 1, pp. 40–44, Nov. 2008.

[175] L. Pardini, B. Kaeffer, A. Trubuil, A. Bourreille, and J. P. Galmiche, “Human intestinal circadian clock: Expression of clock genes in colonocytes lining the crypt,” *Chronobiol. Int.*, 2005.

[176] A. Verlande and S. Masri, “Circadian Clocks and Cancer: Timekeeping Governs Cellular Metabolism,” *Trends in Endocrinology and Metabolism*, vol. 30, no. 7. Elsevier Inc., pp. 445–458, 01-Jul-2019.

[177] F. Sato *et al.*, “PERIOD1 is an anti-apoptotic factor in human pancreatic and hepatic cancer cells,” *J. Biochem.*, 2009.

[178] T. Oshima *et al.*, “Expression of circadian genes correlates with liver metastasis and outcomes in colorectal cancer,” *Oncol. Rep.*, 2011.

[179] X. Yang, P. A. Wood, E. Y. Oh, J. Du-Quiton, C. M. Ansell, and W. J. M. Hrushesky, “Down regulation of circadian clock gene Period 2 accelerates breast cancer growth by altering its daily growth rhythm,” *Breast Cancer Res. Treat.*, 2009.

[180] N. Yang *et al.*, “Cellular mechano-environment regulates the mammary circadian clock,” *Nat. Commun.*, vol. 8, p. 14287, 2017.

[181] H. Breast *et al.*, “Isolation and Characterization of a Spontaneously Immortalized Isolation and Characterization of a Spontaneously Immortalized Human Breast,” *Cancer Res.*, 1990.

[182] S. Xiang *et al.*, “Oscillation of clock and clock controlled genes induced by serum shock in human breast epithelial and breast cancer cells: regulation by melatonin.,” *Breast Cancer (Auckl).*, vol. 6, pp. 137–50, 2012.

[183] H.-H. Lin, M. Qraitem, Y. Lian, S. R. Taylor, and M. E. Farkas, “Analyses of *BMAL1* and *PER2* Oscillations in a Model of Breast Cancer Progression Reveal Changes With Malignancy,” *Integr. Cancer Ther.*, vol. 18, p. 153473541983649, Jan. 2019.

[184] U. Albrecht and G. Eichele, “The mammalian circadian clock,” *Current Opinion in Genetics and Development*. 2003.

[185] S. Ali and R. C. Coombes, “Estrogen receptor alpha in human breast cancer: Occurrence and significance,” *Journal of Mammary Gland Biology and Neoplasia*. 2000.

[186] B. Wörmann, “Breast cancer: basics, screening, diagnostics and treatment.,” *Med. Monatsschr. Pharm.*, 2017.

[187] S. H. Hassanpour and M. Dehghani, “Review of cancer from perspective of molecular,” *J. Cancer Res. Pract.*, 2017.

[188] C. A. Parise and V. Caggiano, “Breast cancer survival defined by the er/pr/her2 subtypes and a surrogate classification according to tumor grade and immunohistochemical biomarkers,” *J. Cancer Epidemiol.*, 2014.

[189] B. T. Hennessy *et al.*, “Characterization of a naturally occurring breast cancer subset enriched in epithelial-to-mesenchymal transition and stem cell characteristics,” *Cancer Res.*, 2009.

[190] T. Sørlie *et al.*, “Gene expression patterns of breast carcinomas distinguish tumor subclasses with clinical implications,” *Proc. Natl. Acad. Sci. U. S. A.*, 2001.

[191] M. L. Telli, “Triple-negative breast cancer,” in *Molecular Pathology of Breast Cancer*, 2016.

[192] A. MacKay *et al.*, “A high-resolution integrated analysis of genetic and expression profiles of breast cancer cell lines,” *Breast Cancer Res. Treat.*, 2009.

[193] J. Kao *et al.*, “Molecular profiling of breast cancer cell lines defines relevant tumor models and provides a resource for cancer gene discovery,” *PLoS One*, 2009.

[194] S. C. Brooks, E. R. Locke, and H. D. Soule, “Estrogen receptor in a human cell line (MCF 7) from breast carcinoma,” *J. Biol. Chem.*, 1973.

[195] K. M. Hatcher, S. E. Royston, and M. M. Mahoney, “Modulation of circadian rhythms through estrogen receptor signaling,” *European Journal of Neuroscience*. 2020.

[196] S. S. Lellupitiyage Don, H. H. Lin, J. J. Furtado, M. Qraitem, S. R. Taylor, and M. E. Farkas, “Circadian oscillations persist in low malignancy breast cancer cells,” *Cell Cycle*, 2019.

[197] A. F. Gazdar *et al.*, “Characterization of paired tumor and non-tumor cell lines established from patients with breast cancer,” *Int. J. Cancer*, 1998.

[198] S. N. Kolomeichuk, E. V. Gurov, T. S. Piskunova, M. L. Tyndyk, and V. N. Anisimov, “Expression of circadian Per1 and Per2 genes in the liver and breast tumor tissues of HER2/neu transgenic mice of different age,” *Bull. Exp. Biol. Med.*, 2011.

[199] C. A. Ramos *et al.*, “A Non-canonical Function of BMAL1 Metabolically Limits Obesity-Promoted Triple-Negative Breast Cancer,” *iScience*, 2020.

[200] G. A. Silverman *et al.*, “The serpins are an expanding superfamily of structurally similar but functionally diverse proteins. Evolution, mechanism of inhibition, novel functions, and a revised nomenclature,” *Journal of Biological Chemistry*, vol. 276, no. 36. Elsevier, pp. 33293–33296, 07-Sep-2001.

[201] S. Kiessling, A. Ucar, K. Chowdhury, H. Oster, and G. Eichele, “Genetic background-dependent effects of murine micro RNAs on circadian clock function,” *PLoS One*, 2017.

[202] L. U. Aguilera, C. Zimmer, and U. Kummer, “A new efficient approach to fit stochastic models on the basis of high-throughput experimental data using a model of IRF7 gene expression as case study,” *BMC Syst. Biol.*, 2017.

[203] E. Nagoshi, C. Saini, C. Bauer, T. Laroche, F. Naef, and U. Schibler, “Circadian Gene Expression in Individual Fibroblasts: Cell-Autonomous and Self-Sustained Oscillators Pass Time to Daughter Cells,” *Cell*, vol. 119, no. 5, pp. 693–705, Nov. 2004.

[204] M. Yalçin, R. El-Athman, K. Ouk, J. Priller, and A. Relógio, “Analysis of the circadian

regulation of cancer hallmarks by a cross-platform study of colorectal cancer time-series data reveals an association with genes involved in huntington's disease," *Cancers (Basel).*, 2020.

[205] S. Yamaguchi *et al.*, "Synchronization of Cellular Clocks in the Suprachiasmatic Nucleus," *Science (80-.).*, 2003.

[206] C. Liu, D. R. Weaver, S. H. Strogatz, and S. M. Reppert, "Cellular construction of a circadian clock: Period determination in the suprachiasmatic nuclei," *Cell*, 1997.

[207] M. E. Futschik and H. Herzel, "Are we overestimating the number of cell-cycling genes? The impact of background models on time-series analysis," *Bioinformatics*, vol. 24, no. 8, pp. 1063–1069, 2008.

[208] A. Kallio, N. Vuokko, M. Ojala, N. Haiminen, and H. Mannila, "Randomization techniques for assessing the significance of gene periodicity results," *BMC Bioinformatics*, vol. 12, p. 330, 2011.

[209] D. hyun Kim, D. Grün, and A. van Oudenaarden, "Dampening of expression oscillations by synchronous regulation of a microRNA and its target," *Nat. Genet.*, vol. 45, no. 11, pp. 1337–1344, Nov. 2013.

[210] P. Zhou, S. Cai, Z. Liu, and R. Wang, "Mechanisms generating bistability and oscillations in microRNA-mediated motifs," *Phys. Rev. E - Stat. Nonlinear, Soft Matter Phys.*, vol. 85, no. 4, p. 041916, Apr. 2012.

[211] N.-H. Du, A. B. Arpat, M. De Matos, and D. Gatfield, "MicroRNAs shape circadian hepatic gene expression on a transcriptome-wide scale," *Elife*, vol. 3, p. e02510, May 2014.

[212] N. Ludwig *et al.*, "Distribution of miRNA expression across human tissues," *Nucleic Acids Res.*, vol. 44, no. 8, pp. 3865–3877, May 2016.

[213] M. A. Baker *et al.*, "Tissue-specific MicroRNA expression patterns in four types of kidney disease," *J. Am. Soc. Nephrol.*, vol. 28, no. 10, pp. 2985–2992, Oct. 2017.

[214] R. A. Ach, H. Wang, and B. Curry, "Measuring microRNAs: Comparisons of microarray and quantitative PCR measurements, and of different total RNA prep methods," *BMC Biotechnol.*, vol. 8, no. 1, p. 69, Sep. 2008.

[215] P. Liu *et al.*, “circGNB1 Facilitates Triple-Negative Breast Cancer Progression by Regulating miR-141-5p-IGF1R Axis,” *Front. Genet.*, vol. 11, p. 193, Mar. 2020.

[216] W. Li, Y. Dong, K. J. Wang, Z. Deng, W. Zhang, and H. F. Shen, “Plasma exosomal mir-125a-5p and mir-141-5p as non-invasive biomarkers for prostate cancer,” *Neoplasma*, vol. 67, no. 6, pp. 1314–1318, 2020.

[217] G. H. Wang, L. Y. Wang, C. Zhang, P. Zhang, C. H. Wang, and S. Cheng, “MiR-1225-5p acts as tumor suppressor in glioblastoma via targeting FNDC3B,” *Open Med.*, vol. 15, no. 1, pp. 872–881, Jan. 2020.

[218] B. Li, F. Zhang, and H. Li, “miR‐1225‐5p inhibits non‐small cell lung cancer cell proliferation, migration and invasion, and may be a prognostic biomarker,” *Exp. Ther. Med.*, vol. 20, no. 6, pp. 1–1, Oct. 2020.

[219] L. Liu, W. Zhang, Y. Hu, L. Ma, and X. Xu, “Downregulation of miR-1225-5p is pivotal for proliferation, invasion, and migration of HCC cells through NFκB regulation,” *J. Clin. Lab. Anal.*, vol. 34, no. 11, p. e23474, Nov. 2020.

[220] W. Zhang, L. Wei, W. Sheng, B. Kang, D. Wang, and H. Zeng, “MiR-1225-5p Functions as a Tumor Suppressor in Osteosarcoma by Targeting Sox9,” *DNA Cell Biol.*, vol. 39, no. 1, pp. 78–91, Jan. 2020.

[221] S. Gao, P. Shi, Z. Tian, X. Yang, and N. Liu, “Overexpression of miR-1225 promotes the progression of breast cancer, resulting in poor prognosis,” *Clin. Exp. Med.*, vol. 21, no. 2, pp. 287–296, May 2021.

[222] Z. Yu *et al.*, “microRNA 17/20 inhibits cellular invasion and tumor metastasis in breast cancer by heterotypic signaling,” *Proc. Natl. Acad. Sci.*, vol. 107, no. 18, pp. 8231–8236, May 2010.

[223] L. Jin *et al.*, “The metastatic potential of triple-negative breast cancer is decreased via caloric restriction-mediated reduction of the miR-17~92 cluster,” *Breast Cancer Res. Treat.*, vol. 146, no. 1, pp. 41–50, Jul. 2014.

[224] Q. Gao, L. Zhou, S.-Y. Yang, and J.-M. Cao, “A novel role of microRNA 17-5p in the modulation of circadian rhythm,” *Sci. Rep.*, vol. 6, p. 30070, Jul. 2016.

[225] L. Castellano *et al.*, “The estrogen receptor-α-induced microRNA signature regulates

itself and its transcriptional response," *Proc. Natl. Acad. Sci.*, vol. 106, no. 37, pp. 15732–15737, Sep. 2009.

[226] E. C. Luo *et al.*, "MicroRNA-769-3p down-regulates NDRG1 and enhances apoptosis in MCF-7 cells during reoxygenation," *Sci. Rep.*, vol. 4, no. 1, pp. 1–8, Aug. 2014.

[227] J.-J. Zhao *et al.*, "MicroRNA-221/222 Negatively Regulates Estrogen Receptorα and Is Associated with Tamoxifen Resistance in Breast Cancer," *J. Biol. Chem.*, vol. 283, no. 45, pp. 31079–31086, Nov. 2008.

[228] M. S. Blattner and M. M. Mahoney, "Estrogen receptor 1 modulates circadian rhythms in adult female mice," *Chronobiol. Int.*, vol. 31, no. 5, pp. 637–644, Jun. 2014.

[229] C. E. Joyce *et al.*, "Deep sequencing of small RNAs from human skin reveals major alterations in the psoriasis miRNAome," *Hum. Mol. Genet.*, vol. 20, no. 20, pp. 4025–4040, Oct. 2011.

[230] J. S. Takahashi, "Transcriptional architecture of the mammalian circadian clock," *Nature Reviews Genetics*, vol. 18, no. 3. Nature Publishing Group, pp. 164–179, 01-Mar-2017.

Published Papers

International Journal of
Molecular Sciences

MDPI

Article

Entrainment of Breast Cell Lines Results in Rhythmic Fluctuations of MicroRNAs

Rafael Chacolla-Huaringa [1,2], Jorge Moreno-Cuevas [1], Victor Trevino [3] and Sean-Patrick Scott [1,*]

1 Grupo de Investigación en Terapia Celular y Medicina Regenerativa, Escuela de Medicina, Tecnológico de Monterrey, Monterrey NL 64710, Mexico; rafael.chacolla@cienciamed.com (R.C.-H.); jemoreno@itesm.mx (J.M.-C.)
2 Cienciamed Company, San Pedro Garza García NL 66278, Mexico
3 Grupo de Investigación en Bioinformática, Escuela de Medicina, Tecnológico de Monterrey, Monterrey NL 64710, Mexico; vtrevino@itesm.mx
* Correspondence: spscott@itesm.mx; Tel.: +52-81-8888-2161

Received: 17 May 2017; Accepted: 5 July 2017; Published: 12 July 2017

Abstract: Circadian rhythms are essential for temporal (~24 h) regulation of molecular processes in diverse species. Dysregulation of circadian gene expression has been implicated in the pathogenesis of various disorders, including hypertension, diabetes, depression, and cancer. Recently, microRNAs (miRNAs) have been identified as critical modulators of gene expression post-transcriptionally, and perhaps involved in circadian clock architecture or their output functions. The aim of the present study is to explore the temporal expression of miRNAs among entrained breast cell lines. For this purpose, we evaluated the temporal (28 h) expression of 2006 miRNAs in MCF-10A, MCF-7, and MDA-MB-231 cells using microarrays after serum shock entrainment. We noted hundreds of miRNAs that exhibit rhythmic fluctuations in each breast cell line, and some of them across two or three cell lines. Afterwards, we validated the rhythmic profiles exhibited by miR-141-5p, miR-1225-5p, miR-17-5p, miR-222-5p, miR-769-3p, and miR-548ay-3p in the above cell lines, as well as in ZR-7530 and HCC-1954 using RT-qPCR. Our results show that serum shock entrainment in breast cells lines induces rhythmic fluctuations of distinct sets of miRNAs, which have the potential to be related to endogenous circadian clock, but extensive investigation is required to elucidate that connection.

Keywords: circadian rhythms; rhythmic fluctuations microRNAs; microarrays; RT-qPCR; breast cancer

1. Introduction

The circadian clock regulates the physiology and behavior of most species with a periodicity of approximately 24 h [1]. Mammalian cells synchronize their external and internal environments, which is critical for their well-being and survival. A lack of synchronicity might trigger diverse disorders, such as depression, diabetes, hypertension, and cancer [2].

Molecularly, the circadian system is involved in transcription, translation, protein–protein interaction, phosphorylation, and protein degradation processes, all of which participate in the biological cycles to 24 h environmental periods [3]. It is known that the circadian clock contains "clock" genes and their protein products are arranged such that they are capable of configuring an auto-regulatory feedback system [4], but the knowledge about other processes is limited. For instance, well-known clock genes such as *PER2* and *BMAL1* are expressed rhythmically in different cell types, such as adipocytes [5], myocytes [6], and stem cells [7]. They may display different phases depending on the tissue [8]. Moreover, these genes also display rhythmic expression for non-tumorigenic breast cell lines but lack of rhythmicity in tumorigenic breast cell lines (defective-clock) [9,10]. Conversely, Gutierrez et al. reported other genes displaying circadian-like expression profiles after entrainment,

even in defective-clock breast cell lines [11]. This evidence suggests that additional regulatory components may be involved in the circadian system.

Recently, post-transcriptional regulatory events have been recognized as important factors in the circadian system [12]. The miRNAs are a group of short, non-coding RNAs of about 23 nucleotides that regulate the level of expression of target genes and subsequent protein translation [13]. A proteomic study of mouse liver revealed that up to 20% of soluble proteins exhibit rhythmic expression, whereas only about 10% of their transcriptional levels are rhythmic, which suggests that miRNAs may conduct a regulatory function [14]. In addition, there have been reports of particular miRNAs exhibiting rhythmic changes in expression over certain time periods in mice [15,16] and rats [17]. Thus, miRNAs seem to be a potential way in which to investigate biological timing processes that might be critical for cancer cells [18,19]. A recent study provides direct evidence that circadian disruption induces changes in miRNA levels in the mammary tissue of rats, which may lead to malignant consequences [20].

Over the last few years, there has been an increasing amount of studies linking abnormal miRNA expression to breast cancer tissue [21,22], but there is still no evidence linking periodicity, circadian clock, and miRNA expression in breast cells. Therefore, in this work, we explored a temporal expression of miRNAs among entrained breast cell lines, regardless of their circadian status (e.g., *PER2* and *BMAL1* profiles). We initiated the study by establishing cultures of breast cells, entraining with 50% horse serum, and obtaining nucleic acid samples at 4 h intervals over 48 h. Next, we analyzed the miRNA expression profiles using microarrays in three human breast cell lines, MCF-10A, MCF-7, and MDA-MB-231—over a period of 28 h. Microarray data was used to identify rhythmic miRNAs. Six miRNAs were selected to confirm their rhythmicity by reverse transcription quantitative PCR (RT-qPCR) assays over 48 h of study and testing in two additional breast cancer cell lines, ZR-7530 and HCC-1954.

2. Results

2.1. Entrainment of Human Breast Cell Cultures

In order to analyze the temporal mRNA expression of human breast cell lines, we entrained cell cultures using the well-known serum shock method [23,24]. In order to verify the entrainment, we measured-the expression level of two known clock genes using RT-qPCR in five breast cell lines. *BMAL1* and *PER2* genes exhibited distinctive, opposite expression profiles in MCF-10A (a non-tumorigenic cell line), with periods of 24.15 and 20.40 h, respectively (see Figure 1A). Previous studies achieved similar results [9–11], which suggests that proper entrainment was used in our experiments. The genes did not exhibit rhythmicity in the tumorigenic cell lines—MCF-7, MDA-MB-231, HCC-1954, and ZR-75-30 (see Figure 1B–E)—as were reported previously [9–11]. In addition, we measured the expression level of *SERPINB1* gene in MCF-7 (see Supplementary Figure S1), which exhibited a particular rhythmic profile, as we reported previously [11]. The results confirm that MCF-10A and MCF-7 were properly entrained and support the validity of the cell culture procedures.

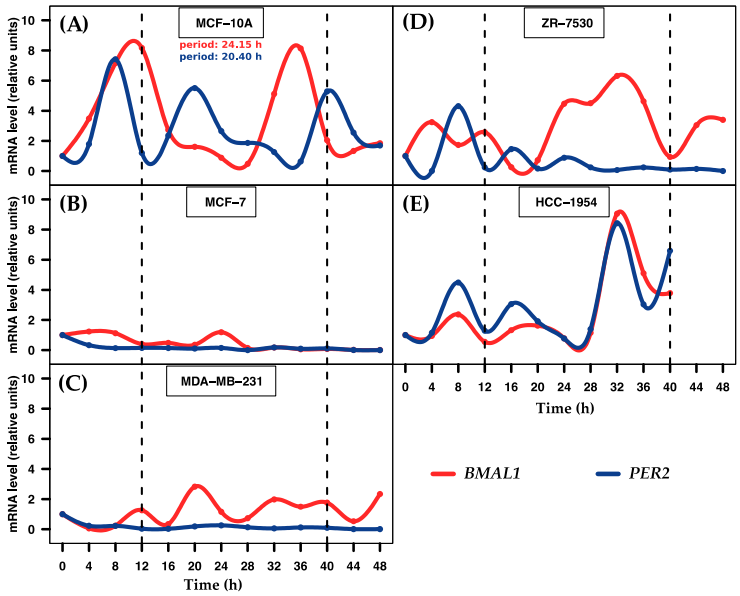

Figure 1. Temporal expression of *BMAL1* and *PER2* genes in five breast cell lines. The graph depicts the level of expression of two clock genes at 4 h intervals over 48 h after 2 h serum shock entrainment. (**A**) MCF-10A cells show rhythmic profiles of both genes; (**B**–**E**) MCF-7, MDA-MB-231, ZR-7530 and HCC-1954 cells do not show rhythmic profiles. Dashed black lines at 12 and 40 h were added to show the period during which the profiles exhibited robustness. Data points (means of two biological replicates) were normalized using GAPDH relative to the first time point (t = 0) within each corresponding cell line.

2.2. Statistical Analysis of miRNA Rhythmic Profiles

We analyzed the temporal expression (8 time points) of 2006 miRNAs in non-tumorigenic breast MCF-10A cells and two tumorigenic cell lines, MCF-7 and MDA-MB-231, using a cosine-fitting function to identify potential rhythmic miRNAs. Prior to this analysis, we generated additional data by running five types of randomization (TL (time-label), RW (row-wise), CW (column-wise), RCW (row-column-wise), and RCWB (row-column-wise by blocks)) on our experimental data (MCF-10A, MCF-7, and MDA-MB-231) to assess whether our microarray data are random. For this purpose, we assessed the distributions of the features associative to rhythmicity, including cosine correlation, period, and phase of the experimental and randomized data.

We found that the distributions of the experimental data were nearly equivalent (see Supplementary Figure S2). However, we observed differences when these distributions were compared with the distributions of randomized data. Specifically, data obtained using the TL and RW methods had similar structures to the experimental data, including similar cosine correlations, periods, and phase distributions. Data obtained using the CW and RCW methods had different structures than the experimental data, including different cosine correlations and phase distributions (but not period distributions). Data obtained using the RCWB method showed marked differences in structure compared with the experimental data, including different cosine correlations, periods, and phases (see Supplementary Figure S3A–C).

We confirmed that the RCWB method changes the structure of the experimental data. Thus, we plotted the cosine correlations and periods for experimental and randomized data. We noted that

randomized data has a high proportion of transcripts with periods less than 0.22, which means they cannot be categorized as rhythmic transcript (periods close to 0.26) (see Supplementary Figure S3D). We also compared periods between the experimental and randomized data, finding that the randomized data features have fewer rhythmic periods than from the experimental data (see Supplementary Figure S3E).

In summary, the similar structures of the experimental and randomized data show that the cosine fitting function can calculate mathematical rhythmic features by chance, it is often observed when statistical analysis is performed in short temporal expression data [25]. However, our last results suggest that the RCWB method effectively removes the biological structure from experimental data and shows that the cosine fitting function can be used to calculate the circadian parameters of transcripts [26]. The current evaluation is consistent with our previous study [11].

2.3. Determination of miRNAs with Rhythmic Expression

We used the cosine-fitting function on temporal microarray data collected from MCF-10A, MCF-7, and MDA-MB-231 to identify putative miRNA with rhythmic patterns. We identified different amounts of rhythmic miRNAs in three tested breast cell lines. A total of 143 (7.12%) rhythmic miRNAs were found in MCF-10A, which can be stratified into six clusters according to phase, with apparently distinct rhythmic expression patterns (see Figure 2A and Figure S4A). MCF-7 and MDA-MB-231 had 183 (9.12%) and 147 (7.32%) rhythmic miRNAs, respectively, and their phase clusters were similar to those of MCF-10A (see Figure 2B,C and Figure S4B,C). Thus, we wondered whether the identified miRNAs were specific to certain cell lines. After our analysis, 9 additional miRNAs were found in MCF-10A and MCF-7. This observation was highly significant (p = 0.03, hypergeometric test). We also noted that 11 miRNAs significantly overlapped across the tumorigenic cell lines MCF-7 and MDA-MB-231 (p = 0.007, hypergeometric test) and 8 miRNAs overlapped across MCF-10A and MDA-MB-231 (p = 0.02, hypergeometric test). We identified 2 rhythmic miRNAs present in the 3 tested breast cell lines (see Figure 2D). Taken together, these diverse results show a large component of specific rhythmic miRNAs and only small common component feature rhythmicity among the tested breast cell lines. This is presented in Tables S1–S3, which depict the miRNAs, cosine correlations, periods, and phases obtained from the cosine-fitting function.

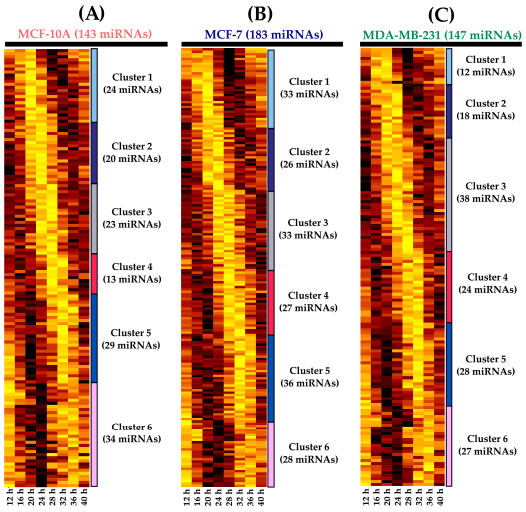

Figure 2. *Cont.*

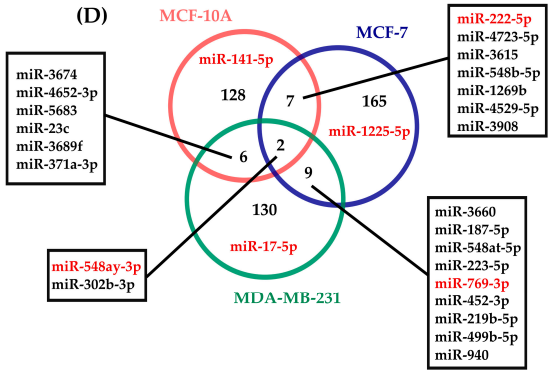

Figure 2. Rhythmic expression of miRNAs identified in three breast cell lines. The heat maps depict the expression level of miRNAs over 28 h (hours 12–40 of the 48 h study) in (**A**) MCF-10A; (**B**) MCF-7; and (**C**) MDA-MB-231 cells. In addition, the heat maps show 6 different clusters of miRNAs that depict marked phases. Brown colors represent higher expression values, while yellow colors represent lower expression values. Expression values are z-scaled relative to each cell line; (**D**) Venn diagram of 143, 183, and 147 miRNAs that were rhythmically expressed over 28 h in MCF-10A, MCF-7, and MDA-MB-231. The diagram also shows miRNAs that exhibited rhythmicity across cell lines and were selected for RT-qPCR validation (red).

2.4. Validation of Rhythmic Expression Profiles Using RT-qPCR

For validation purposes, we selected miRNAs with similar or opposite rhythmic profiles. We selected one miRNA that displayed rhythmicity only for MCF-10A (miR-141-5p), MCF-7 (miR-1225-5p), and MDA-MB-231 (miR-17-5p). Additionally, we selected miR-769-3p because it shared a similar profile for MCF7 and MB-MDA-231 and miR-222-5p because it had opposite profiles for MCF-10A and MCF-7, according to the microarray data. Finally, we included miR-548ay-3p because it exhibited rhythmic expression in MCF-10A, MCF-7, and MDA-MB-231 (see Figure 2D). In order to provide a broader view of the rhythmic expression of miRNAs, we validated the expression using RT-qPCR assays over 48 h. Additionally, we measured the temporal expression of the selected miRNAs in two other tumorigenic breast cell lines, ZR-7530 and HCC-1954 (note that the last two time points of HCC-1954 are missing).

After comparing the miRNAs temporal expression between microarray and RT-qPCR results, we observed similar profiles, suggesting reproducibility among assays (see Figures 3–5). The significance of the rhythmicity of miRNAs was evaluated using MetaCycle [27] ($p < 0.05$). In MCF-10A, miR-141-5p displayed the expected rhythmicity (MetaCycle p-value = 0.023). However, this miRNA also displayed significant rhythmicity in MCF-7 and HCC-1954 (MetaCycle p-values of 0.0011 and 0.041, respectively), which was not observed in the microarray data. We observed that miR-141-5p exhibited lower amplitude in MCF-7 than MCF-10A and HCC-1954 (see Figure 3A). As observed in the microarray analysis, miR-1225-5p did not display significant rhythmicity in MCF-7 cells, but it did display rhythmicity in ZR-7530 and HCC-1954 (MetaCycle p-values of 0.0079 and 0.037, respectively). Nonetheless, it exhibited low amplitudes across five breast cell lines (see Figure 3B). The miR-17-5p displayed the expected rhythmicity in MDA-MB-231 cells (MetaCycle p-value = 0.0018), and it also exhibited rhythmicity in HCC-1954 (MetaCycle p-value = 0.037) (see Figure 3C).

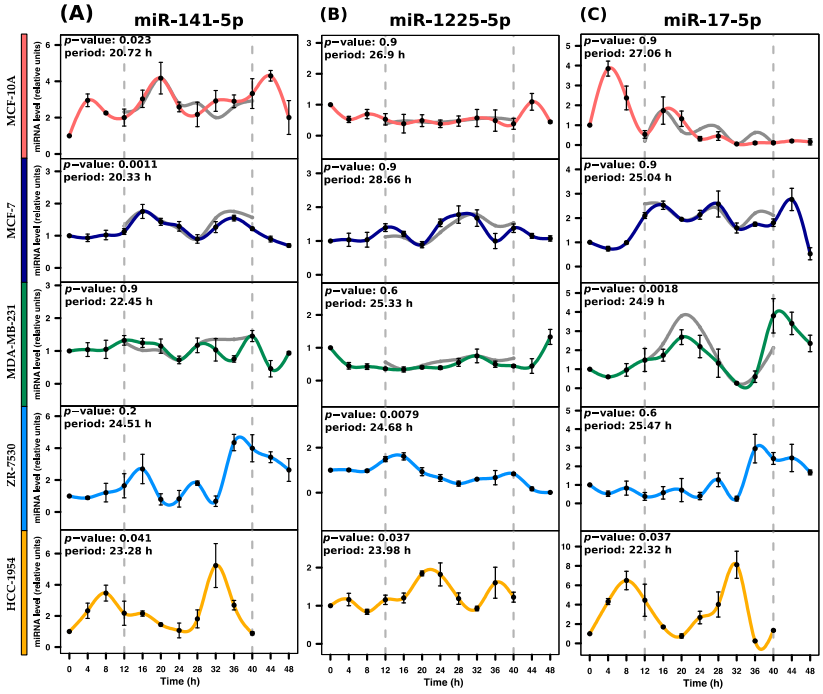

Figure 3. Expression profiles of miR-141-5p, miR-1225-5p, and miR-17-5p across breast cell lines as determined by RT-qPCR. Their rhythmic expression was evaluated by RT-qPCR in serum-shocked MCF-10A, MCF-7, MDA-MB-231, ZR-7530, and HCC-1954 cells over 48 h (4 h intervals). (**A**) miR-141-5p exhibits rhythmic profiles in MCF-10A, MCF-7 and HCC-1954 cells; (**B**) miR-1225-5p exhibits rhythmic profiles in ZR-7530 and HCC-1954 cells; (**C**) miR-17-5p exhibits rhythmic profiles in MDA-MB-231 and HCC-1954 cells. Data points (means of three biological replicates ± standard error of the mean (SEM)) were normalized using miR-106a-5p relative to the first time point (t = 0). The p-value and period values of rhythmic profiles were obtained from the MetaCycle analysis and are illustrated at the top of each plot. Expression profiles with p-values less than 0.05 were considered rhythmic. For comparison purposes, the gray lines in the graphs concerning MCF-10A, MCF-7, and MDA-MB-231 illustrate the expression profiles obtained from the microarray data, which were scaled to the expression profile obtained from RT-qPCR assays. Dashed gray lines at 12 h and 40 h were added to show the period in which profiles were measured by microarray.

The miR-769-3p displayed significant rhythmicity in MCF-7 and MDA-MB-231, both of which featured MetaCycle p-values close to 0.02 and demonstrated profiles consistent with those obtained from the microarray (see Figure 4A). The miR-222-5p displayed significant rhythmic expression in MCF-10A and MCF-7 (MetaCycle p-values of 0.017 and 0.049, respectively) and profiles consistent with the microarray results (see Figure 4B). These miRNAs were also evaluated in the remaining three breast cell lines and demonstrated non-significant rhythmicity (data not shown). The miR-548ay-3p exhibited the expected rhythmic expression in MCF-10A and MDA-MB-231 cells (MetaCycle p-value = 0.021 and 0.0026, respectively), but not in MCF-7 cells (Figure 5). However, it displayed significant rhythmicity in ZR-7530 and HCC-1954 (MetaCycle p-values of 5.51×10^{-7} and 0.0039, respectively). Additionally, we observed that mir-548ay-3p exhibited large-scale peaks of expression in MCF-10A and ZR-7530,

Int. J. Mol. Sci. 2017, 18, 1499

with, interestingly, opposite profiles (Figure 5). See Table 1 for the rhythmic features and statistical significance of the six miRNAs determined by validation.

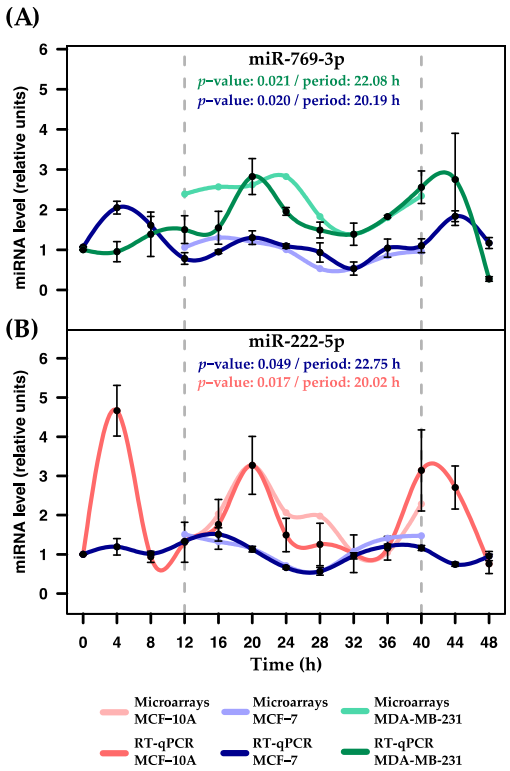

Figure 4. Expression profiles of miR-769-3p and miR-222-5p in three breast cell lines. Rhythmic expression was evaluated using RT-qPCR in serum-shocked MCF-10A, MCF-7, and MDA-MB-231 cells over 48 h (4 h intervals). (**A**) Rhythmic profiles of miR-769-3p obtained from microarray and RT-qPCR assays in MCF-7 and MDA-MB-231 cells; (**B**) Rhythmic profiles of miR-222-5p obtained from microarray and RT-qPCR assays in MCF-10A and MCF-7 cells. Data points (means of three biological replicates ± SEM) were normalized using miR-106a-5p relative to the first time point ($t = 0$). The p-values and period values of rhythmic profiles were obtained from MetaCycle analysis and are illustrated at the top of each plot. Expression profiles with p-values less than 0.05 were considered rhythmic. For comparison purposes, the more lightly colored lines illustrate the expression profiles obtained from microarray assays, which were scaled to the expression profiles obtained from RT-qPCR assays. Dashed gray lines at 12 and 40 h were added to show the periods in which the profiles were measured by microarrays.

Int. J. Mol. Sci. 2017, 18, 1499 8 of 19

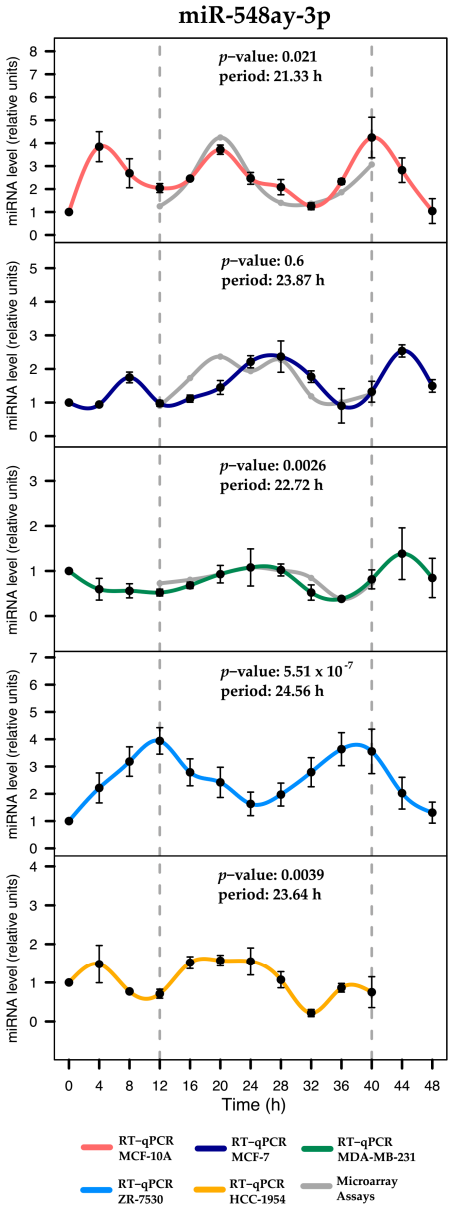

Figure 5. Expression profiles of miR-548ay-3p across breast cell lines. Rhythmic expression was evaluated using RT-qPCR in serum-shocked MCF-10A, MCF-7, MDA-MB-231, ZR-7530, and HCC-1954 cells over 48 h (4 h intervals). Data points (means of three biological replicates ± SEM) were normalized using miR-106a-5p relative to the first time point ($t = 0$). The p-values and period values of rhythmic profiles were obtained from MetaCycle analysis and are illustrated at the top of each plot. For comparison purposes, the gray line illustrates the expression profiles obtained from microarray assays, which were scaled to the expression profiles obtained from RT-qPCR assays. Dashed gray lines at 12 and 40 h were added to show the period in which the profiles were measured by microarrays.

Table 1. Rhythmic features of the miRNA expression profiles obtained over 48 h from the MetaCycle algorithm for non-tumorigenic and tumorigenic breast cell lines.

miRNA	*p*-Value	Period (h)	Phase (h)	Amplitude
MCF-10A				
hsa-miR-141-5p	0.0239 *	20.72	19.97	2.3
hsa-miR-1225-5p	0.9901	26.91	9.12	0.71
hsa-miR-17-5p	0.9659	27.06	4.73	3.79
hsa-miR-769-3p	0.9439	25.33	6.79	1.95
hsa-miR-222-5p	0.0174 *	20.02	0.40	3.91
hsa-miR-548ay-3p	0.0219 *	21.33	20.56	3.2
MCF-7				
hsa-miR-141-5p	0.0012 *	20.34	17.88	1.06
hsa-miR-1225-5p	0.9526	28.67	1.53	0.89
hsa-miR-17-5p	0.9050	25.04	19.81	2.24
hsa-miR-769-3p	0.0205 *	20.19	2.26	1.2
hsa-miR-222-5p	0.0492 *	22.75	13.95	0.94
hsa-miR-548ay-3p	0.6690	23.87	1.99	1.63
MDA-MB-231				
hsa-miR-141-5p	0.9372	22.46	13.76	0.99
hsa-miR-1225-5p	0.6841	25.33	4.72	0.99
hsa-miR-17-5p	0.0018 *	24.90	20.16	3.53
hsa-miR-769-3p	0.0214 *	22.09	19.90	2.55
hsa-miR-222-5p	0.7651	25.80	7.37	1.06
hsa-miR-548ay-3p	0.0027 *	22.73	1.09	1
ZR-7530				
hsa-miR-141-5p	0.2357	24.52	15.42	3.68
hsa-miR-1225-5p	0.0079 *	24.69	13.19	1.6
hsa-miR-17-5p	0.6695	25.47	16.15	2.69
hsa-miR-769-3p	0.9661	28.67	14.22	1.76
hsa-miR-222-5p	0.1897	27.15	7.89	2.24
hsa-miR-548ay-3p	0.00001 *	24.56	12.47	2.63
HCC-1954				
hsa-miR-141-5p	0.0411 *	23.28	9.51	4.35
hsa-miR-1225-5p	0.0373 *	23.99	21.86	1
hsa-miR-17-5p	0.0380 *	22.32	8.14	7.87
hsa-miR-769-3p	0.9610	21.33	18.46	4.65
hsa-miR-222-5p	0.9907	28.67	7.65	6.22
hsa-miR-548ay-3p	0.0040 *	23.64	21.33	1.36

* $p < 0.05$ around 24 h.

2.5. Identification of the Target mRNAs in a Group of miRNAs

After the six miRNAs were validated, we sought their gene targets in multiMiR [28]. It lists the gene targets that were experimentally validated for each miRNA. Of the six miRNAs, only miR-17-5p revealed targets (343 genes in total). We then performed an enrichment analysis using the Reactome enrichment tool, which identified 200 enriched pathways (see Supplementary Table S4). We observed the circadian clock pathways ($p = 0.0027$, FDR = 0.049, rank = 51) of five genes, MEF2D, PPP1CA, NPAS2, PER1, and RPS27A.

3. Discussion

The circadian system is responsible for cell-signaling processes during periods of about 24 h whose disruption might be associated with transcriptional and post-transcriptional changes in normal

and tumorigenic tissues [29]. In this system, BMAL1 and PER2 proteins play a critical role in the functioning of the molecular clock. BMAL1 (also known as ARNTL) and its partner CLOCK comprise a core transcription complex that is needed to generate circadian oscillations in cells [30]. PER2 directly and rhythmically binds to this complex to drive the circadian negative feedback loop [31]. These components are necessary for regulation of circadian rhythms within individual non-tumorigenic cells.

To further understand the circadian clock at the molecular level, the scientific community has begun to explore the non-coding class of small RNAs known as miRNAs, which regulate gene expression [32]. There is evidence that some miRNAs display rhythmic changes in expression over certain periods in mice and rats [15–17]. Hence, we sought to explore the expression changes of miRNAs by a 48 h time-course study after serum shock entrainment of human non-tumorigenic and tumorigenic breast cell lines regardless *BMAL* and *PER2* status. To determine if there are miRNAs that may exhibit rhythmic fluctuation across breast cell lines, we first entrained the cell cultures and measured the temporal expression of *BMAL1* and *PER2* genes to assess the status of the circadian system. These genes displayed the circadian characteristic expression profiles in MCF-10A (non-tumorigenic), but not in the remaining breast cell lines assayed, as previously reported [9–11]. Moreover, the association between disrupted circadian rhythm and cancer is well known [33]. Despite this, we have previously reported some coding genes expressed rhythmically in clock-defective breast cell lines [11]. We confirmed the pattern for SERPINB1 in MCF-7 cells [11]. This evidence suggests that may exist alternative mechanisms that induce rhythmic, but further investigation is required to elucidate this hypothesis.

Diverse post-transcriptional mechanisms have been reported to regulate the circadian clock in mammalian cells [12]. The regulatory function of miRNAs, especially regarding circadian expression, was observed in clock genes [34] and the liver transcriptome [18] of mammalian cells. However, it is still unknown if miRNAs display a rhythmicity feature in non-tumorigenic and tumorigenic cell lines. Prior to identifying these miRNAs, we confirmed that our data results are not random by contrasting the distributions of the rhythmic features calculated from experimental data with those in data without a biological structure (patternless and randomized). The RCWB method changed noticeably the structure of the experimental data. The results can be explained by the simultaneous shuffling of columns and rows in two separate blocks to ensure a lack of intrinsic pattern in the data [26]. Biologically, it might be justified by the assumption that miRNAs feature diverse temporal patterns of expression [35], such as starting and ending expressions with slow peaks or dampened expression. Therefore, our results suggest that short time course data should be randomized using an appropriate method, such as RCWB, to achieve more accurate null distributions [26]. We believe that our validation of miRNA profiles using RT-qPCR is the best evidence that microarray data are not random.

Rhythmic miRNAs were classified based on cosine correlation, period, amplitude, and phase reaching a total of 143, 183, and 147 miRNAs identified for MCF-10A, MCF-7, and MD-MBA-231, respectively. These results showed that less than 10% of miRNAs maintained rhythmicity across distinct breast cell lines, consistent with the hypothesis that the expression of miRNAs depends on the origin of the breast cells [36]. Notably, some rhythmic miRNAs display distinct phases across cell lines (observed in Figures 3–5). Phase changes have been also observed in clock genes in liver and kidney tissues from mice with colorectal liver metastases [37]. Although miRNAs in these conditions have not yet been explored, our observations suggest that shifts in phases are common depending on the cell type origin.

Our analysis identified 9 miRNAs that exhibit rhythmicity in both MCF-10A and MCF-7, but at different phases. This suggests that both cell lines have distinct internal timing in biological processes, likely due to their estrogen receptor (ER) status, which is over-expressed in MCF-7 cells and involved in circadian molecular machinery [38]. In addition, 8 miRNAs were determined to exhibit rhythmicity in both MCF-10A and MDA-MB-231 also with shifts in phases, nevertheless estrogen receptor is

unlikely to be involved in MDA-MB-231 due to its feature of low ER expression. Moreover, 11 miRNAs found in both MCF-7 and MDA-MB-231 also exhibited shifts in phases. This may be due to their subtype of breast cancer or ER status, MCF-7 (ER(+) and PR(+)), while MDA-MB-231 (ER(−), PR(−), and HER2/neu(−)).

Next, we validated the rhythmic expression of six miRNAs that were present in one or more cell lines using RT-qPCR across five breast cell lines. Overall, we observed that the non-validated miRNAs profiles were mostly associated with short amplitudes in the microarray results. This issue often arises in validation assays [39]. Apparently, the short amplitudes may be noise instead of a rhythmic signal. From the miRNAs that exhibited rhythmicity in the microarray results, the miR-141-5p that exhibited rhythmicity only for MCF-10A was also detected in MCF-7 and HCC-1954 by RT-qPCR. The fact that these three breast cell lines with distinct features share this miRNA rhythmicity is intriguing and should be further studied. Notably, one study reported that miR-141-5p showed circadian expression in rat enterocytes [17]. We also found that miR-1225-5p, which was observed in the microarray analysis in MCF-7 was not validated by RT-qPCR, but surprisingly, the profile of miR-1225-5p seems rhythmic in ZR-7530 and HCC-1954 cells although at low amplitudes, suggesting randomness. The miR-17-5p exhibited rhythmic expression in MDA-MB-231 and HCC-1954. Interestingly, both cell lines are negative for ER and PR, but differ in terms of ERBB2 (HER2/neu) expression. Thus, the rhythmicity exhibited in both cell lines appears to be beyond the biological function of the receptor tyrosine-kinase. Additionally, this miRNA is a member of the well-known miR-17/92 cluster, which is largely related to breast cancer as an oncogene and tumor suppressor [40,41]. We also noted that miR-17-5p has potential 343 targeted mRNAs, five genes of which (*MEF2D*, *PPP1CA*, *NPAS2*, *PER1*, and *RPS27A*) are involved in the circadian clock pathway ($p = 0.0027$). Interestingly, a recent study found that miR-17-5p stabilizes the circadian clock period by inhibiting the translation of Clock and Npas2 in mice [42]. These results are encouraging and propose that the other miRNAs identified in the same way than mir-17-5p may play a potential role in rhythmicity. Nevertheless, further investigation is required to validate the remaining molecular associations.

Additionally, we validated the microarray results identifying miRNAs that exhibit shared rhythmicity among MCF-10A, MCF-7, and MDA-MB-231. The miR-769-3p displayed similar rhythmic profiles for MCF-7 and MDA-MB-231. However, the temporal expression of this miRNA for MCF-7 exhibited lower amplitude. These results agrees with evidence showing that miRNA biogenesis is altered in cells with ERα over-expression [43], while MDA-MB-231 are ERα-negative cells that presumably have different miRNA expression. Taken together, this evidence suggests that both cell lines share some inner mechanisms, despite the fact that they are distinct subtypes of breast cancer. The miR-222-5p displayed rhythmicity in MCF-10A and MCF-7 with markedly distinct amplitudes. Previous studies reported that miR-222-5p plays a role in the regulation of ERα expression in breast cancer cells by promoting the transition from ER-positive to ER-negative tumors during the progression of cancer [44] and related to circadian clock outputs [45]. Taken together, this evidence suggests that miR-222-5p expression may participate in different mechanisms between both breast cell lines unknown as of yet. The rhythmic expression of miR-548ay-3p was validated in MCF-10A and MDA-MB-231, but not in MCF-7. Interestingly, it also exhibited rhythmic patterns in ZR-7533 and HCC-1954. To date, no studies have investigated this miRNA because it was discovered only recently [46].

In general, stimuli (e.g., drugs, hormones)—in this case serum shock—might exert transcriptional control (induction) over coding and non-coding genes (see Figure 6), which further play roles in specific cell functions or as a feedback loop in the circadian system. For coding genes, the mechanisms are well known [47]. In breast cell lines, we have previously observed similar number of rhythmic coding genes but at different amplitudes [11]. In this work, we have shown the miRNA may also be rhythmic. It is unknown how this emerges, what is their contribution to tune specific cell functions, or their possible role in the feedback loop. Our data may contribute in this direction.

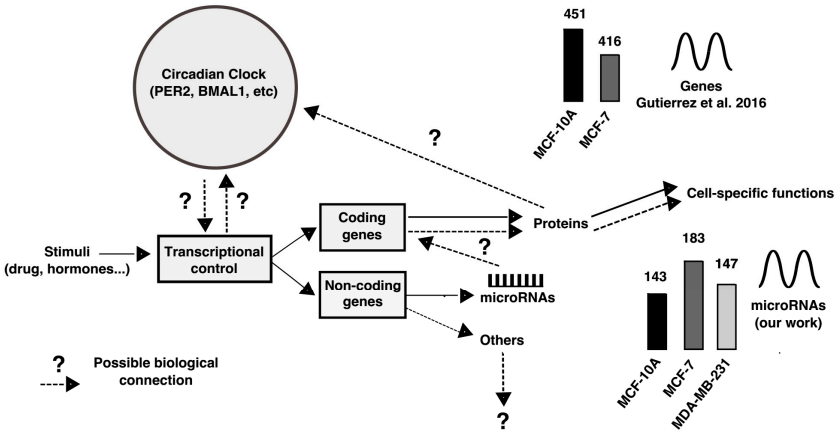

Figure 6. Overview of circadian control and the insight of the rhythmic miRNAs in this system. Continuous lines between concepts represent known facts. Dashed lines represent unknown information. Particularly, derived from our study it is still unknown what could be the role of rhythmic miRNAs to specific cell function and to circadian control. Circadian control inspired in [47].

4. Materials and Methods

4.1. Cell Lines and Culture Procedures

The breast cell lines MCF-10A (ATCC® CRL-110317™), MCF-7 (ATCC® HTB-22™), and HCC-1954 (ATCC® CRL-2338™) were purchased from the American Type Culture Collection (ATCC®, Rockville, MD, USA). MDA-MB-231 and ZR-75-30 cell lines were donated by Nadia Jacobo Herrera from Instituto Nacional de Ciencias Médicas y Nutrición "Salvador Zubirán" in Mexico City, Mexico. Non-tumorigenic human breast cells (MCF-10A) were grown in Mammary Epithelial Basal Medium® supplemented with SingleQuots® from the MEGM® BulletKit® (Lonza, Walkersville, MD, USA). The tumorigenic breast cell lines, ZR-75-30 and HCC-1954, were grown in Gibco® Roswell Park Memorial Institute (RPMI)-1640 medium (Thermo Fisher Scientific, Grand Island, NY, USA) supplemented with 10% and 15% heat-inactivated Gibco® Fetal Bovine Serum (FBS) (Thermo Fisher Scientific), respectively. The MCF-7 and MDA-MB-231 cell lines were grown in Gibco® Dulbecco's Modified Eagle Medium, which features a nutrient mixture of D-MEM and F-12 (Thermo Fisher Scientific), supplemented with 10% heat-inactivated FBS. Each culture medium was supplemented with Gibco® Penicillin-Streptomycin antibiotics (Thermo Fisher Scientific). Cell cultures were grown at 37 °C with 5% CO_2 and 95% air in a humidified incubator.

4.2. Serum Shock Synchronization

Cells were seeded in six-well plates and until they reached near-confluence. Then, cells were synchronized using the serum shock procedure [10]. One day before serum shock, the plates with confluent cells were washed and left overnight in serum-free basal medium (starvation). RPMI-1640 was the basal medium for the ZR-75-30 and HCC-1954 cells, while D-MEM/F-12 was used for the MCF-10A, MCF-7, and MDA-MB-231 cells. After overnight starvation, the medium was exchanged with the appropriate basal medium, which contained 50% horse serum (Biowest, Mountain View, CA, USA). After incubation for 2 h at 37 °C, the medium was replaced with a serum-free basal medium. At this time (time zero), we started to harvest cells every 4 h for 48 h. Time samples were collected separately to confirm synchronization (by duplicate) and miRNA expression (by triplicate; two wells of a six-well plate were merged to make one replicate). This protocol was performed for all breast cell lines.

4.3. Total RNA Purification for mRNA and miRNA Expression

Time samples obtained to confirm synchronization were directly lysed by 400 µL of TRI Reagent® (Sigma-Aldrich, St. Louis, MO, USA) to achieve total RNA isolation according to the manufacturer's instructions. The total RNA was purified using 3 M sodium acetate, with a pH of 5.2 (1/10 volume), and 2.5 volumes of cold 100% ethanol. The mixture was incubated at −80 °C for 30 min. Next, the mixture was centrifuged at 13,500× *g* for 30 min, washed with 1 mL of 75% ethanol, and then dried and re-suspended in pre-warmed nuclease-free water. We then measured the yield and purity of the purified total RNA using NanoDrop 1000 (Thermo Fisher Scientific).

Time samples obtained for miRNA expression were disassociated with 0.4% Trypsin-EDTA (BioVision, Milpitas, CA, USA) and washed with basal medium 2–3 times. Then, the cell pellets were immediately processed to collect cytosolic fractions using the Nuclear/Cytosol Extraction Kit (BioVision) according to the manufacturer's instructions. These fractions were stored at −70 °C. Next, we isolated total RNA from cytosolic time fractions using the MIRVANA miRNA Ambion® Kit (Thermo Fisher Scientific) according to the manufacturer's instructions. The RNA from cytosolic fractions (cyRNA) was purified using 3 M sodium acetate at a pH of 5.2 (1/10 volume) and 2.5 volumes of cold 100% ethanol. Then, the mixture was incubated at −70 °C for 30 min. Next, the mixture was centrifuged at 13,500× *g* for 30 min, washed with 1 mL of 70% ethanol, dried, and re-suspended in pre-warmed nuclease-free water. We then measured the yield and purity of the cyRNA using NanoDrop 1000 (Thermo Fisher Scientific). In addition, cyRNA samples were assessed using an RNA HighSense Analysis Kit (Bio-Rad Laboratories, Irvine, CA, USA) in Experion (Bio-Rad Laboratories) in order to ensure the quality of RNA (RIN, RNA integrity number) for microarray hybridization assays.

4.4. Quantitative RT-qPCR for mRNA Expression

Reverse transcription of mRNA to cDNA was carried out with 400 ng of total RNA using an AffinityScript Multi-Temperature cDNA synthesis kit (Agilent Technologies, Santa Clara, CA, USA) according to the manufacturer's instructions. Next, qPCR was carried out using the Applied Biosystems® StepOne™ Real-Time PCR System (Thermo Fisher Scientific). The reaction involved 20 ng of cDNA, 200 nM of forward and reverse primers for circadian clock genes, *BMAL1*, and *PER2*, and one rhythmic gene for MCF-7, SERPINB1, which we described in a previous study [11] (Table 2), 1× Brilliant II Fast SYBR® Green qPCR Master Mix (Agilent Technologies), 300 nM passive reference dye, and molecular grade water to reach a final volume of 12 µL. The initial activation step was performed at 95 °C for 3 m, then a cycling program was begun, which involved denaturing at 95 °C for 6 s and annealing/extension at 60 °C for 12 s, and a melting curve analysis was performed to ensure the efficiency of the reaction. Relative expression was calculated using the $\Delta\Delta C_t$ method [48] with GAPDH serving as the reference gene for normalization. The expression level of each biological replicate was calculated separately and averaged, and the SEM was calculated for each time point. The relative expression results of each gene were plotted over 48 h at 4 h intervals.

Table 2. List of primers for clock genes.

Gene	Primer	Sequence (5′→3′)	NCBI RefSeq
BMAL1	Forward Reverse	CATTGTGCACAGAAGCATCA ACAAGGAAGAATAAACGGCTTT	NM_001178.4
PER2	Forward Reverse	TGCCAAAATCTTACTCTGCTG GGCATCACGTAAACAAATTCA	NM_022817.2
SERPINB1	Forward Reverse	AGGTTCATTCAAGATTCCAGAGT AGTTTCAGAATATAAGACGCTCCA	NM_030666.3 70
GAPDH	Forward Reverse	AGCCACATCGCTCAGACAC TGGCAACAATATCCACTTTACCAGA	NM_002046.4

4.5. Microarray Processing and Analysis

The miRNAs' temporal expression was profiled using a Human miRNA Microarray 8 × 60 K Kit (Agilent Technologies), which contained 2006 human miRNAs, based on miRBase Release 19.0 (http://www.mirbase.org/). These assays were performed using cyRNA time samples during a period of 28 h (hours 12–40 of the 48 h study) because they show the beginning of gene-sustained oscillations in living cells upon serum shock [23,49]. Thus, we used two slides (eight arrays per slide) for to profiling MCF-10A, MCF-7, and MDA-MB-231.

In total, 100 ng of cyRNA time samples was used for hybridization with miRNA complete labeling and the Hyb Kit (Agilent Technologies) according to the manufacturer's instructions. The first slide was hybridized with cyRNA time samples from MCF-10A labeled with Cy3 fluorochrome, while cyRNA time samples from MCF-7 and MDA-MB-231 were labeled with Cy3 and pCp (Cytidine-5′-phosphate-3′-(6-aminohexyl)phosphate)-Cy5 (277 µM) fluorochromes, respectively, and hybridized with the second slide, according to the manufacturer's instructions [50]. Next, standard washing procedures and hybridization with microarray slides were performed according to the manufacturer's instructions. Slides were scanned using the GenePix® 4000B Microarray Scanner (Molecular Devices, Downingtown, PA, USA) with GenePix® Pro 6.0.1.25 Acquisition and Analysis Software (Molecular Devices). The GenePix® results (GPR) files were imported into the software R, version 2.12.2 (http://www.R-project.org). Spot intensities were background subtracted using the Linear Models for Microarray Data package (Limma, version 3.20.5, https://bioconductor.org/packages/limma/) [51,52]. The miRNA array contained an average of 30 replicates per probe sequence, with a total of 60,000 unique features and controls. The data were normalized between arrays by quantile normalization and log10 transformed, and the median was applied to the replicated probes [53]. The miRNA expression data contains one to four different probes associated with each miRNA, which were considered individually for further analysis. However, miRNAs were selected for validation based on restrictive parameters, as described in Section 4.6. The miRNA microarray data will be submitted to GEO NCBI.

4.6. Identification of miRNAs with Rhythmic Expression

The miRNAs with rhythmic patterns were identified by analyzing miRNA expression over 28 h (hours 12–40 of the 48 h study) for MCF-10A, MCF-7, and MDA-MB-231. Firstly, data was arranged from 0–28 h in order to perform the cosine-fitting algorithm. This interval, which avoids the first 12 h, is appropriate for identifying miRNAs with robust rhythmicity [49]. The cosine function is defined as $g = \beta \times \cos(\omega \times t + \varphi)$, where the cosine parameters β, ω, and φ were limited to [0, 30], [0, π], and [-2π, 2π], respectively. The cosine fitting function was evaluated by comparing the distributions of the cosine correlations, periods, and phases in the experimental and randomized data. Afterward, restrictive values for amplitude, period, and cosine correlation were selected to identify rhythmic miRNAs. These values were $r > 0.82$ for cosine correlation, 0.22–0.29 for period, and >0.045 for amplitude. The miRNAs that fulfilled those parameters were grouped using hierarchical clustering (ward agglomeration) to identify miRNAs with similar phases. Next, miRNAs were selected for confirmation using RT-qPCR. They were chosen if they featured cosine-fitting correlation values of r were close to 1, a period of about 24 h, and a high amplitude value. Additionally, we restricted the selection of miRNAs for longer probe sequences, lengths of at least 15 nt, and/or high correlation among probes that belong to the selected miRNA. These parameters were used to ensure the reproducibility of the RT-qPCR assays [54]. Finally, the newly developed MetaCycle package (version 1.0.0; https://github.com/gangwug/MetaCycleV100.git) was used to confirm the significance of the periodicity and rhythmicity of the miRNAs validated by RT-qPCR [27]. The miRNAs that exhibited p-values of less than 0.05 were considered rhythmic. All the statistical analyses were performed using R programming language.

4.7. Quantitative RT-qPCR for miRNA Expression

Reverse transcription of cyRNA time samples (performed separately in triplicate) was conducted using miRNA-specific stem-loop RT primers (see Table 3), which featured a 3′ overhang of 6 or 7 nucleotides complementary to the 3′ portion of the associated mature miRNA sequence [55]. We made a pool of seven stem-loop RT primers that included one endogenous control at 10 nM, allowing simultaneous reverse transcriptions in one tube [56]. Reverse transcriptase reactions contained 200 ng of cyRNA, a stem-loop RT primer pool, and reagents from a TaqMan MicroRNA Reverse Transcription Kit (Thermo Fisher Scientific) according to the manufacturer's instructions. A negative control (no template) was included in all reactions.

Next, we performed pre-amplification of cDNA prior to quantification [57,58]. We facilitated two separate pre-amplification reactions using two miRNA primer pools. The first primer pool contained miR-1225-5p, miR-548ay-3p, and miR-769-3p, and the second contained miR-141-5p, miR-222-5p, and miR-17-5p. Both pools included miR-106a-5p as an endogenous control. For each reaction, 3 µL of cDNA, 100 nM of the miRNA primer pool (forward primers), 12.5 µL of 2× Universal Master Mix with no UNG (Thermo Fisher Scientific), 1 uM of universal reverse primer, 1 µL of 5 U/µL AmpliTaq Gold (Promega Corp, Madison, WI, USA), 0.5 µL of 100 mM dNTPs (Promega Corp), 0.5 µL of 100 mM MgCl2 (Promega Corp), and molecular grade water were used to achieve a final volume of 25 µL. Regarding the temperature profile of the reaction, incubation at 95 °C for 10 m, was followed by incubation at 55 °C for 2 m and 14 cycles of 95 °C for 1 s and 65 °C for 1 m. A negative pre-amplified control (no-cDNA) was included. Next, both pre-amplified cDNAs were diluted 10 times using molecular grade water and stored at −20 °C before further processing.

Finally, the qPCR was run using an Applied Biosystems® StepOne™ Real-Time PCR System (Thermo Fisher Scientific). Seven miRNAs were profiled using 1X Brilliant II Fast SYBR® Green qPCR Master Mix (Agilent Technologies). The reaction consisted of 1 µL of pre-amplified cDNA, 150 nM of forward and reverse primers (Table 3), 300 nM of passive reference dye, and molecular grade water to achieve a final volume of 12 µL. The following three-step cycling program was used: 95 °C for 3 min and 40 cycles of 95 °C for 6 s, 55 °C for 12 s, and 70 °C for 10 s. Melting curves were performed to ensure an efficient reaction. The relative expression was calculated using the $\Delta\Delta C_t$ [48], with miR-106a-5p used for normalization [15]. The level of expression of each biological replicate was calculated separately and averaged, and the SEM was calculated for each time point. The relative expression results of each miRNA were plotted over 48 h at 4 h intervals.

Table 3. List of primers for miRNA validation.

miRNA	Primer	Sequence (5′→3′)	Mature Accession Number
hsa-miR-141-5p	Stem-loop	GTC GTA TCC AGT GCA GGG TCC GAG GTA TTC GCA CTG GAT ACG AC TCCAAC	MIMAT0004598
	Forward	CAC GCA CAT CTT CCA GTA C	
hsa-miR-1225-5p	Stem-loop	GTC GTA TCC AGT GCA GGG TCC GAG GTA TTC GCA CTG GAT ACG AC CCCCCC	MIMAT0005572
	Forward	CAACAGTGGGTACGGCCCA	
hsa-miR-17-5p	Stem-loop	GTC GTA TCC AGT GCA GGG TCC GAG GTA TTC GCA CTG GAT ACG AC CTACCT	MIMAT0000070
	Forward	CAC GCA CAA AGT GCT TAC A	
hsa-miR-769-3p	Stem-loop	GTC GTA TCC AGT GCA GGG TCC GAG GTA TTC GCA CTG GAT ACG AC AACCAA	MIMAT0003887
	Forward	CAA CAC TGG GAT CTC CGG	

Table 3. *Cont.*

miRNA	Primer	Sequence (5′→3′)	Mature Accession Number
hsa-miR-222-5p	Stem-loop	GTC GTA TCC AGT GCA GGG TCC GAG GTA TTC GCA CTG GAT ACG AC AGGATC	MIMAT0004569
	Forward	CAG CAC TCA GTA GCC AGT	
hsa-miR-548ay-3p	Stem-loop	GTC GTA TCC AGT GCA GGG TCC GAG GTA TTC GCA CTG GAT ACG AC TGCAAG	MIMAT0025453
	Forward	CAG CAC AAA ACC GCG AT	
hsa-miR-106a-5p	Stem-loop	GTC GTA TCC AGT GCA GGG TCC GAG GTA TTC GCA CTG GAT ACG AC GCTACC	MIMAT0000103
	Forward	CAC GCA AAAAGTGCTTACAGT	
	Universal	TCG TA TCC AGT GCA GGG T	

4.8. Identification of Targeted mRNAs and Pathway Analysis

The MultiMiR package (version 1.0.1; http://multimir.ucdenver.edu/) was established to identify targeted miRNAs that were experimentally validated [28]. The Reactome pathway analysis tool (www.reactome.org/PathwayBrowser/#TOOL=AT) was used to perform annotation enrichment analysis using lists of targeted mRNAs [59].

5. Conclusions

Our results indicate that serum shock entrainment of breast cell lines induces rhythmic fluctuations in some miRNAs. Additionally, some miRNAs exhibit different expression profiles across breast cell lines, which suggests that tumorigenic and non-tumorigenic cells respond differently to serum shock in terms of transcription. Our results indirectly link the hypothesis that miRNAs may play a potential role in circadian architecture of breast cells. Further studies are required to understand the possible effects of the rhythmicity of miRNAs in breast cells and determine whether they can be used as potential biomarkers.

Supplementary Materials: Supplementary materials can be found at www.mdpi.com/1422-0067/18/7/1499/s1.

Acknowledgments: The authors would like to thank Ana Cristina González and Raul Cantú for their technical support with RNA purification. Rafael Chacolla-Huaringa expresses his gratitude to the Mexican National Council for Science and Technology (CONACyT) for the Ph.D. grant scholarship (#290649). This work was funded by Cátedras de Hematologia y Cancer and Terapia Celular y Medicina Regenerativa, part of the Tecnológico de Monterrey, Monterrey campus.

Author Contributions: Designed research: Rafael Chacolla-Huaringa and Sean-Patrick Scott. Performed experiments: Rafael Chacolla-Huaringa. Analyzed data: Rafael Chacolla-Huaringa. Interpreted the results of experiments: Rafael Chacolla-Huaringa, Victor Trevino, and Sean-Patrick Scott. Prepared figures: Rafael Chacolla-Huaringa. Drafted manuscript: Rafael Chacolla-Huaringa. Edited and revised manuscript: Rafael Chacolla-Huaringa, Jorge Moreno-Cuevas, Victor Trevino, and Sean-Patrick Scott. Approved final version of manuscript: Rafael Chacolla-Huaringa, Jorge Moreno-Cuevas, Victor Trevino and Sean-Patrick Scott.

Conflicts of Interest: The authors declare no conflict of interest.

Abbreviations

BMAL1	also known arntl, aryl hydrocarbon receptor nuclear translocator like
PER2	Period circadian clock 2
SERPINB1	Serpin family B member 1
TL	Time-label
RW	Row-wise
CW	Column-wise
RCW	Row-column-wise
RCWB	Row-column-wise by blocks

References

1. Golombek, D.A.; Rosenstein, R.E. Physiology of circadian entrainment. *Physiol. Rev.* **2010**, *90*, 1063–1102. [CrossRef] [PubMed]
2. Rana, S.; Mahmood, S. Circadian rhythm and its role in malignancy. *J. Circadian Rhythm.* **2010**, *8*, 1–13. [CrossRef] [PubMed]
3. Garbarino-Pico, E.; Green, C.B. Posttranscriptional regulation of mammalian circadian clock output. *Cold Spring Harb.* **2007**, *72*, 145–156. [CrossRef] [PubMed]
4. Buhr, E.D.; Takahashi, J.S. Molecular components of the Mammalian circadian clock. *Handb. Exp. Pharmacol.* **2013**, *15*, 3–27. [CrossRef]
5. Bray, M.S.; Young, M.E. Circadian rhythms in the development of obesity: Potential role for the circadian clock within the adipocyte. *Obes. Rev.* **2007**, *8*, 169–181. [CrossRef] [PubMed]
6. Leibetseder, V.; Humpeler, S.; Svoboda, M.; Schmid, D.; Thalhammer, T.; Zuckermann, A.; Marktl, W.; Ekmekcioglu, C. Clock genes display rhythmic expression in human hearts. *Chronobiol. Int.* **2009**, *26*, 621–636. [CrossRef] [PubMed]
7. Gutierrez-Monreal, M.A.; Cuevas-Diaz, R.; Moreno-Cuevas, J.E.; Scott, S.P. A Role for 1α, 25-dihydroxyvitamin D_3 in the expression of circadian genes. *J. Biol. Rhythms* **2014**, *29*, 384–388. [CrossRef] [PubMed]
8. Harbour, V.L.; Weigl, Y.; Robinson, B.; Amir, S.; Brooks, A. Phase differences in expression of circadian clock genes in the central nucleus of the amygdala, dentate gyrus, and suprachiasmatic nucleus in the rat. *PLoS ONE* **2014**, *9*, e103309. [CrossRef] [PubMed]
9. Xiang, S.; Mao, L.; Duplessis, T.; Yuan, L.; Dauchy, R.; Dauchy, E.; Blask, D.E.; Frasch, T.; Hill, S.M. Oscillation of clock and clock controlled genes induced by serum shock in human breast epithelial and breast cancer cells: Regulation by melatonin. *Breast Cancer* **2012**, *6*, 137–150. [CrossRef] [PubMed]
10. Rossetti, S.; Esposito, J.; Corlazzoli, F.; Gregorski, A.; Sacchi, N. Entrainment of breast (cancer) epithelial cells detects distinct circadian oscillation patterns for clock and hormone receptor genes. *Cell Cycle* **2012**, *11*, 350–360. [CrossRef] [PubMed]
11. Gutiérrez-Monreal, M.A.; Treviño, V.; Moreno-Cuevas, J.E.; Scott, S.-P. Identification of circadian-related gene expression profiles in entrained breast cancer cell lines. *Chronobiol. Int.* **2016**, *33*, 392–405. [CrossRef] [PubMed]
12. Kojima, S.; Green, C.B. Circadian genomics reveal a role for post-transcriptional regulation in mammals. *Biochemistry* **2015**, *54*, 124–133. [CrossRef] [PubMed]
13. He, L.; Hannon, G.J. MicroRNAs: Small RNAs with a big role in gene regulation. *Nat. Rev. Genet.* **2004**, *5*, 522–531. [CrossRef] [PubMed]
14. Reddy, A.B.; Karp, N.A.; Maywood, E.S.; Sage, E.A.; Deery, M.; O'Neill, J.S.; Wong, G.K.Y.; Chesham, J.; Odell, M.; Lilley, K.S.; et al. Circadian orchestration of the hepatic proteome. *Curr. Biol.* **2006**, *16*, 1107–1115. [CrossRef] [PubMed]
15. Lee, K.H.; Kim, S.H.; Lee, H.R.; Kim, W.; Kim, D.Y.; Shin, J.C.; Yoo, S.H.; Kim, K.T. MicroRNA-185 oscillation controls circadian amplitude of mouse cryptochrome 1 via translational regulation. *Mol. Biol. Cell* **2013**, *24*, 2248–2255. [CrossRef] [PubMed]
16. Kinoshita, C.; Aoyama, K.; Matsumura, N.; Kikuchi-Utsumi, K.; Watabe, M.; Nakaki, T. Rhythmic oscillations of the microRNA miR-96-5p play a neuroprotective role by indirectly regulating glutathione levels. *Nat. Commun.* **2014**, *5*, 3823. [CrossRef] [PubMed]
17. Balakrishnan, A.; Stearns, A.T.; Park, P.J.; Dreyfuss, J.M.; Ashley, S.W.; Rhoads, D.B.; Tavakkolizadeh, A. MicroRNA mir-16 is anti-proliferative in enterocytes and exhibits diurnal rhythmicity in intestinal crypts. *Exp. Cell Res.* **2010**, *316*, 3512–3521. [CrossRef] [PubMed]
18. Du, N.-H.; Arpat, A.B.; Matos, M.; De Gatfield, D. MicroRNAs shape circadian hepatic gene expression on a transcriptome-wide scale. *Elife* **2014**, *3*, e02510. [CrossRef] [PubMed]
19. Gotoh, T.; Vila-Caballer, M.; Liu, J.; Schiffhauer, S.; Finkielstein, C.V. Association of the circadian factor Period 2 to p53 influences p53's function in DNA-damage signaling. *Mol. Biol. Cell* **2015**, *26*, 359–372. [CrossRef]
20. Kochan, D.Z.; Ilnytskyy, Y.; Golubov, A.; Deibel, S.H.; McDonald, R.J.; Kovalchuk, O. Circadian disruption-induced microRNAome deregulation in rat mammary gland tissues. *Oncoscience* **2015**, *2*, 428–442. [CrossRef] [PubMed]

21. Sempere, L.F.; Christensen, M.; Silahtaroglu, A.; Bak, M.; Heath, C.V.; Schwartz, G.; Wells, W.; Kauppinen, S.; Cole, C.N. Altered microrna expression confined to specific epithelial cell subpopulations in breast cancer. *Cancer Res.* **2007**, *67*, 11612–11620. [CrossRef] [PubMed]
22. Mulrane, L.; McGee, S.F.; Gallagher, W.M.; O'Connor, D.P. miRNA dysregulation in breast cancer. *Cancer Res.* **2013**, *73*, 6554–6562. [CrossRef] [PubMed]
23. Balsalobre, A.; Damiola, F.; Schibler, U.A. Serum shock induces circadian gene expression in mammalian tissue culture cells. *Cell* **1998**, *93*, 929–937. [CrossRef]
24. Nagoshi, E.; Saini, C.; Bauer, C.; Laroche, T.; Naef, F.; Schibler, U. Circadian gene expression in individual fibroblasts: Cell-autonomous and self-sustained oscillators pass time to daughter cells. *Cell* **2004**, *119*, 693–705. [CrossRef] [PubMed]
25. Futschik, M.E.; Herzel, H. Are we overestimating the number of cell-cycling genes? The impact of background models on time-series analysis. *Bioinformatics* **2008**, *24*, 1063–1069. [CrossRef] [PubMed]
26. Kallio, A.; Vuokko, N.; Ojala, M.; Haiminen, N.; Mannila, H. Randomization techniques for assessing the significance of gene periodicity results. *BMC Bioinform.* **2011**, *12*, 330. [CrossRef] [PubMed]
27. Wu, G.; Anafi, R.C.; Hughes, M.E.; Kornacker, K.; Hogenesch, J.B. MetaCycle: An integrated R package to evaluate periodicity in large scale data. *Bioinformatics* **2016**, *32*, 3351–3353. [CrossRef] [PubMed]
28. Ru, Y.; Kechris, K.J.; Tabakoff, B.; Hoffman, P.; Radcliffe, R.A.; Bowler, R.; Mahaffey, S.; Rossi, S.; Calin, G.A.; Bemis, L.; Theodorescu, D. The multiMiR R package and database: Integration of microRNA–target interactions along with their disease and drug associations. *Nucleic Acids Res.* **2014**, *42*, 133. [CrossRef] [PubMed]
29. Sahar, S.; Sassone-Corsi, P. Metabolism and cancer: The circadian clock connection. *Nat. Rev. Cancer* **2009**, *9*, 886–896. [CrossRef] [PubMed]
30. Xu, H.; Gustafson, C.L.; Sammons, P.J.; Khan, S.K.; Parsley, N.C.; Ramanathan, C.; Lee, H.W.; Liu, A.C.; Partch, C.L. Cryptochrome 1 regulates the circadian clock through dynamic interactions with the BMAL1 C terminus. *Nat. Struct. Mol. Biol.* **2015**, *22*, 476–484. [CrossRef] [PubMed]
31. Chen, R.; Schirmer, A.; Lee, Y.; Lee, H.; Kumar, V.; Yoo, S.H.; Takahashi, J.S.; Lee, C. Rhythmic PER abundance defines a critical nodal point for negative feedback within the circadian clock mechanism. *Mol. Cell* **2009**, *36*, 417–430. [CrossRef] [PubMed]
32. Hausser, J.; Zavolan, M. Identification and consequences of miRNA-target interactions—Beyond repression of gene expression. *Nat. Rev. Genet.* **2014**, *15*, 599–612. [CrossRef] [PubMed]
33. Savvidis, C.; Koutsilieris, M. Circadian rhythm disruption in cancer biology. *Mol. Med.* **2012**, *18*, 1249–1260. [CrossRef] [PubMed]
34. Na, Y.J.; Sung, J.H.; Lee, S.C.; Lee, Y.J.; Choi, Y.J.; Park, W.Y.; Shin, H.S.; Kim, J.H. Comprehensive analysis of microRNA-mRNA co-expression in circadian rhythm. *Exp. Mol. Med.* **2009**, *41*, 638–647. [CrossRef] [PubMed]
35. Kim, D.H.; Grün, D.; van Oudenaarden, A. Dampening of expression oscillations by synchronous regulation of a microRNA and its target. *Nat. Genet.* **2013**, *45*, 1337–1344. [CrossRef] [PubMed]
36. Chen, B.; Zhang, B.; Luo, H.; Yuan, J.; Skogerbø, G.; Chen, R. Distinct MicroRNA Subcellular Size and Expression Patterns in Human Cancer Cells. *Int. J. Cell Biol.* **2012**, *2012*. [CrossRef] [PubMed]
37. Huisman, S.A.; Oklejewicz, M.; Ahmadi, A.R.; Tamanini, F.; Ijzermans, J.N.M.; van der Horst, G.T.J.; de Bruin, R.W.F. Colorectal liver metastases with a disrupted circadian rhythm phase shift the peripheral clock in liver and kidney. *Int. J. Cancer* **2015**, *136*, 1024–1032. [CrossRef] [PubMed]
38. Gery, S.; Virk, R.K.; Chumakov, K.; Yu, A.; Koeffler, H.P. The clock gene Per2 links the circadian system to the estrogen receptor. *Oncogene* **2007**, *26*, 7916–7920. [CrossRef] [PubMed]
39. Menger, G.J.; Lu, K.; Thomas, T.; Cassone, V.M.; Earnest, D.J. Circadian profiling of the transcriptome in immortalized rat SCN cells. *Physiol. Genom.* **2005**, *21*, 370–381. [CrossRef] [PubMed]
40. Yu, Z.; Willmarth, N.E.; Zhou, J.; Katiyar, S.; Wang, M.; Liu, Y.; McCue, P.A.; Quong, A.A.; Lisanti, M.P.; Pestell, R.G. microRNA 17/20 inhibits cellular invasion and tumor metastasis in breast cancer by heterotypic signaling. *Proc. Natl. Acad. Sci. USA* **2010**, *107*, 8231–8236. [CrossRef] [PubMed]
41. Jin, L.; Lim, M.; Zhao, S.; Sano, Y.; Simone, B.A.; Savage, J.E.; Wickstrom, E.; Camphausen, K.; Pestell, R.G.; Simone, N.L. The metastatic potential of triple-negative breast cancer is decreased via caloric restriction-mediated reduction of the miR-17~92 cluster. *Breast Cancer Res. Treat.* **2014**, *146*, 41–50. [CrossRef] [PubMed]

42. Gao, Q.; Zhou, L.; Yang, S.-Y.; Cao, J.-M. A novel role of microRNA 17-5p in the modulation of circadian rhythm. *Sci. Rep.* **2016**, *6*, 30070. [CrossRef] [PubMed]
43. Castellano, L.; Giamas, G.; Jacob, J.; Coombes, R.C.; Lucchesi, W.; Thiruchelvam, P.; Barton, G.; Jiao, L.R.; Wait, R.; Waxman, J.; et al. The estrogen receptor-α-induced microRNA signature regulates itself and its transcriptional response. *Proc. Natl. Acad. Sci. USA* **2009**, *106*, 15732–15737. [CrossRef] [PubMed]
44. Zhao, J.J.; Lin, J.; Yang, H.; Kong, W.; He, L.; Ma, X.; Coppola, D.; Cheng, J.Q. MicroRNA-221/222 negatively regulates estrogen receptorα and is associated with tamoxifen resistance in breast cancer. *J. Biol. Chem.* **2008**, *283*, 31079–31086. [CrossRef] [PubMed]
45. Blattner, M.S.; Mahoney, M.M. Estrogen receptor 1 modulates circadian rhythms in adult female mice. *Chronobiol. Int.* **2014**, *31*, 637–644. [CrossRef] [PubMed]
46. Joyce, C.E.; Zhou, X.; Xia, J.; Ryan, C.; Thrash, B.; Menter, A.; Zhang, W.; Bowcock, A.M. Deep sequencing of small RNAs from human skin reveals major alterations in the psoriasis miRNAome. *Hum. Mol. Genet.* **2011**, *20*, 4025–4040. [CrossRef] [PubMed]
47. Takahashi, J.S. Transcriptional architecture of the mammalian circadian clock. *Nat. Rev. Genet.* **2016**, *18*, 164–179. [CrossRef] [PubMed]
48. Livak, K.J.; Schmittgen, T.D. Analysis of relative gene expression data using real-time quantitative PCR and the 2(-Delta Delta C(T)) method. *Methods* **2001**, *408*, 402–408. [CrossRef] [PubMed]
49. Izumo, M.; Sato, T.R.; Straume, M.; Johnson, C.H. Quantitative analyses of circadian gene expression in mammalian cell cultures. *PLoS Comput. Biol.* **2006**, *2*, e136. [CrossRef] [PubMed]
50. Wang, H.; Ach, R.A.; Curry, B. Direct and sensitive miRNA profiling from low-input total RNA. *RNA* **2007**, *13*, 151–159. [CrossRef] [PubMed]
51. Ritchie, M.E.; Silver, J.; Oshlack, A.; Holmes, M.; Diyagama, D.; Holloway, A.; Smyth, G.K. A comparison of background correction methods for two-colour microarrays. *Bioinformatics* **2007**, *23*, 2700–2707. [CrossRef] [PubMed]
52. Smyth, G.K.; Speed, T. Normalization of cDNA microarray data. *Methods* **2003**, *31*, 265–273. [CrossRef]
53. López-Romero, P.; González, M.A.; Callejas, S.; Dopazo, A.; Irizarry, R.A. Processing of Agilent microRNA array data. *BMC Res. Notes* **2010**, *3*, 18. [CrossRef] [PubMed]
54. Chou, C.-C.; Chen, C.-H.; Lee, T.-T.; Peck, K. Optimization of probe length and the number of probes per gene for optimal microarray analysis of gene expression. *Nucleic Acids Res.* **2004**, *32*, e99. [CrossRef] [PubMed]
55. Chen, C.; Ridzon, D.A.; Broomer, A.J.; Zhou, Z.; Lee, D.H.; Nguyen, J.T.; Barbisin, M.; Xu, N.L.; Mahuvakar, V.R.; Andersen, M.R.; et al. Real-time quantification of microRNAs by stem–loop RT–PCR. *Nucleic Acids Res.* **2005**, *33*, e179. [CrossRef] [PubMed]
56. Mestdagh, P.; Feys, T.; Bernard, N.; Guenther, S.; Chen, C.; Speleman, F.; Vandesompele, J. High-throughput stem-loop RT-qPCR miRNA expression profiling using minute amounts of input RNA. *Nucleic Acids Res.* **2008**, *36*, e143. [CrossRef] [PubMed]
57. Lao, K.; Xu, N.L.; Yeung, V.; Chen, C.; Livak, K.J.; Straus, N.A. Multiplexing RT-PCR for the detection of multiple miRNA species in small samples. *Biochem. Biophys. Res. Commun.* **2006**, *343*, 85–89. [CrossRef] [PubMed]
58. Pezzolesi, M.G.; Satake, E.; McDonnell, K.P.; Major, M.; Smiles, A.M.; Krolewski, A.S. Circulating TGF-β1–regulated miRNAs and the risk of rapid progression to ESRD in type 1 diabetes. *Diabetes* **2015**, *64*, 3285–3293. [CrossRef] [PubMed]
59. Fabregat, A.; Sidiropoulos, K.; Garapati, P.; Gillespie, M.; Hausmann, K.; Haw, R.; Jassal, B.; Jupe, S.; Korninger, F.; McKay, S.; et al. The reactome pathway knowledgebase. *Nucleic Acids Res.* **2016**, *44*, D481–D487. [CrossRef] [PubMed]

Curriculum Vitae

Rafael Julián Chacolla Huaringa was born in Lima, Peru, on December 27, 1985. He earned the Medical Technologist degree from the Universidad Nacional Federico Villarreal, Lima in February 2008. He was accepted in the graduate program in Biotechnology Master in August 2009. He acquired skills and knowledge, which influenced him to decide to achieve a new challenge. Thus, He decided to pursue a PhD program in August 2011, where he achieved two international poster conferences, one of them was in San Antonio, Texas, EEUU, and the second one was in Tampa, Florida, EEUU. Additionally, he obtained an article published in a prestigious international scientific journal. All of above achievements made him a gather valuable experience to continue his career in diverse fields, such as academics and industry.

This document was typed in using Microsoft Word by Rafael Julián Chacolla Huaringa